# Transmission and feedback strategies for energy harvesting wireless communication systems

Rajeev Gangula

ParisTech
INSTITUT DES SCIENCES ET TECHNOLOGIES
PARIS INSTITUTE OF TECHNOLOGY

TELECOM ParisTech

2015-ENST-0042

EDITE - ED 130

# Doctorat ParisTech

# T H È S E

**pour obtenir le grade de docteur délivré par**

## TELECOM ParisTech

**Spécialité « Communication et Electronique »**

*présentée et soutenue publiquement par*

**Rajeev GANGULA**

le 21 juillet 2015

# Stratégies de transmission et feedback pour les systèmes de communication sans-fil à récupération de l'énergie

Directeur de thèse : **David GESBERT**

**Jury**

| | |
|---|---|
| **Mme. Elif Uysal-Biyikoglu**, Professeur, METU, Turquie | Rapporteur |
| **Mme. Mari Kobayashi**, Professeur, Supélec, France | Rapporteur |
| **M. Dirk Slock**, Professeur, EURECOM, France | Examinateur |
| **M. Deniz Gündüz**, Professeur, Imperial College London, UK | Examinateur |

**TELECOM ParisTech**
école de l'Institut Télécom - membre de ParisTech

THÈSE



# DISSERTATION

In Partial Fulfillment of the Requirements
for the Degree of Doctor of Philosophy
from TELECOM ParisTech

Specialization : Communication and Electronics

**Rajeev Gangula**

# Transmission and Feedback Strategies for Energy Harvesting Wireless Communication Systems

Defense scheduled on the 21st of July 2015 before a committee composed of :

| | |
|---|---|
| Reviewers | Prof. Elif Uysal-Biyikoglu, METU, Turkey |
| | Dr. Mari Kobayashi, Supélec, France |
| Examiners | Prof. Dirk Slock, EURECOM, France |
| | Dr. Deniz Gündüz, Imperial College London, UK |
| Thesis supervisor | Prof. David Gesbert, EURECOM, France |

# Abstract

Over the last decade, we have witnessed a rapid growth in the number of communication devices, and this trend is expected to continue as the key technologies such as Internet of Things (IoT), wearable devices, are shaping the future of information and communication technology (ICT) industry. This growth has resulted in a tremendous increase in the energy demand, and hence the carbon footprint of the ICT ecosystem can no longer be ignored.

Additionally, in traditional battery powered communication systems where energy infrastructure is not available after deployment, the limited available energy in the battery becomes the bottleneck as it determines the network lifetime.

Powering up nodes with ambient energy sources, thanks to the energy harvesting technology, not only reduces the carbon footprint of ICT sector but also increases the autonomy of battery powered communication networks. An energy harvesting node can scavenge energy from the surrounding environment (typical sources are solar, wind, vibration, thermal, etc.). However, time varying nature of the ambient energy makes the design of communication strategies quite different from the traditional communication systems.

Besides energy harvesting, higher throughput can be obtained in a wireless communication system by designing transmission schemes on the basis of propagation channel information. As channel adaptation techniques require to have some knowledge of the wireless channel conditions feedback to the transmitter, the gain in throughput comes at the cost of pilot-based training and feedback which consume resources in a communication system, especially, energy. In addition when the goal in a communication system is to send information about the source to a destination such that mean squared error distortion is minimized, transmission and compression strategies has to be designed based on both the time varying channel conditions and the source statistics.

This dissertation focuses on the design of transmission strategies taking into account the cost of obtaining the channel state information (CSI) at the transmitter, and time varying source statistics when the communication nodes rely on harvested energy (hence time-varying energy) supplies. Specifically, in Chapter 2, we consider a point-to-point multiple-input single-output

(MISO) communication system in which both the transmitter and the receiver have energy harvesting capabilities. The receiver is interested in sending the CSI to the transmitter to help improve the transmission rate. By modeling the energy consumed in obtaining the CSI, we aim to maximize the throughput, subject to the energy harvesting constraints at the transmitter and the receiver.

As an extension of the point-to-point MISO scenario, in Chapter 3, a MISO broadcast channel where a multi-antenna transmitter serves multiple single antenna energy harvesting user terminals is studied. The transmitter obtains the CSI by estimating the channel from the pilot symbols sent by the user terminals. Training schemes that optimize the throughput are obtained under energy harvesting constraints at the user terminals.

Next, in Chapter 4, we consider a system consisting of two sensor nodes where each node observes and samples a common physical phenomenon locally, and hence the samples are correlated. Then the nodes send their information to the destination over orthogonal wireless channels. In this scenario, we determine the achievable distortion region for the data transmitted by both sensor nodes.

Finally, we consider a communication system where the goal is to send information about the energy source itself to a destination (measurement node) with minimized mean squared error distortion. Specifically, the sensor measures and sends information about the source signal while at the same time relies on the energy harvested from it. In this scenario, we come up with some practical schemes that efficiently utilizes the electrical signal generated from the ambient energy source to minimize the average end-to-end distortion.

# Acknowledgements

I would like to thank my supervisor David Gesbert for first actually offering me a master thesis and then a doctoral thesis to work on. Beyond his well known qualities in the academia, his personal qualities made an enjoyable work environment in our group. He offered me enough freedom in work and at the same time was always available for providing important guidence. I would also like to thank Deniz Gunduz for hosting me at Imperial college and for the fruitful collaboration we had throughout this work.

During the 4 years i have spent at EURECOM, i had an amazing chance to make friends from different countries and cultures. This international exposure equipped me with different ways of thinking and seeing things from various perspectives in life. A special thanks to Giovanni for bringing liveliness (at times chaos!) into a rather monotonic work atmosphere, Robin for being a cool roomie in all these years in Antibes, Anikó for organising nice dinners (Italian rather than Hungarian), Leela and Shashank for making me not miss my mother tongue and home and José for being a cool Spaniard to be around. I would also like to thank my friends and colleagues Paul de Kerret, Miltos filippou and Xinping Yi for making a nice work environment in our group.

Finally, if it is not for my parents' endless love and their efforts in providing me with good education and moral values, and an elder brother who is always there for me, I wouldn't have reached this far.

# Table of Contents

# List of Figures

# Acronyms

Here are the main acronyms used in this document. The meaning of an acronym is usually indicated once, when it first appears in the text.

| | |
|---|---|
| AWGN | Additive White Gaussian Noise |
| BC | Broadcast Channel |
| CSI | Channel State Information |
| DL | DownLink |
| DP | Dynamic programming |
| DWF | Directional Water-Filling |
| EH | Energy Harvesting |
| FDD | frequency-division-duplex |
| HPN | Harvested Power to Noise ratio |
| i.i.d. | Independent and Identically Distributed |
| KKT | Karush-Kuhn-Tucker |
| MISO | Multiple Input Single Output |
| MDP | Markov Decision Processes |
| MG | Multiplexing Gain |
| MIMO | Multiple Input Multiple Output |
| p2p | Point-to-Point |
| QoS | Quality of Service |
| RVQ | Random Vector Quantization |
| RX | Receiver |
| SNR | Signal to Noise Ratio |
| TDD | time-division-duplex |
| TX | Transmitter |
| UL | UpLink |
| WF | Water-Filling |
| w.r.t. | with respect to |
| ZF | Zero Forcing |

# Notations

Here is a list of main operators and symbols used in this document. For vectors and matrices, the dimensions are frequently indicated when they appear in the text. We have tried to keep the notation consistent throughout the thesis, but rarely symbols have different definitions in different chapters and in that case they are defined very explicitly to avoid any confusion.

| | |
|---|---|
| $x$ or $X$ | Scalar |
| $\boldsymbol{x}$ | Vector |
| $(.)^*$ | Conjugate operation |
| $(.)^T$ | Transpose operation |
| $(.)^{\mathrm{H}}$ | Hermitian operation |
| $\lvert x \rvert$ | Absolute value of scalar |
| $\lVert \boldsymbol{x} \rVert$ | Euclidean norm of vector |
| $\mathrm{E}\,(.)$ | Mathematical expectation |
| $\mathbf{A}\,(i,j)$ | Entry at the $i$-th row and $j$-th column of matrix $\mathbf{A}$ |
| $[1:K]$ | Set of integers $\{1,\ldots,K\}$ |
| $\mathbb{N}$ | Set of natural numbers |
| $\mathbb{R}$ | Set of real numbers |
| $\mathbb{R}_+$ | Set of positive real numbers |
| $\mathcal{CN}$ | Complex Normal Distribution |
| $\mathbb{C}$ | Complex space |
| $\mathbb{C}^{M\times 1}$ | $M$-dimensional complex space |
| $\lvert\mathcal{A}\rvert$ | Cardinality of set $\mathcal{A}$ |
| $\boldsymbol{x} \preceq \boldsymbol{y}$ | $\boldsymbol{x}$ is *majorized* by $\boldsymbol{y}$ |

# Chapter 1

# Introduction

Energy harvesting (EH) is a process in which energy is scavenged from the ambient external sources (e.g. solar energy, wind energy, thermal energy, vibrational, and kinetic energy etc.). The usage of EH capable devices in wireless communication networks has attracted a lot of attention in recent years as it reduces the dependency of network on energy infrastructure. This chapter is composed of four sections. The first section motivates the need behind the study and development of communication systems with EH technologies. A typical mathematical model of an EH communication device, and some characterizations of harvested energy are given in the second section. Based on the characteristics of the EH profiles, different frameworks that allows us to study and evaluate the performance of EH communication systems, along with the state of the art are described in section Three. The final section provides an outline and the main contributions of this dissertation.

## 1.1 Motivation

The study of communication systems where the terminals are powered by renewable ambient energy addresses two fundamental problems : reduction of the carbon footprint of information and communication technologies (ICTs) and increase the autonomy of battery-run communication networks.

Growth in the energy demands leading to an increase in the energy obtained from non-renewable sources is a growing concern in our society. Exchange of information in a fast and efficient manner across the globe, thanks to ICTs, has resulted in a significant reduction in the carbon footprint of several sectors in our economy.

However, with an increase in our daily digital activities, and with the

key trends such as Big Data, Cloud Computing, Internet of Things (IoT) etc., shaping the future of the ICT industry, there is a predicted exponential growth in the number of communicating devices, and the amount of data being exchanged.

Now the question is, can we still ignore the carbon footprint of the ICT ecosystem ? To get an insight, we present some statistics taken from a documentary [1]. From 1990 to 2003, the world produced 5 million Gigabytes (GB) of data. In 2011, it took only two days to produce the same quantity, while in 2013, only 10 minutes. Today, we exchange an average of 10 million e-mails per hour, which requires energy that is equivalent to the energy consumed in 4000 round trip journeys between Paris and New York by plane. Hence, there is a strong requirement in coming up with "green" ICTs.

To address this issue, plenty of research effort has been invested in studying energy efficient transmission and reception techniques [1–3], network protocols [4] and computing and storage [5], under the umbrella of "green communication networks". In addition to the design of energy efficient ICTs, significant reductions in the carbon footprint of ICTs can be attained by using EH nodes in communication networks, which can recycle the clean and ambient energy from the environment.

Apart from being an environment friendly technology, EH improves the autonomy of battery powered communication systems. In traditional wireless networks nodes get their energy from the power grid by always or periodically connecting to it. While it is easy to connect the terminals to the grid in some networks, in others, such as sensor networks, energy infrastructure is usually not available after deployment. Therefore, in such networks a node's lifetime, and hence, the network lifetime, is constrained by the limited initial energy in the battery. Providing EH capabilities to the communication nodes is an attractive solution to the network lifetime problem [6]. An EH node can scavenge energy from the environment (typical sources are solar, wind, vibration, thermal, etc.) [7]. With EH nodes in the network, in principle, one can guarantee perpetual lifetime without the need of replacing batteries. With EH technology, the "plug and play" deployment of networks, in principle, can be made "drop and play", i.e., we can build communication networks on the fly without the need of any energy infrastructure.

However, EH poses a new design challenge as the energy sources are typically sporadic and random. The main challenge lies in ensuring the quality of service (QoS) constraints of the network given the random and time varying nature of energy sources. This calls for the intelligent management of various parameters involved in a communication system.

In summary, EH technology offers a promising approach in not only reducing the carbon foot print of communication systems but also in improving

1. "Internet, la pollution cachée", Directed by : Coline Tison and Laurent Lichtenstein. A nice documentary providing awareness of the lesser known digital pollution.

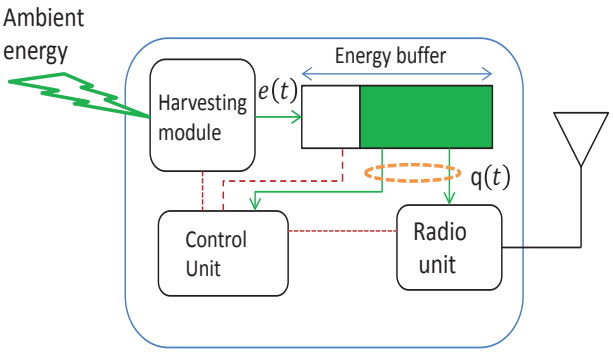


FIGURE 1.1 – A mathematical model for an energy harvesting communication device.

the life time of battery powered communication networks. However, the intermittent nature of harvested energy makes the design quite different from traditional communication systems which has constant power supply. Hence, the classical theory of communication and resource optimization need to be revisited taking into account the time-varying energy supplies.

## 1.2 Mathematical Model for EH Nodes

An abstract mathematical model for a typical EH wireless communication device is shown in Figure. 1.1. A brief description and modeling assumptions of each component are given below.

- The harvesting module converts the ambient energy into electrical signal. Examples of harvesters include photovoltaic cells for solar harvesting, and piezoelectric materials for vibration based energy harvesting. Since the ambient energy is typically a time varying process, we model the harvested energy i.e, the output of the harvesting module as a time varying process $e(t)$. Note that $e(t)$ represents the cumulative harvested energy by time $t$, and it is given by

$$e(t) = e_0 + \int_0^t h(\tau)\, d\tau, \tag{1.1}$$

where $h(\tau)$ is the instantaneous energy arrival rate and $e_0 \geq 0$ is the initial energy in the energy buffer. Depending on the nature of

the energy source, and the type of harvester, $e(t)$ can be discrete or continuous in time, and random or deterministic. The time-scale of variation in $e(t)$ plays an important role in the design of EH communication systems. The harvested energy $e(t)$ , for example when the energy source is radio frequency (RF) waves, may vary over the time-scales on the order of coding duration. On the other hand, in some EH processes, for example solar energy, $e(t)$ varies much slowly and can be assumed to be constant during the coding duration.

- The harvested energy can be stored in an energy buffer of size $B_{max}$ units. Typically the energy buffer is either a rechargeable battery or a super capacitor. The stored energy can be later used to power different sub systems in the node. If the energy arrives when the energy buffer is already full it is discarded.
- Based on the harvested energy $e(t)$ and the energy buffer status, the control unit is responsible for controlling the energy consumption $q(t)$ of the node by taking decisions such as power allocation for transmission and other subsystems, make the node idle or active etc..
- The radio unit is used for transmitting and receiving data over the wireless medium. Studies have shown that the radio/transceiver unit consumes significant portion of the power compared to the other tasks such as sensing and processing [8–10]. Hence, in this dissertation we only model the energy consumed in sending information and ignore the energy consumed in other components of the EH node.

## 1.3 State-of-the-art and Literature Survey

Depending on the time-scale variations of EH profiles and communication system models, the literature of EH communication systems can be depicted as a tree shown in Fig. 1.2. A brief explanation of information theoretic and resource allocation studies is provided in this section.

### 1.3.1 Information Theoretic Studies

Information theoretic analysis provides the fundamental limits of communication over a stochastic channel. Generally, it involves characterizing the capacity (in point-to-point channels) or capacity region (in multiuser settings). In traditional communication devices, typically capacity is evaluated under average or peak power constraints, nonetheless fixed for a transmitted codeword. However, in communication channels with EH devices, one may encounter random and time varying harvested energy over the code duration, and hence, a fixed power budget for the transmitted codeword cannot always be guaranteed. In such channels, capacity is evaluated under new type of constraints introduced by the EH process and the energy buffer size at the transmitter (TX).

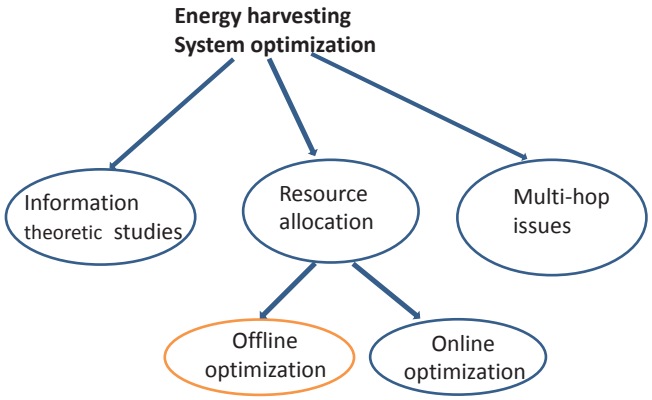


FIGURE 1.2 – Literature tree.

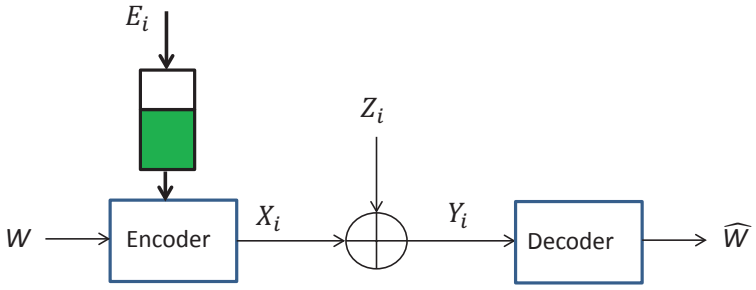


FIGURE 1.3 – AWGN channel with EH TX.

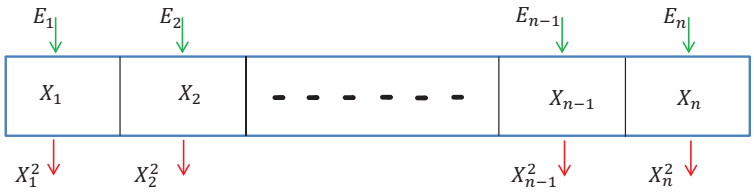


FIGURE 1.4 – Codeword with time-varying energy. $E_i$ units of energy arrives and $X_i^2$ units of energy spent in $i$-th channel use.

In [11], [12], the authors consider a memoryless additive white Gaussian noise channel (AWGN) with an EH TX as shown in Fig. 1.3. The transmitter wishes to send a message $W$ to the receiver reliably over $n$ channel uses. The TX harvests $E_i$ units of energy just before the beginning of the $i$-th channel use. While [11] models the energy arrival process as a stationary and ergodic random sequence over the code word duration, [12] considers $E_i$'s to be i.i.d. In both cases, the energy arrival process has mean $\mathrm{E}[E_i] = \overline{P}$. The harvested energy can be stored in an unlimited energy buffer. The transmission of $X_i$ in the $i$-th channel use, results in an energy expenditure of $X_i^2$ units. Therefore, at channel use $i$, $E_i$ and $X_i^2$ units of energy enter and leave the energy buffer of the TX, respectively. This is illustrated in Fig. 1.4.

Therefore, the transmitted codeword has to satisfy the following cumulative energy constraints

$$\sum_{i=1}^{k} X_i^2 \leq \sum_{i=1}^{k} E_i, \quad k = 1, \ldots, n. \tag{1.2}$$

The constraints in (1.2) are known as *energy neutrality constraints* or *energy causality constraints*, represent the fact that for each channel use, the total energy consumed can not be more than the energy harvested till that channel use.

For the above problem it is shown that the capacity is equal to that of a classical AWGN channel with an average power constraint $\overline{P}$. This approach has been extended to a zero buffer [13], finite buffer [14], [15], deterministic energy arrivals [16], and multiple access scenarios [17] .

Note that the ergodic capacity results mentioned in this section requires coding over long energy arrival sequences. In some EH processes, for example solar, the harvested energy changes over time scales which are very large compared to the normal communication delay requirements, and hence, these studies do not capture delay-limited rates achievable in such systems.

### 1.3.2 Resource Allocation Problems

Resource allocation problems deal with the intelligent management of energy over EH intervals such that a utility (e.g. throughput in a finite horizon) is optimized. The optimal resource allocation policy then depends on the EH profile and the knowledge available about the EH process. These problems can be classified into two sub groups based on causal and non-causal information about the energy arrivals.

#### A Offline optimization

In the offline optimization framework, resource allocation problems are formulated under the assumption that the involved nodes have non-causal knowledge of the random and time varying parameters such as, energy arrival information, channel state information etc.

The study of offline policies has the following important merits.

- It is suitable for systems in which the EH process is either deterministic or accurately predictable. For example, the harvested solar energy can be accurately predicted depending on the harvesting device characteristics, location, weather data and time of the day.
- Even when the EH process is not predictable, the solution gives a bound on the performance that can be obtained by any schemes that rely only on causal knowledge.
- The optimal solution obtained using the offline framework is independent of the nature of EH profiles. The insight gained from the structure of optimal offline solution can be used to design low complexity heuristic online algorithms.

To obtain a flavor of such problems, we provide some examples.

Consider the problem of throughput maximization by a deadline $T$ seconds in a p2p AWGN channel with an EH TX. The total time duration $T$ is divided into $N$ unit duration time slots (TSs). At the beginning of the $n$-th TS ($n = 1, \ldots, N+1$), denoted by $t_{n-1}$, an energy packet of size $e_{n-1}$ units arrives at the TX. The harvested energy can be stored in an infinite energy buffer. The time frame structure is shown in Fig. 1.5.

The problem of maximizing the number of successful bits transmitted by time $T$ is formulated as

$$\max_{p \geq 0} \int_0^T \log\left(1 + p\left(t\right)\right) dt \;\; \text{s.t} \int_0^{t^{'}} p\left(t\right) \leq E(t^{'}),\; 0 \leq t^{'} \leq T$$

where the cumulative energy $E(t^{'}) = \sum_{i=0}^{k-1} e_i,\; t_{k-1} \leq t^{'} \leq t_k$. A graphical illustration of the optimal power allocation is shown in Fig. 1.5. The energy consumed by any feasible power allocation policy $p\left(t\right)$ should lie below $E\left(t\right)$. This constraint is known as *energy neutrality constraint*, represents the fact that energy consumed cannot be more than the energy harvested till that

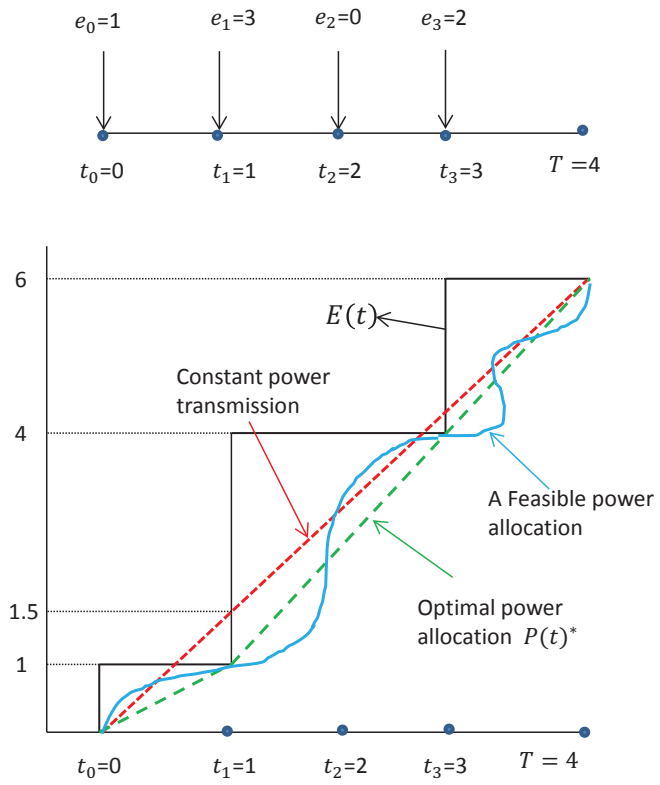


FIGURE 1.5 – Optimal power allocation with time-varying energy arrivals

time. Since the objective is a concave function, using Jensen's inequality it is easy to see that the constant power allocation is desirable, however, it violates the energy neutrality constraint. Therefore, the optimal policy tries to make the power allocation as constant as possible while being under the cumulative energy curve $E(t)$. The solution has the "string tying" interpretation, i.e., can be interpreted as tying a tightest possible string starting from $t_0$ and ending at $T$ while lying below the staircase $E(t)$.

A similar problem in p2p fading channels can be formulated under the assumption of non-causal knowledge of the energy arrivals and the channel gains. The optimization problem is given by :

$$\underset{p_n \geq 0}{\text{maximize}} \quad \sum_{n=1}^{N+1} \log\left(1 + h_n p_n\right) \tag{1.3a}$$

$$\text{s.t.} \quad \sum_{i=1}^{l} L_i p_i \leq \sum_{i=0}^{l-1} e_i, \forall l \in [1 : N+1]. \tag{1.3b}$$

The optimal power allocation of the problem (1.3) is derived in [18]. The solution has a *directional water filling* (DWF) interpretation, and it reduces to the classical water filling algorithm for power allocation in fading channels when there is only single energy arrival at TS $t_0$. The power allocated in the $n$-th TS is given by

$$p_n^* = \left[W_n - \frac{1}{h_n}\right]^+,$$

where $W_n$ represents the water level in TS $n$, and is found by the analysis of the Karush-Kuhn-Tucker (KKT) optimality conditions. A graphical illustration of the solution of DWF is given in Fig. 1.6. The optimal power in each TS is given by the height of the water level. A notable feature of DWF is the *right preamble taps* which allow the flow of water level (Energy) in only the forward direction. This represents the fact that the future energy arrivals cannot be used in current or past time instants.

Recently, a significant number of works have appeared studying the optimal transmission schemes within the offline optimization framework. Optimal transmission schemes are studied for the p2p AWGN channel [19], fading channel [18, 20], broadcast channel [21], [22], [23] and relay channel [24, 25]. Extensions, taking into account the imperfections in battery [23] as well as circuit power consumption [26], [27] are also investigated. An extensive overview can be found in [28].

The above mentioned works focus on optimizing transmission schemes and hence ignore the energy consumption aspects at the RX. The authors in [29] considers the optimization of a p2p communication system with an EH RX. Taking into account the power consumption of analog-to-digital converter (ADC), number of antennas used for reception, resolution of the ADC

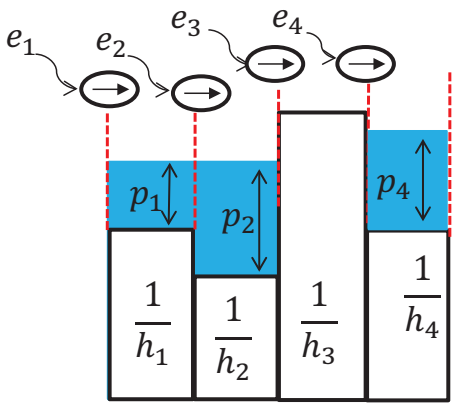


FIGURE 1.6 – DWF with Channel gains
$h_1 = 0.2, h_2 = 0.3, h_3 = 0.01, h_4 = 0.2$, Energy arrivals
$e_1 = 3, e_2 = 3, e_3 = 4, e_4 = 4$.

and the transmission bandwidth is optimized. Using a constant energy expenditure model per successfully received bit, [30] considers the optimization of both transmission and reception policies with EH TX and EH RX.

### B Online optimization

Some EH processes are highly random (e.g. wind), and hence the knowledge about the future energy arrivals is hard to obtain in practice. In this case, the system must make decisions at each time based on the current and past system states and possibly some statistical information about the future energy arrivals. This problem falls into the general category of "sequential decision making under uncertainty". When the statistics of the EH process is known, the study of such problems can be carried out using Markov Decision Processes (MDP) framework [31–33]. The optimal policy consists of a sequence of decision rules that maximizes the expected throughput over a time-horizon. Generally, Dynamic programming (DP) is used to obtain the optimal policies. However, due to the *curse of dimensionality* involved with the DP, i.e., the implementation complexity grows with the number of states involved. Therefore, many low complexity heuristic algorithms are proposed in literature whose performance can be compared with the offline benchmark [18], [20] [34].

When statistics of the EH process are not available, [35] applies Lyapunov optimization and queue stability techniques to obtain the scheduling policies that maximize the time averaged utility in a EH communication network. In [36], the authors introduced "learning theoretic approach", to study a p2p fading channel governed by a Markov processes. The expected throughput is maximized while not assuming any a priori information on the Markov processes.

### 1.3.3 Multi-antenna Systems with Imperfect CSI

It is now well known that channel adaptation and precoding techniques in multi-antenna systems provide large improvements in the throughput [37]. These techniques require some knowledge of the wireless channel conditions also known as CSI at the transmitter (CSIT). In p2p multi-antenna systems, CSIT is used to design transmission schemes such as beamforming, spatial power allocation among the antennas and transmit antenna selection, that provide gains in signal to noise ratio (SNR) and diversity. In contrast to a p2p multi-antenna system where the RX antennas can jointly process the received signal and remove the inter-stream interference when multiple parallel data streams are transmitted, the distributed nature of the RXs makes the joint processing impossible in the multi-user system. If the RXs have limited or single antennas, this leaves the TX with the task of designing precoding filters that removes the inter-user interference. In this scenario, CSIT plays an even more crucial role as it allows the TX to serve multiple RXs in parallel.

Accurate CSIT plays an important role in achieving the throughput gains with the above mentioned transmission strategies. In practice, CSIT is obtained by a limited rate feedback link in a two-way communication systems where the two links operate in different frequency bands, or by estimating the known pilot symbols sent by the RX when the two links operating on the same frequency band in time-sharing fashion. However, in both systems, acquisition of CSIT creates overhead in the communication resources. The works in [38], [39], have considered training and feedback overhead optimization in a p2p multi-antenna channel where feedback is used in designing beamforming vectors at the TX. An extension to the multi-user scenario where interference canceling precoders are used is analyzed in [40]. A common aspect all these works is that the overhead is modeled in terms of the bandwidth i.e., no of channel uses for sending feedback or number of pilot symbols for training, assuming the RXs have constant power supply. In this thesis, we model the overhead not only in terms of the bandwidth but also in the energy consumed as in our case the terminals depend on limited time-varying harvested energy.

## 1.4 Outline of the Dissertation

The main focus of this dissertation is to design intelligent transmission as well as feedback strategies in multi-node and/or multi-antenna communication systems, given the time-varying nature of harvested energy at the nodes. Precisely, we formulate and solve problems within the offline optimization framework that gives the best possible performance bounds independent of the nature of harvesting profiles at the nodes.

An outline of the dissertation along with a brief summary of the contributions of each chapter is provided below.

#### Chapter 2 - Optimization of Point-to-point EH MISO channel

Most prior works in EH communication networks assume that the TX has access to the perfect CSI. However, in practice, the RX needs to send this information either via a feedback channel or by sending pilot symbols, and hence, incurs some cost (especially energy). Therefore, a natural question to ask is

- How do we design the transmission and feedback schemes in an EH communication system if the cost of obtaining CSI is taken into account ?

In this chapter, we address this question in the context of a point-to-point multiple-input single-output (MISO) communication system when both the TX and the RX have EH capabilities. Feedback and transmission schemes that optimize the throughput are devised taking into account the time-varying energy arrivals at the TX and the RX.

Part of the work in this chapter has resulted in the following publications :

- *Rajeev Gangula, David Gesbert, Deniz Gunduz "Optimizing feedback in energy harvesting MISO communication channels", in proc. of IEEE Global Conference on Signal and Information Processing, December 3-5, 2013, Austin, TX, USA.*
- *Rajeev Gangula, David Gesbert, Deniz Gunduz "Optimization of energy harvesting MISO communication system with feedback", IEEE Journal on Selected Areas in Communications, vol.33, no.3, pp.396-406, March 2015.*

#### Chapter 3 - Training Optimization in TDD MISO Broadcast Channels

As pointed out in Section 1.3.3, CSI at the TX plays an even more crucial role in multi-user settings in dealing with inter-user interference. In this chapter, we consider a MISO broadcast channel where a multi-antenna TX serves multiple single antenna EH user terminals. The CSI at the TX is obtained by estimating the channel from the pilot symbols sent by the user

terminals. Training schemes that optimize the throughput are obtained under the constraints of time-varying energy arrivals at the user terminals. The optimal policy turns out to be quite different from single user case considered in the previous chapter.

The contributions of this chapter will be soon submitted for publication :

- *Rajeev Gangula, David Gesbert, Deniz Gunduz "Training optimization for Multiuser MISO Downlink with Energy Harvesting users" To be submitted.*

### Chapter 4 - Distributed Compression and Transmission with Energy Harvesting Sensors

In this chapter, distributed source coding with EH nodes from a rate-distortion perspective is studied. In the considered scenario, two sensor nodes observe correlated source samples, and wish to communicate their samples to the destination with the minimum average end-to-end distortion. The goal is to see how the correlation and the EH constraints affect the coordination among the nodes in compression and transmission schemes.

The work in this chapter has resulted in the following publication :

- *Rajeev Gangula, Deniz Gunduz, David Gesbert "Distributed compression and transmission with energy harvesting sensors", in Proc. of IEEE ISIT, Hong Kong, 2015.*

### Chapter 5 - Harvesting and Compression of Information from an Ambient Energy Source

In a traditional EH sensor node, energy harvested from the environment is used to sample, process and send information about a physical phenomenon in its surrounding environment. In some scenarios, the ambient energy source from which the sensor harvests energy and the information source from which the sensor collects samples are the same. For example, a sensor node wishes to send information about the intensity of the solar irradiation in its surroundings, and at the same time depends on the energy harvested from it. In this chapter, we come up with some practical schemes that efficiently utilizes the electrical signal generated from the ambient energy/information source for both communication and harvesting purposes. The aim is to communicate the source to a destination with minimum average end-to-end distortion while using the harvested energy from the same source. We also investigate the situation where the sensor has two energy supplies, one from traditional limited energy in the battery, and the other form harvest energy from the source itself. In this case, we design schemes that intelligently use both the traditional and the harvested energy, so as to satisfy some QoS constraints on the average distortion while minimizing the usage of traditional limited energy.

### Chapter 6

Finally, this chapter concludes the dissertation and points out some possible future research problems.

### Other research contributions

Some of the work not dealing with EH systems performed during this PhD thesis has not been included in this dissertation ; however, the results have been published in the following :

- *R. Gangula, D. Gesbert, J. Lindblom, E.G., Larsson " On the value of spectrum sharing among operators in Multicell networks", in proc. of IEEE Vehicular Technology Conference, Dresden, June 2013.*

# Chapter 2

# Optimization of p2p EH MISO Communication Channels

## 2.1 Introduction

To the best of our knowledge, a common aspect of most prior works dealing with resource allocation problems in EH communication networks is that the transmitter (TX) is provided with perfect channel state information (CSI). Knowledge of the CSI at the TX is beneficial in designing the optimal channel adaptation techniques and the TX filters in multi-antenna systems. However, in practice, the TX obtains this information either via a feedback channel where the receiver (RX) sends quantized CSI bits or by estimating the channel from the pilot symbols sent by the RX. Recent studies have demonstrated that, although feedback enhances the system performance, feedback resources, namely power and bandwidth, are limited, and must be spent wisely [41]. As a result, an important question arises : How do the EH constraints affect the design of feedback enabled wireless networks ?

In this chapter, optimization of a feedback enabled EH MISO channel, where feedback is used to improve the rate through array gain is studied. Using different feedback models, throughput optimization problems are formulated under the EH constraints at the TX and RX. We try to address the following questions : In the case of EH, the available energy at the RX varies over time. Should the RX allocate resources such that same quality of CSI is maintained at the TX at all times ? If so, can the CSI quality be improved by using more bandwidth when the RX has less harvested energy ? When both the TX and the RX harvest energy, how the transmission power policy and the feedback policy are coupled ?

The main contributions of the chapter are the following :

- Introducing for the first time energy harvesting constraints in a feedback enabled MISO fading channel.
- Using offline optimization framework, upper bounds lower bounds on the ergodic rate under the EH constraints are obtained.
- Tools from majorization theory are used in devising simple algorithms to solve the formulated optimization problems.

We start by giving a brief preliminary description of majorization theory in Section 2.2. In the following section, feedback/training schemes are optimized under EH constraints at the RX, while the TX is assumed to have a constant power supply. Section 2.5 considers the case when both TX and RX harvest energy. Numerical results validating the analysis are provided in Section 2.6.

## 2.2 Preliminaries

In this section, the basic notion of majorization is introduced and some important inequalities on convex functions that are used in this work are stated. The readers are referred to [42], [43] for a complete reference. We start by stating the Edmundson-Madansky's inequality.

**Theorem 1.** *[42] If $f$ is a convex function and $x$ is a random variable with values in an interval $[a, b]$, then*

$$\mathrm{E}\left[f\left(x\right)\right] \leq \frac{b-\mu}{b-a} f\left(a\right) + \frac{\mu-a}{b-a} f\left(b\right),$$

*where $\mu = \mathrm{E}\left[x\right]$.*

Let $\boldsymbol{x} = [x_1, \ldots, x_n]$ and $\boldsymbol{y} = [y_1, \ldots, y_n]$, be two vectors and $\boldsymbol{x}, \boldsymbol{y} \in \mathbb{R}^n$. Majorization theory formalizes the notion that the components of a vector $\boldsymbol{x}$ are "less spread out" than the components of a vector $\boldsymbol{y}$.

**Definition 1.** *Let $x_{(i)}$ denote the $i$-th largest component of $\boldsymbol{x}$. Then $\boldsymbol{x}$ is said to be majorized by $\boldsymbol{y}$, denoted by $\boldsymbol{x} \preceq \boldsymbol{y}$, if*

$$\sum_{i=1}^{l} x_{(i)} \leq \sum_{i=1}^{l} y_{(i)}, \qquad \forall l \in [1 : n-1]$$
$$\sum_{i=1}^{n} x_{(i)} = \sum_{i=1}^{n} y_{(i)}.$$

**Definition 2.** *[43, 2.A.1] An $n \times n$ matrix $\mathbf{D}$ with elements $d_{i,j}$ is doubly stochastic if*

$$d_{i,j} \geq 0, \qquad \forall i, j \in [1 : n],$$
$$\sum_{i=1}^{n} d_{i,j} = 1, \ \forall j \in [1 : n] \ \text{ and } \ \sum_{j=1}^{n} d_{i,j} = 1, \ \forall i \in [1 : n].$$

**Theorem 2.** *[43, 4.A.1, 4.B.1] For $\boldsymbol{x}, \boldsymbol{y} \in \mathbb{R}^n$, the following conditions are equivalent :*

- $\boldsymbol{x} \preceq \boldsymbol{y}$.
- $\boldsymbol{x} = \boldsymbol{y}\mathbf{D}$ *for some doubly stochastic matrix* $\mathbf{D}$.
- *For all continuous concave functions* $g : \mathbb{R} \to \mathbb{R}$, $\sum_{i=1}^{n} g(x_i) \geq \sum_{i=1}^{n} g(y_i)$.

**Definition 3.** *[43, 15.A.2] Let* $\mathbf{X}$ *and* $\mathbf{Y}$ *be* $m \times n$ *real matrices. Then* $\mathbf{X}$ *is said to be majorized by* $\mathbf{Y}$*, written* $\mathbf{X} \preceq \mathbf{Y}$*, if* $\mathbf{X} = \mathbf{YD}$*, where the* $n \times n$ *matrix* $\mathbf{D}$ *is doubly stochastic.*

**Theorem 3.** *[43, 15.A.4] Let* $\mathbf{X}$ *and* $\mathbf{Y}$ *be* $m \times n$ *real matrices. Then,* $\mathbf{X} \preceq \mathbf{Y}$ *if and only if*

$$\sum_{i=1}^{n} g(\boldsymbol{x}_i^c) \geq \sum_{i=1}^{n} g(\boldsymbol{y}_i^c),$$

*for all continuous concave functions* $g : \mathbb{R}^m \to \mathbb{R}$*; here* $\boldsymbol{x}_i^c$ *and* $\boldsymbol{y}_i^c$ *denote the* $i$*-th column vector of* $\mathbf{X}$ *and* $\mathbf{Y}$*, respectively.*

## 2.3 System model

We consider a p2p MISO fading channel as shown in Fig. 2.1, where both the TX and the RX harvest energy from the environment. Each node is equipped with an individual energy buffer, i.e., a rechargeable battery, that can store the locally harvested energy.

### 2.3.1 Energy Harvesting Model

The total observation time is divided into $K$ equal length EH intervals. At the beginning of the $k$-th EH interval, $k \in [1 : K]$, energy packets of size $e_k^t, e_k^r$ units arrive at the TX and the RX, respectively. At each node, this energy is first stored in an infinite size energy buffer, and used only for communication purposes. We assume that all $e_k^t, e_k^r$'s are known in advance by both terminals i.e., we formulate the problem within the offline optimization framework.

### 2.3.2 Communication System Model

A bidirectional communication link between the TX and RX is considered in which the downlink (DL) and the uplink (UL) takes place in the same frequency band. Each EH interval consists of $L$ data frames, each of length $T$ channel uses. We assume a block fading channel model. The channel is constant during $T$ channel uses of each frame, but changes in an independent and identically distributed (i.i.d.) fashion from one frame to another. The time frame structure is shown in Fig. 2.2. The TX has $M > 1$ antennas,

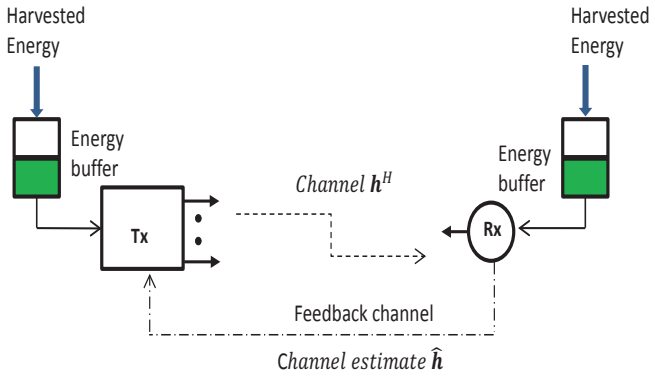


FIGURE 2.1 – MISO channel with EH nodes.

while the RX has a single antenna. The received signal in the DL on a given channel use is given by

$$y = \boldsymbol{h}^{\mathrm{H}}\boldsymbol{w}s + \eta, \tag{2.1}$$

where $\boldsymbol{h} \in \mathbb{C}^{M\times 1}$ represents the vector of channel coefficients from TX to the RX with i.i.d. $\mathcal{CN}(0,1)$ elements, $\boldsymbol{w} \in \mathbb{C}^{M\times 1}$ denotes the beamforming vector, the input symbol maximizing the achievable ergodic rate in the $k$-th EH interval is $s \sim \mathcal{CN}(0, p_k^t)$, and $\eta \sim \mathcal{CN}(0,1)$ represents the noise at the RX.

### 2.3.3 Feedback Models

We consider two models for the acquisition of CSI at the TX. In a time-division-duplex (TDD) system with perfectly calibrated devices, UL and DL channels are reciprocal, and therefore DL channel can be estimated using the pilot symbols sent by the RX in the UL. When the devices are not self-calibrated, the UL and DL channel are no more reciprocal. In this case, the RX has to quantize the DL channel state and send this information to the TX via a feedback channel [39], [40]. In all cases, perfect CSI is assumed at the terminals where information is decoded.

#### A TDD system with non self-calibrated devices

We assume that the RX perfectly estimates the channel state at the beginning of each data frame, and feeds back the quantized CSI to the TX

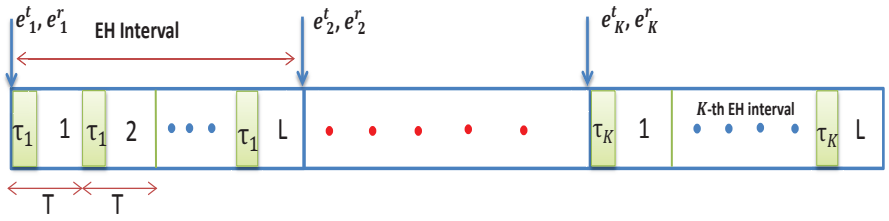


FIGURE 2.2 – Energy harvesting time frame structure.

within the same frame. In the $k$-th EH interval, the frame structure is as follows : The RX in $\tau_k$ channel uses sends the CSI in the UL, and in the remaining $T-\tau_k$ channel uses, TX sends data to the RX in the DL exploiting the obtained CSI. In this work we model it as an additive white Gaussian noise (AWGN) channel, which captures the essential behavior of feedback with EH constraints.

In the $k$-th EH interval, quantization of the channel state is performed using a codebook $\mathcal{C}_k$ known at both the TX and RX. The receiver uses Random Vector Quantization (RVQ). The codebook consists of $M$-dimensional unit vectors $\mathcal{C}_k \triangleq \left\{\boldsymbol{f}_1, \ldots, \boldsymbol{f}_{2^{b_k}}\right\}$, where $b_k$ is the number of bits used for quantization. The RX chooses the beamforming vector according to $\boldsymbol{w}_k = \arg\max_{\boldsymbol{f}\in\mathcal{C}_k} |\tilde{\boldsymbol{h}}^{\mathrm{H}}\boldsymbol{f}|^2$, where $\tilde{\boldsymbol{h}} \triangleq \frac{\boldsymbol{h}}{||\boldsymbol{h}||}$. We assume that the length of the EH interval is very large compared to the channel coherence time (i.e., $L$ is very large). As a result, the achievable ergodic rate in the $k$-th EH interval is given by

$$R_k = \left(1 - \frac{\tau_k}{T}\right) \mathrm{E}_{||\boldsymbol{h}||^2,\nu_k}\left[\log_2\left(1 + \frac{p_k^t}{\left(1-\frac{\tau_k}{T}\right)}\|\boldsymbol{h}\|^2 \nu_k\right)\right], \tag{2.2}$$

where $\nu_k = |\tilde{\boldsymbol{h}}^{\mathrm{H}}\boldsymbol{w}_k|^2$. Note that $\nu_k$ and $||\boldsymbol{h}||^2$ are independent [44], and $\nu_k$ depends on the number of bits used for quantization $b_k$.

By using the AWGN feedback channel model, the number of feedback bits $b_k$ can be related to the power used by the RX, $p_k^r$, and the number of

channel uses $\tau_k$ as follows :

$$b_k = \tau_k \log_2 \left(1 + \frac{p_k^r}{\sigma^2}\right), \tag{2.3}$$

where $\sigma^2$ is the noise variance in the uplink.

### B TDD system with self-calibrated devices

In this scenario, since UL and DL channels are reciprocal, TX estimates the DL channel by using the known pilot (training) symbols sent by the RX. The RX sends $\tau_k$ pilot symbols with an average power $p_k^r$ in the UL. On a given channel use in the $k$-th EH interval, we model the channel as [45], [46]

$$\boldsymbol{h} = \sqrt{1-\delta_k^2}\hat{\boldsymbol{h}} + \sqrt{\delta_k^2}\boldsymbol{e}, \tag{2.4}$$

where $\hat{\boldsymbol{h}}$ is the channel estimate and is independent of the error vector $\boldsymbol{e}$. The elements of $\hat{\boldsymbol{h}}$, $\boldsymbol{e}$ are i.i.d. with $\mathcal{CN}(0,1)$. Assuming minimum mean square error (MMSE) estimation, the estimation error variance is [46]

$$\delta_k^2 = \frac{1}{1 + p_k^r \tau_k / \sigma^2}, \tag{2.5}$$

where $\sigma^2$ is the noise variance in the UL. We assume that the length of the EH interval is very large compared to the channel coherence time (i.e., $L$ is very large). As a result, the achievable ergodic rate in the $k$-th EH interval is given by

$$R_k = \left(1 - \frac{\tau_k}{T}\right) \mathrm{E}_{\hat{\boldsymbol{h}},\boldsymbol{e}} \log_2 \left(1 + \frac{p_k^t}{\left(1 - \frac{\tau_k}{T}\right)} \left| \boldsymbol{h}^{\mathrm{H}} \frac{\hat{\boldsymbol{h}}}{||\hat{\boldsymbol{h}}||} \right|^2 \right) \tag{2.6}$$

### 2.3.4 Optimization Problem

Using the above mentioned feedback models, for each model, the problem of maximizing the sum throughput by the end of the $K$-th EH interval can be formulated as

$$\max_{p_k^t, p_k^r, \tau_k} \quad \sum_{k=1}^{K} R_k \tag{2.7a}$$

$$\text{s.t.} \quad L \sum_{i=1}^{l} \tau_i p_i^r \leq \sum_{i=1}^{l} e_i^r, \ \forall l \in [1:K], \tag{2.7b}$$

$$LT \sum_{i=1}^{l} p_i^t \leq \sum_{i=1}^{l} e_i^t, \ \forall l \in [1:K], \tag{2.7c}$$

$$\tau_k \in [0, T), \ \tau_k \in \mathbb{N}, \ p_k^t \geq 0, \ \text{and} \ p_k^r \geq 0, \forall k \in [1:K]. \tag{2.7d}$$

The constraints (2.7b) and (2.7c) guarantee the *energy neutrality* of the system, i.e., at each node, energy consumed can not be more than the energy harvested till that time. Also note that $\tau_k$ impacts the achievable rate $R_k$ in each EH interval.

Before tackling the above problem, first, we consider a special case in which only the RX harvests energy. Later, the general case with both the TX and the RX harvesting energy is studied.

## 2.4 EH Receiver

In this setting, the RX harvests energy from the environment, whereas the TX is connected to the power grid so that it has a fixed power supply at all times. Therefore, there are no EH constraints at the TX, and constraints (2.7c) can be ignored. However, there is now a constraint on the average transmission power at each data frame of the $k$-th EH interval i.e., $p_k^t \leq p, \forall k$. We start with the feedback model where UL and DL channel are not identical.

### 2.4.1 Non-reciprocal channels

For the case of non-reciprocal channels, the ergodic rate expression in (2.2) is used as the objective function in the optimization problem (2.7). Note that the optimization problem is non-convex due to the constraints in (2.7b). We perform a change of variables with $q_k \triangleq \tau_k p_k^r, \ \forall k$ to make the constraints in (2.7b) linear. Now the number of feedback bits $b_k$ can be related to the energy used by the RX, $q_k$, and the number of channel uses $\tau_k$ as follows :

$$b_k = \tau_k \log_2 \left(1 + \frac{q_k}{\tau_k \sigma^2}\right), \tag{2.8}$$

For analytical tractability, we neglect the practical constraint that $\tau_k$ and $b_k$ should be integers. Using the ergodic rate expression given in [44, Equation (27)] and (2.8), the ergodic rate $R_k \triangleq R\left(p_k^t, q_k, \tau_k\right)$ is found to be

$$\begin{aligned} R_k = \left(1 - \frac{\tau_k}{T}\right) \log_2 e \Bigg( & e^{\rho_k} \sum_{l=0}^{M-1} E_{l+1}\left(\rho_k\right) - \\ & \int_{\nu_k=0}^{1} \left(1 - \left(1-\nu_k\right)^{M-1}\right)^{N_k} \frac{M}{\nu_k} e^{\left(\frac{\rho_k}{\nu_k}\right)} E_{M+1}\left(\frac{\rho_k}{\nu_k}\right) d\nu_k \Bigg) \end{aligned} \tag{2.9}$$

where $\rho_k = \left(\frac{1-\frac{\tau_k}{T}}{p_k^t}\right)$, $N_k = \left(1 + \frac{q_k}{\tau_k \sigma^2}\right)^{\tau_k}$, and $E_n\left(x\right) \triangleq \int_1^\infty e^{-xt} x^{-n} dt$ is the $n$-th order exponential integral.

Coming up with simple algorithms to solve the optimization problem is desirable in EH networks as the nodes may not have the computational and

energy resources for running complex optimization algorithms. However, the ergodic rate expression to be used in the optimization problem is not in closed form and offers little insight into the convexity of the problem which is required to reduce the complexity of optimization. This motivates the use of convex bounds on (2.9) as the objective function in the following optimization problems. Solving these modified problems provides an upper bound on the throughput. Since the constraints in the original and the modified optimization problems are the same, the solution for the modified problem is also feasible in the original problem, and if used in evaluating the exact rate expression in (2.9), we obtain a lower bound on the throughput. In some settings, we show that the bounds used are very close to the ergodic rate.

Applying Jensen's inequality on (2.2) we obtain,

$$R_k \leq \left(1 - \frac{\tau_k}{T}\right) \log_2 \left(1 + \frac{p_k^t}{\left(1 - \frac{\tau_k}{T}\right)} M \, \mathrm{E}[\nu_k]\right). \tag{2.10}$$

The expected value $\nu_k$ is given by [44], [47]

$$\mathrm{E}[\nu_k] = 1 - 2^{b_k} \beta\left(2^{b_k}, \frac{M}{M-1}\right), \tag{2.11}$$

where $\beta(x, y)$ denotes the beta function. Using the quantization error bound in [47, Lemma 6], (2.11) can be bounded as [1]

$$\mathrm{E}[\nu_k] \leq \nu_k^u \triangleq 1 - \left(\frac{M-1}{M}\right) 2^{\frac{-b_k}{M-1}}. \tag{2.12}$$

Using (2.12) and (2.10), an upper bound on the ergodic rate $R_k^u \triangleq R^u\left(p_k^t, q_k, \tau_k\right)$ is obtained as

$$R_k^u = t_k \log_2 \left[1 + \frac{p_k^t M}{t_k} \left(1 - \frac{M-1}{M} \left(1 + \frac{q_k}{\tau_k \sigma^2}\right)^{\frac{-\tau_k}{M-1}}\right)\right], \tag{2.13}$$

where $t_k \triangleq \left(1 - \frac{\tau_k}{T}\right)$.

We now illustrate the tightness of the upper bound. Applying the Jensen's inequality on (2.2), $R_k^u - R_k$ can be lower bounded as

$$\begin{aligned} R_k^u - R_k \geq t_k \log_2 \left(1 + \frac{p_k^t}{t_k} M \nu_k^u\right) - \\ t_k \, \mathrm{E}_{||\boldsymbol{h}||^2} \log_2 \left(1 + \frac{p_k^t}{t_k} \left\|\boldsymbol{h}\right\|^2 \mathrm{E}[\nu_k]\right). \end{aligned} \tag{2.14}$$

1. This bound is universal in the sense that it applies to any $b_k$-bit quantization of an isotropically distributed vector, not necessarily limited to RVQ.

Since (2.2) is a concave function of $\nu_k$ and $\nu_k \in [0,1]$, applying Theorem 1 on (2.2), we have

$$R_k \geq t_k \, \mathrm{E}_{||\boldsymbol{h}||^2} \log_2 \left(1 + \frac{p_k^t}{t_k} \|\boldsymbol{h}\|^2\right) \mathrm{E}[\nu_k] \tag{2.15}$$

Now using (2.15), $R_k^u - R_k$ can be upper bounded as

$$\begin{aligned} R_k^u - R_k \leq t_k \log_2 \left(1 + \frac{p_k^t}{t_k} M \nu_k^u\right) - \\ t_k \, \mathrm{E}_{||\boldsymbol{h}||^2} \log_2 \left(1 + \frac{p_k^t}{t_k} \|\boldsymbol{h}\|^2\right) \mathrm{E}[\nu_k] \end{aligned} \tag{2.16}$$

Since both $\lim_{b_k \to \infty} \nu_k^u = 1$ and $\lim_{b_k \to \infty} \mathrm{E}[\nu_k] = 1$ [44], and using (2.14) and (2.16), we have,

$$\Delta R_k \triangleq \lim_{b_k \to \infty} R_k^u - R_k = t_k \, \mathrm{E}_{||\boldsymbol{h}||^2} \log_2 \left(\frac{t_k + p_k^t M}{t_k + p_k^t \|\boldsymbol{h}\|^2}\right). \tag{2.17}$$

Further, for all feasible $\tau_k$, in the low power regime,

$$\lim_{p_k^t \to 0} \Delta R_k = 0, \tag{2.18}$$

and in the high power regime,

$$\begin{aligned} \lim_{p_k^t \to \infty} \Delta R_k &= t_k \left(\log_2 M - \mathrm{E}_{||\boldsymbol{h}||^2} \log_2 ||\boldsymbol{h}||^2\right) \\ &\leq \log_2 M - \mathrm{E}_{||\boldsymbol{h}||^2} \log_2 ||\boldsymbol{h}||^2. \end{aligned} \tag{2.19}$$

From the above analysis, it can be seen that when the RX has enough harvested energy to send large number of feedback bits, in the low power regime the bound is tight, and in the high power regime the difference is bounded by a constant. For example, it is 0.1958 for $M = 4$, and also note that $\lim_{M \to \infty} \log_2 M - \mathrm{E}_{||\boldsymbol{h}||^2} \log_2 ||\boldsymbol{h}||^2 = 0$.

Using (2.13) as the objective function, the modified optimization problem can be written as follows,

$$\max_{p_k^t, q_k, \tau_k} \quad \mathfrak{U} = \sum_{k=1}^{K} R_k^u \tag{2.20a}$$

$$\text{s.t.} \quad L \sum_{i=1}^{l} q_i \leq \sum_{i=1}^{l} e_i^r, \forall l \in [1:K], \tag{2.20b}$$

$$p_k^t \leq p, \quad \text{and } p_k^t \geq 0, \ \forall k \in [1:K], \tag{2.20c}$$

$$\tau_k \in [0, T), \quad \text{and} \quad q_k \geq 0, \quad \forall k \in [1:K], \tag{2.20d}$$

where $p$ is the power constraint at the transmitter.

As the objective function is monotonic in $q_k$ and $p_k^t$, the constraint in (2.20b) must be satisfied with equality for $l = K$, and the first constraint in (2.20c) must be satisfied with equality, i.e., $p_k^t = p, \forall k$, otherwise, we can always increase $q_K, p_k^t$, and hence, the objective function, without violating any constraints. Now it remains to optimize over the variables $q_k$ and $\tau_k$.

The feasible set is represented as

$$\mathfrak{F} = \{\boldsymbol{q}, \boldsymbol{\tau} | q_k, \tau_k \text{ satisfy (2.20b), (2.20d) } \forall k\}, \tag{2.21}$$

where $\boldsymbol{q} = [q_1, \ldots, q_K]$ and $\boldsymbol{\tau} = [\tau_1, \ldots, \tau_K]$. To show that the above problem is a convex optimization problem, we make use of the following lemma.

**Lemma 1.** *If the function $f(x,t) : \mathbb{R}_+^2 \to \mathbb{R}_+$ is concave, and $g(y,z) : \mathbb{R}_+^2 \to \mathbb{R}_+$ is concave and monotonically increasing in each argument, then the function $h(x,y,t) = \left(1 - \frac{t}{T}\right) g\left(\frac{y}{1-\frac{t}{T}}, \frac{f(x,t)}{1-\frac{t}{T}}\right)$ is concave $\forall (x,y) \in \mathbb{R}_+^2, t \in [0,T)$.*

*Proof.* The proof is similar to that of showing the perspective of a concave function is concave. See Appendix. □

**Proposition 1.** *The objective function of the optimization problem (2.20) is concave.*

*Proof.* See Appendix. □

Since the objective function in (2.20) is concave and the constraints are linear, it has a unique maximizer [48]. Using the concavity of the objective function, we show that the optimal energy allocation vector is the most majorized feasible energy vector.

**Proposition 2.** *The global optimum of (2.20) is obtained at $(\boldsymbol{q}^*, \boldsymbol{\tau}^*)$, where $\boldsymbol{q}^* \preceq \boldsymbol{q}, \forall (\boldsymbol{q}, \boldsymbol{\tau}) \in \mathfrak{F}$, and $\tau_k^*$ is the solution of the following equation*

$$\frac{\partial R_k^u}{\partial \tau_k}|_{(q_k^*, \tau_k^*)} = 0, \ \forall k \in [1:K]. \tag{2.22}$$

*Proof.* Consider the following equivalent form of (2.20), where the optimization is performed in two steps.

$$\max_{\boldsymbol{q}} \tilde{\mathcal{U}}(\boldsymbol{q}) \ \text{ s.t. } \forall (\boldsymbol{q}, \boldsymbol{\tau}) \in \mathfrak{F}, \tag{2.23}$$

where $\tilde{\mathcal{U}}(\boldsymbol{q})$ is obtained by

$$\tilde{\mathcal{U}}(\boldsymbol{q}) = \max_{\boldsymbol{\tau}} \mathcal{U}(\boldsymbol{q}, \boldsymbol{\tau}) \ \text{ s.t. } \forall (\boldsymbol{q}, \boldsymbol{\tau}) \in \mathfrak{F}. \tag{2.24}$$

Since $\mathcal{U}$ is a concave function over the convex set $\mathfrak{F}$, the function $\tilde{\mathcal{U}}(\boldsymbol{q})$ is concave, where the domain of $\tilde{\mathcal{U}}$ is the set $\tilde{\mathfrak{F}} = \{\boldsymbol{q} | (\boldsymbol{q}, \boldsymbol{\tau}) \in \mathfrak{F}\}$ [48, 3.2.5].

$\mathcal{U} = \sum_{k=1}^{K} R_k^u$ is continuous, differentiable and concave in $\tau_k \in [0, T)$. Furthermore, for given $q_k$, $R_k^u$ approaches $\log_2(1+p)$ and 0, as $\tau_k$ approaches 0 and $T$, respectively. Therefore, the unique maximizer of (2.24) lies in $[0, T)$, and it is obtained at

$$\frac{\partial \mathcal{U}}{\partial \tau_k}|_{\tau_k^*} = \frac{\partial R_k^u}{\partial \tau_k}|_{\tau_k^*} = 0, \ \forall k \in [1:K]. \tag{2.25}$$

From above, as $\tau_k^*$ is only a function of $q_k$,

$$\tilde{\mathcal{U}}(\boldsymbol{q}) = \sum_{k=1}^{K} \tilde{R}_k^u \tag{2.26}$$

where $\tilde{R}_k^u \triangleq \tilde{R}^u(q_k) = R^u(q_k, \tau_k^*(q_k))$. Using (2.26) and Theorem 2, $\tilde{\mathcal{U}}(\boldsymbol{q}^*) \geq \tilde{\mathcal{U}}(\boldsymbol{q}), \forall \boldsymbol{q} \in \tilde{\mathfrak{F}}$. Finding the optimal energy allocation vector $\boldsymbol{q}^*$ under the EH constraints turns out be a well known problem, and the algorithm to construct $\boldsymbol{q}^*$ is given in various works [12], [20] and [49, 50]. The proof that the algorithm constructs the most majorized feasible energy vector is given in [12]. Since the optimal energy allocation vector is $\boldsymbol{q}^*$, the optimal $\boldsymbol{\tau}^*$ is obtained by (2.22). □

A brief description of the algorithm tailored to this work is given next, while the details can be found in [12], [20] and [49,50]. There is no closed form expression for the solution of (2.22), hence we resort to numerical methods to obtain $\boldsymbol{\tau}^*$. Fig. 2.3 shows the behavior of $\tau_k^*$ as a function of the allocated energy $q_k^*$. From Fig. 2.3 we can see that, in each interval, the optimal number of channel uses for sending feedback is an increasing function of the energy allocated for sending feedback up to a threshold and after the threshold it becomes a decreasing function.

### A Optimal Energy Allocation

From Definition 1, we can see that the components of the most majorized energy vector are "less spread out" than any other feasible energy vector. Therefore, the algorithm essentially try to make the energy vector as equalized as possible. This is done by spreading the energy to future intervals, however, note that energy arriving in later intervals cannot be spread to earlier intervals due to the EH constraints. The Optimal Energy Allocation (OEA) algorithm, given in Algorithm 1, divides the EH intervals into $|\mathcal{S}|$ energy bands whose indices form the set $\mathcal{S} = \{B_0, B_1, \dots B_{|\mathcal{S}|}\}$, where $B_i < B_j, \forall i < j$, $B_0 = 0$, and $B_{|\mathcal{S}|} = K$. The $i$-th energy band contains the EH intervals with indices $k \in [B_{i-1}+1 : B_i]$. Moreover, the optimal allocated energy values in each EH interval belonging to the $i$-th energy band are equal, and denoted by $q_{(i)}^*$. The energy vector $\boldsymbol{q}^*$ obtained by $[\boldsymbol{q}^*, \mathcal{S}_r] = \text{OEA}(K, \{e_i^r/L\})$, has the following properties :

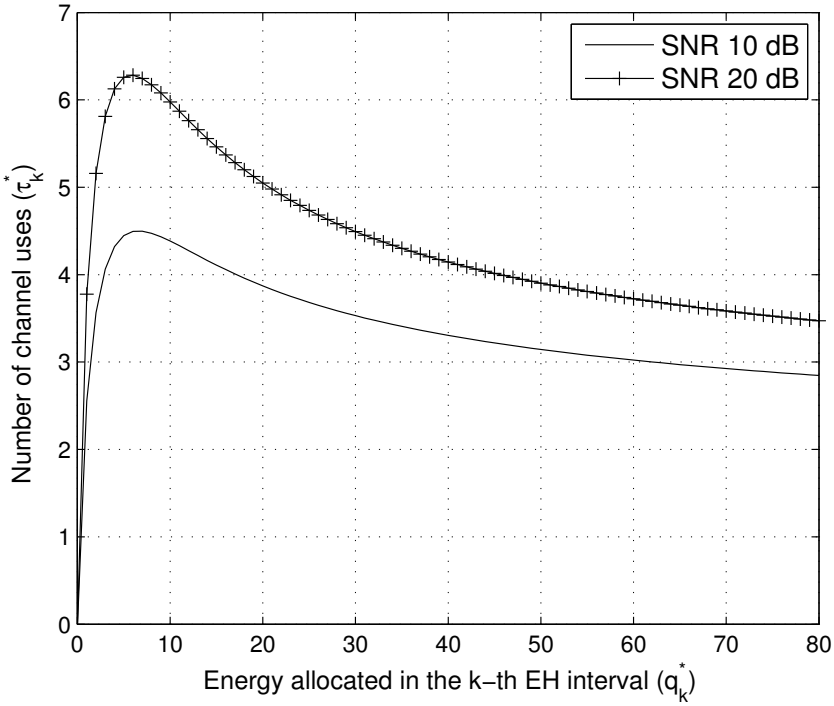


FIGURE 2.3 – Optimal number of channel uses for sending feedback.

(P1) $q_k^* = q_{(i)}^* = \frac{\sum_{l=B_{i-1}+1}^{B_i} e_l^r}{L(B_i - B_{i-1})},\ \forall k \in [B_{i-1}+1 : B_i]$.
(P2) The entries $q_{(i)}^*$ are strictly monotonic, i.e., $q_{(1)}^* < q_{(2)}^* < ... < q_{(|\mathcal{S}|)}^*$.

**Input** : EH intervals $K$ ; Harvested energy $\{e_i\}$
**Output**: Energy allocation $\boldsymbol{o}^\star$, Energy band indices $\mathcal{S} = \{B_0, B_1, \dots B_{|\mathcal{S}|}\}$

```
// initialization
```
$B_0 := 0$;

**for** $i = 1 : K$ **do**
  **for** $k = K : -1 : (B_{i-1}+1)$ **do**
    (i) $o_l^\star = \frac{\sum_{j=B_{i-1}+1}^{k} e_j}{k - B_{i-1}},\ l \in \{B_{i-1}+1, \dots, k\}$
    **if** $\sum_{i=1}^{l} o_i^\star \le \sum_{i=1}^{l} e_i, l = 1, ..., K$ **then**
      $B_i = k$ ;
      Save $\{o_1^\star, \cdots, o_k^\star\}$
      **break** ;
    **end**
  **end**
  **if** $B_i == K$ **then**
    **break** ;
  **end**
**end**

**Algorithm 1:** Optimal Energy Allocation (OEA) algorithm

### 2.4.2 Reciprocal channels

Following the similar approach as in the non-reciprocal case, we use an upper bound on the ergodic rate expression in (2.6) as the objective for the throughput maximization problem. Applying Jensen's inequality on (2.6) and then substituting (2.5), an upper bound on the ergodic rate $R_k^u \triangleq R^u\left(p_k^t, p_k^r, \tau_k\right)$ is given by

$$\begin{aligned} R_k^u &= \left(1 - \frac{\tau_k}{T}\right) \log_2 \left[1 + \frac{p_k^t}{\left(1 - \frac{\tau_k}{T}\right)} \mathrm{E}_{\hat{\boldsymbol{h}}, \boldsymbol{e}} \left( \left| \boldsymbol{h}^{\mathrm{H}} \frac{\hat{\boldsymbol{h}}}{||\hat{\boldsymbol{h}}||} \right|^2 \right) \right] \\ &\overset{(a)}{=} \left(1 - \frac{\tau_k}{T}\right) \log_2 \left[1 + \frac{p_k^t}{\left(1 - \frac{\tau_k}{T}\right)} \left( M - (M-1) \frac{1}{(1 + p_k^r \tau_k / \sigma^2)} \right) \right], \end{aligned} \tag{2.27}$$

where

(a) follows by using (2.4) and (2.5), and from the fact that $\boldsymbol{e}$ and $\hat{\boldsymbol{h}}$ are independent with zero mean.

Using (2.27) as the objective function, the modified optimization problem can be written as follows :

$$\max_{p_k^t, p_k^r, \tau_k} \quad \mathcal{U} = \sum_{k=1}^{K} R_k^u \tag{2.28a}$$

$$\text{s.t.} \quad L \sum_{i=1}^{l} \tau_i p_i^r \leq \sum_{i=1}^{l} e_i^r, \forall l \in [1:K], \tag{2.28b}$$

$$0 \leq p_k^t \leq p, \quad \text{and } p_k^r \geq 0, \ \forall k \in [1:K], \tag{2.28c}$$

$$\tau_k \in [0, T) \ \text{ and } \tau_k \in \mathbb{N} \ \ \forall k \in [1:K], \tag{2.28d}$$

where $p$ is the power constraint at the transmitter.

The above problem is non-convex since the objective function is not a concave function and the constraints in (2.28b), (2.28d) are not convex. However, using the following remarks we can simplify the optimization problem.

**Remark 1.** *Since the objective function in (2.28) is monotonically increasing in the transmission power, $p_k^t$, for the optimal solution $p_k^t = p, \forall k$.*

**Remark 2.** *Note that the estimation error in the k-th EH interval, $\delta_k^2$ in (2.5), depends only on the energy used for sending pilot symbols $q_k = \tau_k p_k^r$. Since $R_k^u$ is a monotonically decreasing function of $\tau_k$ given $q_k$ is fixed, and the estimation error depends only on $q_k$, and from the fact that the constraints in (2.28b) also only depend on $q_k$, we can see that any value $\tau_k$ such that $\tau_k > 1$ is not optimal. Therefore, the optimal number of pilot symbols $\tau_k^*$ can take only the values in the set $\{0, 1\}$.*

Using the above remarks, we have

$$\max_{\tau_k} R_k^u = \max_{\tau_k \in \{0,1\}} R_k^u = \max\left\{\log_2(1+p), R^u(p, q_k)\right\}, \tag{2.29}$$

where

$$R^u(p, q_k) = \left(1 - \frac{1}{T}\right) \log_2 \left[1 + \frac{p}{\left(1 - \frac{1}{T}\right)} \left(M - (M-1)\frac{1}{(1 + q_k/\sigma^2)}\right)\right], \tag{2.30}$$

and $q_k = \tau_k p_k^r$. Now the optimization problem in (2.28) can be simplified to

$$\max_{q_k} \quad \sum_{k=1}^{K} \max\left\{\log_2(1+p), R^u(p, q_k)\right\}, \tag{2.31a}$$

$$\text{s.t.} \quad L \sum_{i=1}^{l} q_i \leq \sum_{i=1}^{l} e_i^r, \forall l \in [1:K], \tag{2.31b}$$

$$q_k \geq 0, \ \forall k \in [1:K]. \tag{2.31c}$$

It can be easily verified that the function $R^u(p, q_k)$ is concave in $q_k$, however, the objective function is not concave (in fact quasi concave/convex) and hence (2.31) is not a convex optimization problem. Using the following observations we construct an optimal power allocation scheme.

**Lemma 2.** *For the objective function in (2.31), either* $\log_2(1+p) \geq R^u(p, q_k)$ , $\forall q_k$ *or* $\exists\ \tilde{q} \in [0, \infty)$*, where* $\tilde{q}$ *is the solution of*

$$R^u(p, q_k) = \log_2(1+p)\,,\ \forall p \geq 0 \tag{2.32}$$

*Proof.* Consider the asymptote

$$\lim_{q_k \to \infty} R^u(p, q_k) = \left(1 - \frac{1}{T}\right) \log_2\left(1 + \frac{pM}{\left(1 - \frac{1}{T}\right)}\right). \tag{2.33}$$

The function $R_k^u$ is strictly monotonic in $q_k$ with $R^u(p, 0) < \log_2(1+p)$, and approaches the value in (2.33) as $q_k$ approaches $\infty$. Therefore, if

$$\log_2(1+p) < \lim_{q_k \to \infty} R^u(p, q_k)\,,$$

then $\exists\ \tilde{q} \in [0, \infty)$ satisfying (2.32), otherwise, $\log_2(1+p) \geq R^u(p, q_k)\,,\ \forall q_k$. □

Thanks to Lemma 2, in the rest of the section we do not deal with the case where $\log_2(1+p) \geq R^u(p, q_k)\,,\ \forall q_k$, since the solution of (2.31) is trivial as the RX doesn't send any pilot symbols.

**Lemma 3.** *Without loss of optimality, we only consider schemes where the energy allocated by the RX in the k-th interval satisfies* $q_k \notin (0, \tilde{q}]$*, where* $\tilde{q}$ *is the solution of (2.32).*

*Proof.* From Lemma 2, we have $\log_2(1+p) \geq R^u(p, q_k)\,,\ \forall q_k \in [0, \tilde{q}]$. Therefore, the the objective function in (2.31) becomes $\log_2(1+p)\,,\ \forall q_k \in [0, \tilde{q}]$. Hence, if there is optimal solution such that $q_k \in (0, \tilde{q}]$ we can make $q_k = 0$ without changing the value of the objective function. □

**Remark 3.** *The optimal energy allocation vector* $\boldsymbol{q}^* = [q_1^*, \ldots, q_K^*]$ *for (2.31) may not be unique. If there is an optimal policy* $\boldsymbol{q}^*$*, such that there exists* $q_i^* > q_j^*$ *for some* $1 \leq i < j \leq K$*, then we can switch the energy allocated in intervals i and j without violating the EH constraints in (2.31b) while achieving the same objective value. Therefore, we are interested in obtaining energy allocation policies which are monotonically increasing in time.*

**Proposition 3.** *Without loss of optimality, we are interested in optimal energy allocation vectors of the form* $\boldsymbol{q}^o = \left[\boldsymbol{0}_{1\times k_o}\ \boldsymbol{q}^m_{1\times(K-k_o)}\right]$*, where* $0 \leq k_o \leq K-1$*,* $\boldsymbol{q}^m$ *denotes the most majorized feasible vector for the EH profile* $\boldsymbol{e}^o_{1\times(K-k_o)} = \left[\sum_{i=1}^{k_o+1} e_i^r, e_{k_o+2}^r, \ldots, e_K^r\right]$*, and it is obtained by using Algorithm 1,* $\boldsymbol{q}^m = OEA(K-k_o, \boldsymbol{e}^o/L)$*.*

*Proof.* Using Lemma 3 and Remark 3, we are interested in optimal energy policies that are monotonically increasing in time and satisfy $q_k \notin (0, \tilde{q}], \forall k$. Therefore for we are interested in the optimal energy allocation of the form $\hat{\boldsymbol{q}}^o = \left[\mathbf{0}_{1\times k_o}\ \hat{\boldsymbol{q}}_{1\times(K-k_o)}\right]$, $0 \leq k_o \leq K-1$. The remaining proof is by contradiction. Suppose that $\hat{\boldsymbol{q}}^o$ is an optimal energy allocation vector, and $\hat{\boldsymbol{q}} \neq \boldsymbol{q}^m$. Since $\hat{\boldsymbol{q}}^o$ is an optimal policy, the elements of $\hat{\boldsymbol{q}}$ must be greater than $\tilde{q}$ given in (2.32). Since the objective function $R_k^u$ given in (2.29) is concave for $q_k \geq \tilde{q}$, and by Theorem 2, we can see the power allocation $\boldsymbol{q}^m \preceq \hat{\boldsymbol{q}}$ increases the objective. Now, it needs to be verified that the elements of $\boldsymbol{q}^m$ are greater than $\tilde{q}$. By using Theorem 2, we have $\boldsymbol{q}^m = \hat{\boldsymbol{q}}\mathbf{D}$ for some doubly stochastic matrix $\mathbf{D}$. We can write $q_k^m = \sum_{j=1}^{K-k_o} \hat{q}_j d_{j,k}$. Using the property of doubly stochastic matrix in Definition 2, and the fact that $\hat{q}_j > \tilde{q}$, we have $q_k^m > \tilde{q}$. Therefore, $\hat{\boldsymbol{q}} \neq \boldsymbol{q}^m$ cannot be optimal. □

Based on the above analysis, the problem (2.31) simplifies to an optimization over a single variable $1 \leq k_o \leq K$, and for each choice of $k_o$, the optimal energy allocation is obtained by using Proposition 3.

Note that for large values of $T$, $\left(1 - \frac{\tau_k}{T}\right) \approx 1$, and the objective function in (2.31) can be approximated as $R^u\left(p, q_k\right)$. In this case, the optimal power allocated for sending pilot symbols tends to the most majorized feasible vector. i.e., $\boldsymbol{q}^* \preceq \boldsymbol{q}$, $\forall \boldsymbol{q}$ satisfying the constraints in (2.31b) and (2.31c).

## 2.5 EH Transmitter and Receiver

In this section, we consider the general case where both the TX and the RX harvest energy. Note that if the TX is silent in $k$-th interval, i.e., $p_k^t = 0$, there is no incentive for the RX to send feedback in this interval. Therefore, without loss of optimality we only consider EH profiles where $e_1^t > 0$. Otherwise, if there is an EH profile such that $e_k^t = 0, k \in [1 : m-1]$, then $p_k^t = 0, k \in [1 : m-1]$ due to the constraints in (2.7c). In these intervals the RX simply accumulates the harvested energy, and without loss of optimality we can have a new EH profile with $\tilde{e}_1^t = e_{i+m-1}^t, \forall i \in [1 : K-m+1]$, and $\tilde{e}_1^r = \sum_{k=1}^m e_k^r$ and $\tilde{e}_i^r = e_{i+m-1}^r, \forall i \in [2 : K-m+1]$ for further analysis. We start with the feedback model where UL and DL channel are not identical.

### 2.5.1 Non-reciprocal channels

The ergodic rate upper bound in (2.13) is not concave, but concave in each variable given the other variables are fixed. To obtain a simple algorithm and an upper bound on the throughput, we follow a similar approach as in the previous section, and use a concave upper bound on (2.13) as the objective function for throughput optimization.

This bound is obtained by using a hypothetical system in which the transmission power is 1 unit higher than the actual transmission power of

the system, which is $p_k^t/t_k$. Plugging this into the upper bound in (2.13), a new upper bound $R_k^{ub} \triangleq R^{ub}\left(p_k^t, q_k, \tau_k\right)$ on the ergodic rate is obtained :

$$R_k^{ub} = t_k \log_2\left(1 + \left(1 + \frac{p_k^t}{t_k}\right)\frac{f_k}{t_k}\right), \tag{2.34}$$

where $t_k \triangleq 1 - \frac{\tau_k}{T}$ and $f_k \triangleq M - (M-1)\left(1 + \frac{q_k}{\tau_k \sigma^2}\right)^{\frac{-\tau_k}{M-1}}$. We now illustrate the tightness of the upper bound in (2.34) in the low and high power regimes. For all feasible $\tau_k, p_k^t$ and $q_k$, we can see that $0 < t_k \leq 1$ and $1 \leq f_k \leq M$. Consider

$$R_k^{ub} - R_k^u = t_k \log_2\left(\frac{t_k^2 + t_k f_k + p_k^t f_k}{t_k + p_k^t f_k}\right) - t_k \log_2\left(t_k\right) \tag{2.35}$$

Note that (2.35) is decreasing in $p_k^t$ for fixed $\tau_k$ and $q_k$. Since $\tau_k, f_k$ are bounded, for fixed $\tau_k$ and $q_k$, in the low power regime

$$\begin{aligned}\lim_{p_k^t \to 0} R_k^{ub} - R_k^u &= t_k \log_2\left(1 + \frac{f_k}{t_k}\right) \\ &\leq \log_2\left(1 + M\right),\end{aligned} \tag{2.36}$$

and in the high power regime,

$$\lim_{p_k^t \to \infty} R_k^{ub} - R_k^u = -t_k \log_2(t_k) \leq 0.5. \tag{2.37}$$

From the above analysis, it can be seen that, (2.35) decreases as the power is increased, and it is bounded by a constant in the high power regime. By using (2.34), the modified throughput maximization problem is formulated as

$$\max_{p_k^t, q_k, \tau_k} \quad \mathcal{U}_1 = \sum_{k=1}^{K} R_k^{ub} \tag{2.38a}$$

$$\text{s.t.} \quad L\sum_{i=1}^{l} q_i \leq \sum_{i=1}^{l} e_i^r, \forall l \in [1:K], \tag{2.38b}$$

$$LT\sum_{i=1}^{l} p_i^t \leq \sum_{i=1}^{l} e_i^t, \forall l \in [1:K], \tag{2.38c}$$

$$\tau_k \in [0, T),\ p_k^t \geq 0,\ q_k \geq 0, \text{ and } \forall k \in [1:K]. \tag{2.38d}$$

Since the objective function is monotonic in $q_k$ and $p_k^t$, the constraints in (2.38b) and (2.38c) must be satisfied with equality for $l = K$, otherwise, we can always increase $q_K, p_k^t$, and hence the objective function, without violating any constraints. The feasible set is represented as

$$\mathfrak{J} = \left\{(\boldsymbol{p}, \boldsymbol{q}, \boldsymbol{\tau})\, | p_k^t, q_k, \tau_k \text{ satisfy (2.38b), (2.38c) and (2.38d) } \forall k\right\},$$

where $\boldsymbol{p} = \left[p_1, \ldots, p_k^t\right]$, $\boldsymbol{q} = [q_1, \ldots, q_K]$ and $\boldsymbol{\tau} = [\tau_1, \ldots, \tau_K]$.

**Proposition 4.** *The objective function in the optimization problem (2.38) is concave.*

*Proof.* See Appendix. □

Since the objective function in (2.38) is concave and the constraints are linear, it has a unique maximizer [48]. Consider the following equivalent form of (2.38), where the optimization is performed in two steps.

$$\max_{\boldsymbol{p},\boldsymbol{q}} \tilde{\mathcal{U}}_1(\boldsymbol{p},\boldsymbol{q}) \text{ s.t. } \forall(\boldsymbol{p},\boldsymbol{q},\boldsymbol{\tau}) \in \mathfrak{J}, \tag{2.39}$$

where $\tilde{\mathcal{U}}_1(\boldsymbol{p},\boldsymbol{q})$ is obtained by

$$\tilde{\mathcal{U}}_1(\boldsymbol{p},\boldsymbol{q}) = \max_{\boldsymbol{\tau}} \mathcal{U}_1(\boldsymbol{p},\boldsymbol{q},\boldsymbol{\tau}) \text{ s.t. } \forall(\boldsymbol{p},\boldsymbol{q},\boldsymbol{\tau}) \in \mathfrak{J}. \tag{2.40}$$

Since $\mathcal{U}_1$ is a concave function over the convex set $\mathfrak{J}$, the function $\tilde{\mathcal{U}}_1$ is concave with domain $\tilde{\mathfrak{J}} = \{(\boldsymbol{p},\boldsymbol{q}) \,|\, (\boldsymbol{p},\boldsymbol{q},\boldsymbol{\tau}) \in \mathfrak{J}\}$ [48, 3.2.5]. $\mathcal{U}_1 = \sum_{k=1}^{K} R_k^{ub}$ is continuous, differentiable and concave in $\tau_k \in [0,T)$. Furthermore, for given $p_k^t$ and $q_k$, $R_k^{ub}$ approaches $\log_2\left(2+p_k^t\right)$ and 0, as $\tau_k$ approaches 0 and $T$, respectively. Therefore, the unique maximizer of (2.40), $\tau_k^*, \forall k$ lies in $[0,T)$, and it is obtained as

$$\frac{\partial \mathcal{U}_1}{\partial \tau_k}|_{\tau_k^*} = \frac{\partial R_k^{ub}}{\partial \tau_k}|_{\tau_k^*} = 0, \ \forall k \in [1:K]. \tag{2.41}$$

As $\tau_k^*$ is only a function of $q_k$ and $p_k^t$, (2.39) can be written as

$$\max_{p_k^t, q_k} \ \tilde{\mathcal{U}}_1 = \sum_{k=1}^{K} \tilde{R}_k^{ub} \text{ s.t. } \forall k, \left(p_k^t, q_k\right) \in \tilde{\mathfrak{J}}, \tag{2.42}$$

where $\tilde{R}_k^{ub} \triangleq \tilde{R}^{ub}\left(p_k^t, q_k\right) = R^{ub}\left(p_k^t, q_k, \tau_k^*\left(p_k^t, q_k\right)\right)$.

In order to get an insight on how the optimal solution of (2.39) may look like, consider a simple scenario in which there is only a sum power constraint at the TX and the RX, i.e., the constraints in (2.38b), (2.38c) has to be satisfied for only $l = K$. In this case, by Jensen's inequality, the uniform power allocation at the TX and the RX is optimal [2]. However, due to the EH constraints, this may not be feasible. Using this intuition, we can see that the optimal policy tries to equalize the powers as much as possible, while satisfying the EH constraints. Next, we consider the case in which the EH profiles at the TX and the RX are similar, and show that the optimization problem is considerably simplified.

2. In this section, with slight abuse of terminology we use the terms RX power and RX energy interchangeably.

## A Similar EH Profiles

The EH profiles are similar in the sense that the most majorized feasible vectors obtained from the EH profiles of the TX and RX, $\boldsymbol{p}^*$ and $\boldsymbol{q}^*$, have the same structure, i.e., if $p_i^* = c_1, \forall i \in [m:n]$, then $q_i^* = c_2, \forall i \in [m:n]$ for some constants $c_1, c_2 \geq 0$. We now give a formal definition.

**Definition 4.** *By using the OEA algorithm, let* $[\boldsymbol{q}^*, \mathcal{S}_r] = OEA(K, \{e_i^r/L\})$ *and* $[\boldsymbol{p}^*, \mathcal{S}_t] = OEA(K, \{e_i^t/LT\})$. *EH profiles at the TX and the RX are said to be similar if* $\mathcal{S}_r = \mathcal{S}_t$.

From Section 2.2, we can see that the definition of majorization for the vector case does not directly extend to the matrix case. If OEA algorithm is used at the TX and RX separately, we get the most individually majorized power vectors, which in general may not be the optimal solution of (2.39). However, we now show that if the EH profiles are similar, the above mentioned approach is indeed optimal.

**Proposition 5.** *If the EH profiles at the TX and the RX are similar then* $(\boldsymbol{q}^*, \boldsymbol{p}^*, \boldsymbol{\tau}^*)$ *is the global optimum of (2.38), where* $\boldsymbol{q}^* \preceq \boldsymbol{q}, \boldsymbol{p}^* \preceq \boldsymbol{p}$, $\forall\, (\boldsymbol{q}, \boldsymbol{p}, \boldsymbol{\tau}) \in \mathfrak{J}$, *and* $\tau_k^*$ *is the solution of*

$$\frac{\partial R_k^{ub}}{\partial \tau_k}|_{(p_k^*, q_k^*, \tau_k^*)} = 0,\ \forall k \in [1:K]\,. \tag{2.43}$$

*Proof.* See Appendix. □

## B Different EH Profiles

Unfortunately, we could not find a simple algorithm to solve (2.38) in a general setting where the EH profiles are not similar. In (2.42), if one variable is fixed, optimizing over the other variable has a *directional* or *staircase water-filling* interpretation [18], [20], however, the difficulty lies in the fact that there is no closed form expression for $\tilde{R}_k^{ub}$. Nonetheless, based on the convexity of the objective function, some properties of the optimal solution are given below.

**Lemma 4.** *Under the optimal policy, the transmission power* $p_k^t$, *and the energy used to send the feedback* $q_k$ *are non-decreasing in* $k, \forall k \in [1:K]$.

**Lemma 5.** *Under the optimal policy, at the time instants at which* $R^{ub}$ *changes, the energy buffer of either the TX or the RX is emptied.*

The proofs of the above lemmas are given in Appendix.

### 2.5.2 Reciprocal channels

Using the analysis and the ergodic rate upper bound provided in Section 2.4.2, the throughput maximization problem for reciprocal channels scenario when both TX and RX harvest energy can be formulated as

$$\max_{p_k^t, q_k} \quad \sum_{k=1}^{K} \max\left\{\log_2\left(1+p_k^t\right), R^u\left(p_k^t, q_k\right)\right\}, \tag{2.44a}$$

$$\text{s.t.} \quad L\sum_{i=1}^{l} q_i \leq \sum_{i=1}^{l} e_i^r, \forall l \in [1:K], \tag{2.44b}$$

$$LT\sum_{i=1}^{l} p_i^t \leq \sum_{i=1}^{l} e_i^t, \forall l \in [1:K], \tag{2.44c}$$

$$p_k^t \geq 0 \text{ and } q_k \geq 0 \ \forall k \in [1:K]. \tag{2.44d}$$

However, the objective function is not jointly concave in $p_k^t$ and $q_k$, therefore, following a similar approach as in the above section we use an upper bound on $R_k^u$ in (2.30) as the objective function. An upper bound on the ergodic rate $R_k^{ub} \triangleq R^{ub}\left(p_k^t, q_k\right)$ is given by

$$R_k^{ub} = \log_2\left[1+\left(1+\frac{p_k^t}{\left(1-\frac{1}{T}\right)}\right)\left(M-(M-1)\frac{1}{(1+q_k/\sigma^2)}\right)\right]. \tag{2.45}$$

This bound is obtained by using a hypothetical system in which the transmission power is 1 unit higher than the actual transmission power and neglecting the $\left(1-\frac{1}{T}\right)$ term in front of the logarithm in $R^u\left(p_k^t, q_k\right)$. Using this bound as the objective function, the modified throughput maximization problem is formulated as

$$\max_{p_k^t, q_k} \quad \mathcal{U}_1 = \sum_{k=1}^{K} R_k^{ub} \tag{2.46a}$$

$$\text{s.t.} \quad L\sum_{i=1}^{l} q_i \leq \sum_{i=1}^{l} e_i^r, \forall l \in [1:K], \tag{2.46b}$$

$$LT\sum_{i=1}^{l} p_i^t \leq \sum_{i=1}^{l} e_i^t, \forall l \in [1:K], \tag{2.46c}$$

$$p_k^t \geq 0 \text{ and } q_k \geq 0 \ \forall k \in [1:K]. \tag{2.46d}$$

Since the objective function is monotonic in $p_k^t$ and $q_k$, the constraints in (2.46b) and (2.46c) must be satisfied with equality for $l = K$, otherwise, we can always increase $q_K, p_k^t$, and hence the objective function, without violating any constraints. The feasible set is represented as

$$\mathfrak{H} = \left\{(\boldsymbol{p}, \boldsymbol{q}) \,|p_k^t, q_k \text{ satisfy (2.46b), (2.46c) and (2.46d) } \forall k\right\},$$

where $\boldsymbol{p} = \left[p_1, \ldots, p_k^t\right]$ and $\boldsymbol{q} = [q_1, \ldots, q_K]$.

**Proposition 6.** *The objective function in the optimization problem (2.46) is concave.*

*Proof.* See Appendix. □

The same analysis provide in Section 2.5.1 can be used to obtain similar results for the case of reciprocal channels. The results are stated below, however, the proofs are omitted as they follow same methods and steps as in the non-reciprocal case in Section 2.5.1.

**Proposition 7.** *If the EH profiles at the TX and the RX are similar then* $(\boldsymbol{p}^*, \boldsymbol{q}^*)$ *is the global optimum of (2.46), where* $\boldsymbol{p}^* \preceq \boldsymbol{p}, \boldsymbol{q}^* \preceq \boldsymbol{q},\ \forall\, (\boldsymbol{p}, \boldsymbol{q}) \in \mathfrak{H}$.

When the EH profiles are not similar, following lemmas gives some properties of the optimal solution.

**Lemma 6.** *Under the optimal policy, the transmission power* $p_k^t$*, and the energy used to send pilot symbols* $q_k$ *are non-decreasing in* $k, \forall k \in [1 : K]$.

**Lemma 7.** *Under the optimal policy, at the time instants at which* $R^{ub}$ *changes, the energy buffer of either the TX or the RX is emptied.*

## 2.6 Numerical Results

We start by considering the case in which the RX harvests energy, while the TX has a constant power supply. We assume that the RX is equipped with a solar EH device. Following [51], solar irradiance data is taken from the database reported in [52]. Each EH interval is of duration $\Delta = 1$ hour, $T = 200$ ms, resulting in $L = 18000$ frames. The harvested power from the irradiance data can be calculated as, $p_{harv} = I[\text{Watt}/m^2] \times Area[m^2] \times \rho$, where $\rho$ is the efficiency of the harvester. A hypothetical solar panel of variable area is assumed. The area of the panel is adjusted such that we have the EH profile shown in Fig. 2.4 at the RX. In Fig. 2.4, the **harvested power to noise ratio (HPN)** in the $k$-th EH interval $\frac{e_k^r}{\Delta\sigma^2}$ is shown.

Using this EH profile, throughput of different feedback policies for the non-reciprocal channels scenario is shown in Fig. 2.5. In Fig. 2.5, OEA represents the proposed policy in which the energy vector is obtained by using the OEA algorithm, and then the optimal time span of feedback $\tau_k^*$ is obtained by solving (2.25). In the greedy scheme, the consumed energy is equal to the harvested energy in that interval, i.e., $q_k = e_k^r/L$, and then optimization is performed only over $\tau_k$, given $q_k$. The performance of the above policies when the feedback bits are rounded to the largest previous integer is also shown. We can see that the proposed approach outperforms the greedy policy by 1.6 dB at a rate of 4 bits/s/Hz. Also the rate loss due to bit rounding is

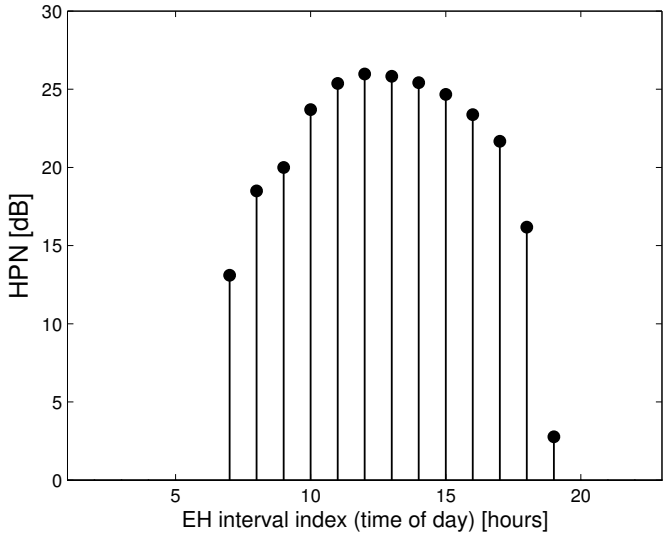


FIGURE 2.4 – Model for a solar energy harvesting profile.

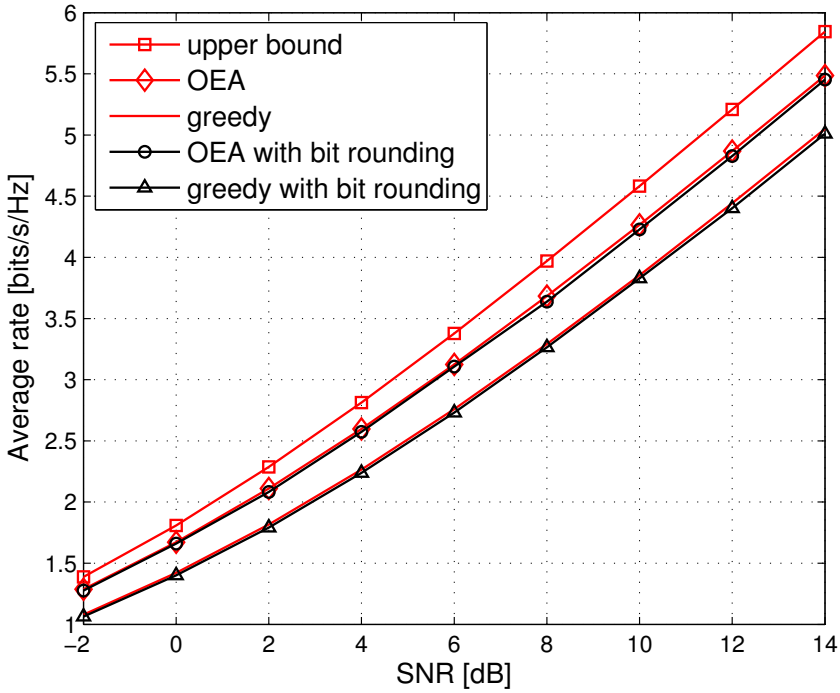


FIGURE 2.5 – Ergodic rate for non-reciprocal channel scenario with only an EH RX, and $M = 4$.

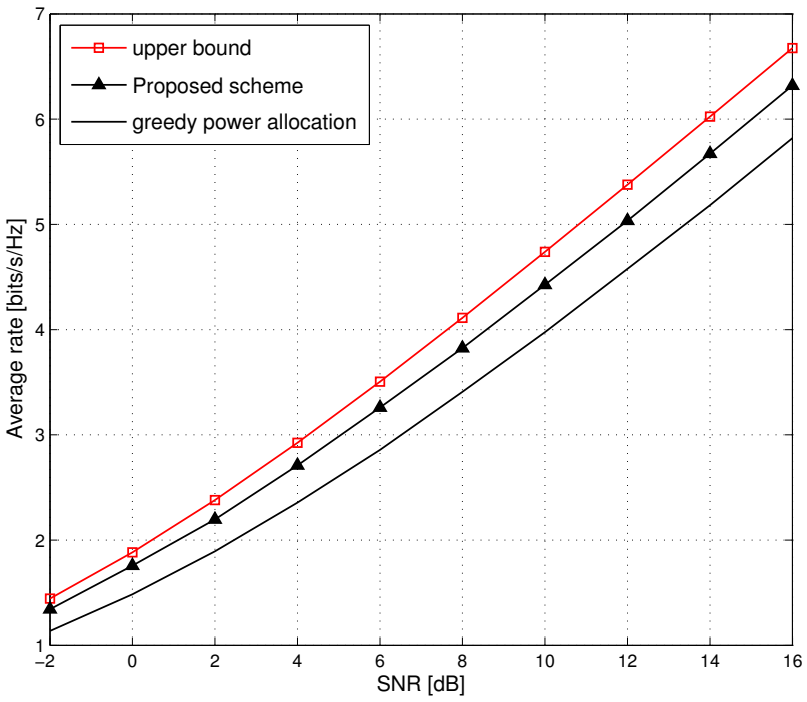


FIGURE 2.6 – Ergodic rate for reciprocal channel scenario with only an EH RX, and $M = 4$.

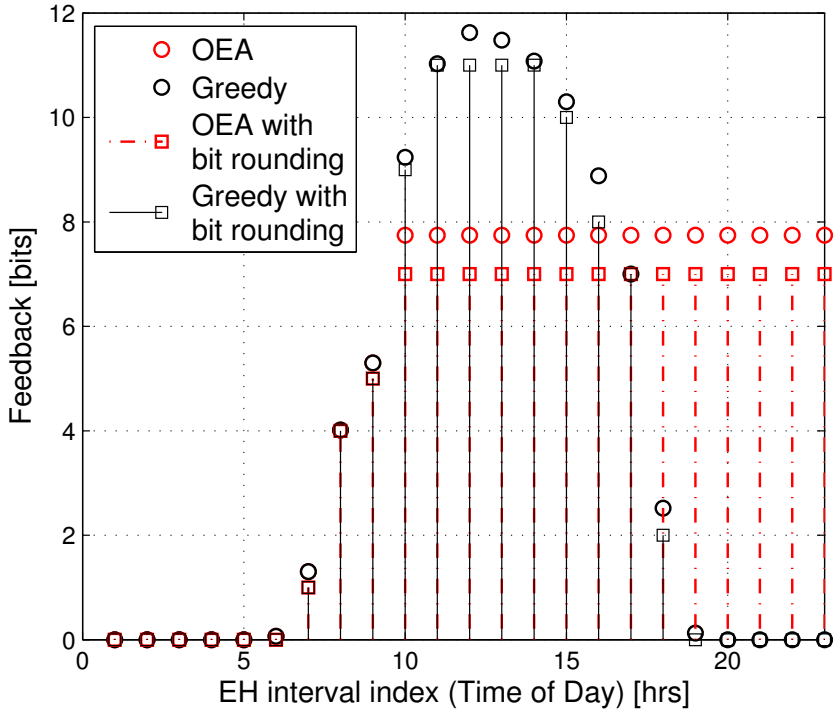


FIGURE 2.7 – Feedback load at downlink SNR of 10 dB, $M = 4$.

negligible. By using the same EH profile in Fig. 2.4, throughput of different feedback policies for the reciprocal channels scenario is shown in Fig. 2.6.

In Fig. 2.7, feedback bit allocation is shown for the above mentioned policies for a downlink SNR of 10 dB. From Fig. 2.7, we can see that with the proposed strategy, feedback bit allocation is equalized as much as possible. Similarly, the energy allocated for the pilot symbols in the reciprocal channel scenario is shown in Fig. 2.8. Here also energy allocation is as equalized as much as possible.

In Fig. 2.9 we compare the achievable ergodic rates for two feedback models using the EH profile from Fig. 2.4. It can be seen that the rate achieved is higher in the reciprocal channels scenario.

We now consider the case in which both the TX and the RX harvest energy, with similar EH profiles. The same EH profile in Fig. 2.4 is separately used at both the RX and the TX, hence the EH profiles are similar. In Fig. 2.10, the throughput of different schemes is shown at various mean HPN values at the TX for the non-reciprocal channel scenario. The results for the reciprocal channels scenario are shown in Fig. 2.11. The mean HPN at the TX is varied by increasing the harvester area at the TX, i.e., the EH profile is multiplied by a positive number (area), while keeping the same

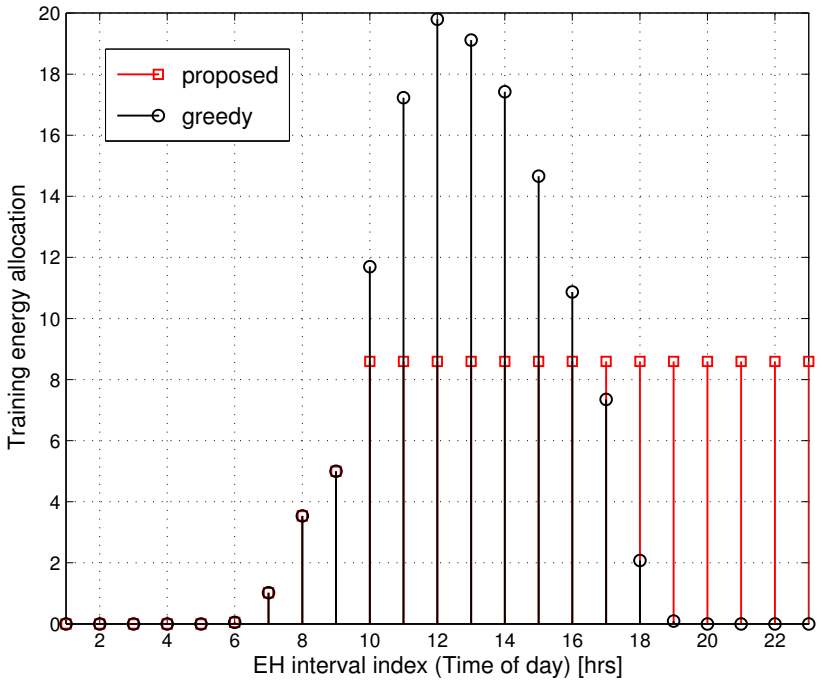


FIGURE 2.8 – Energy used in training at downlink SNR of 10 dB, $M = 4$.

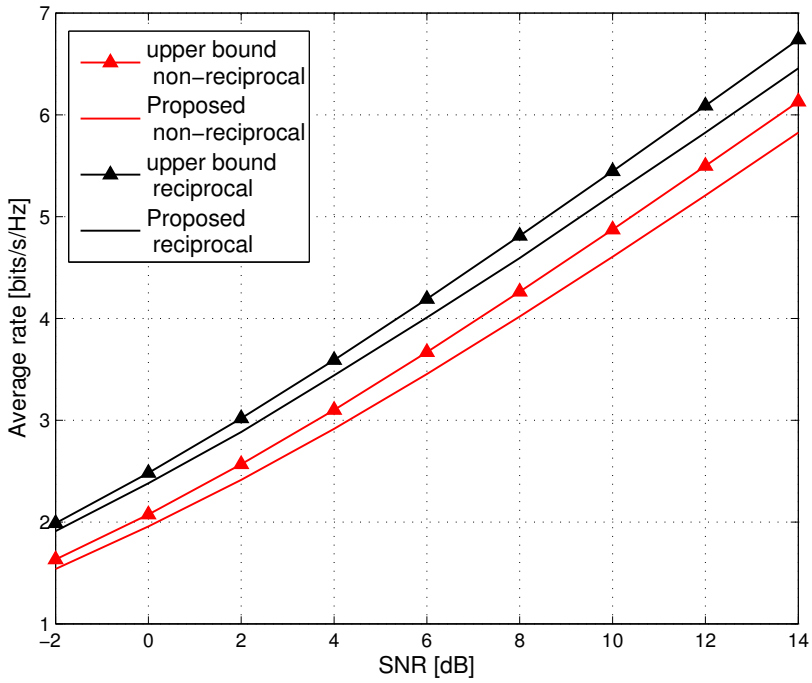


FIGURE 2.9 – Ergodic rate for reciprocal and non-reciprocal channels with only an EH RX, and $M = 8$.

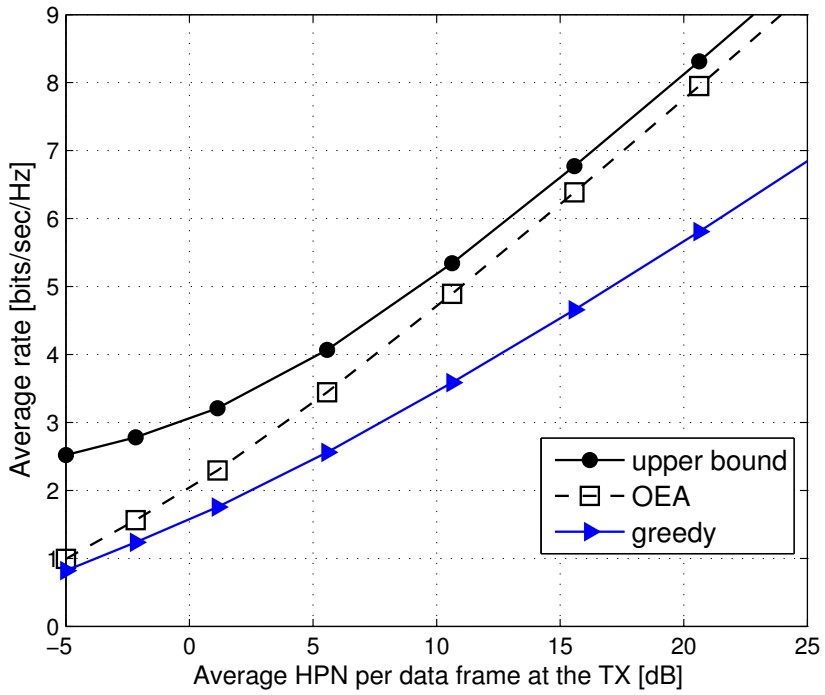


FIGURE 2.10 – Ergodic rate for similar EH profiles in non-reciprocal channel scenario, $M = 4$.

shape and efficiency. In Fig. 2.10, OEA represents the proposed policy in which the energy vector at the TX and the RX is obtained by using the OEA algorithm, and then the optimal time span of feedback $\tau_k^*$ is obtained by solving (2.41). In the greedy scheme, the allocated energy is equal to the harvested energy in that interval, i.e., at the TX $p_k^t = e_k^t/LT$, at the RX $q_k = e_k^r/L$, and then optimization is performed only over $\tau_k$, given $p_k^t$ and $q_k$. The difference in throughput between the greedy and OEA is small when the average HPN is low, and it increases with the HPN. In contrast to the OEA scheme, using the greedy approach with the solar EH profile results in some EH intervals being allocated zero energy, and therefore does not scale by increasing the harvester area. This particularly hurts the greedy policy's throughput in the high HPN regime as the multiplexing gain (pre-log factor) is reduced.

Finally, we consider a case with non-similar EH profiles, where the EH profiles are generated independently at the TX and the RX, and they are i.i.d. with exponential distribution. EH profiles are verified so that they are not similar according to Definition 4. Similarly to Fig. 2.10, in Fig. 2.12, the mean HPN at the TX is varied by multiplying the EH profile by a constant, while keeping the same shape. Since we could not find a simple algorithm in

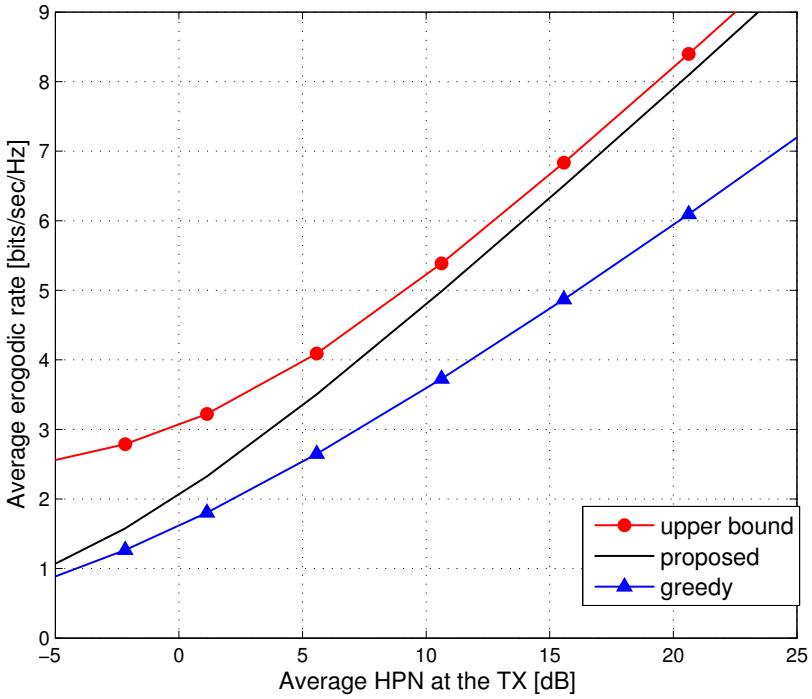


FIGURE 2.11 – Ergodic rate for similar EH profiles in reciprocal channel scenario, $M = 4$.

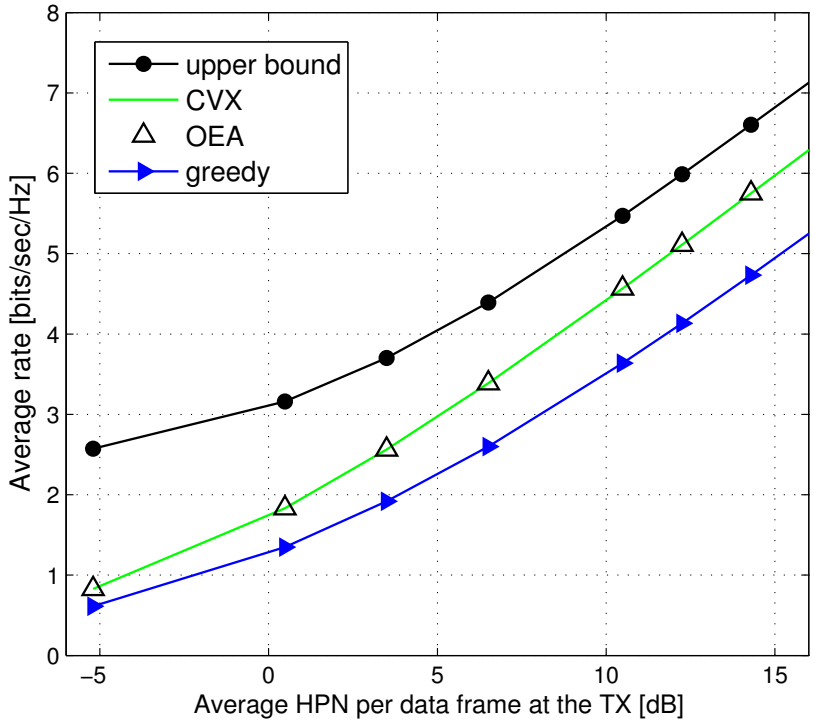


FIGURE 2.12 – Ergodic rate for non-similar EH profiles, $M = 4$.

this case, CVX solver is used to solve the optimization problem [48], and is denoted as CVX in Fig. 2.12. As we can see, the heuristic of using the OEA approach performs quite well even in the non-similar EH profile scenario. The energy allocation at the TX and the RX are shown in Fig. 2.13 for the above mentioned policies at an average per frame HPN of 0.5 dB at the TX. Different from Fig. 2.10, in Fig. 2.12 the rate scaling with average HPN is same for both the greedy and the OEA policy. For the greedy policy, the allocated energy in an EH interval scales with the increasing mean HPN, in contrast to the solar EH profile, for which the allocated energy is zero in some intervals.

## 2.7 Conclusion

We have studied the problem of feedback design with EH constraints in a p2p MISO channel when both the TX and the RX harvest energy. Since the exact expressions of throughput are complicated, concave upper bounds have been used in the optimization problems. We have first considered the case in which only the RX harvests energy, and optimized the feedback policy. Later,

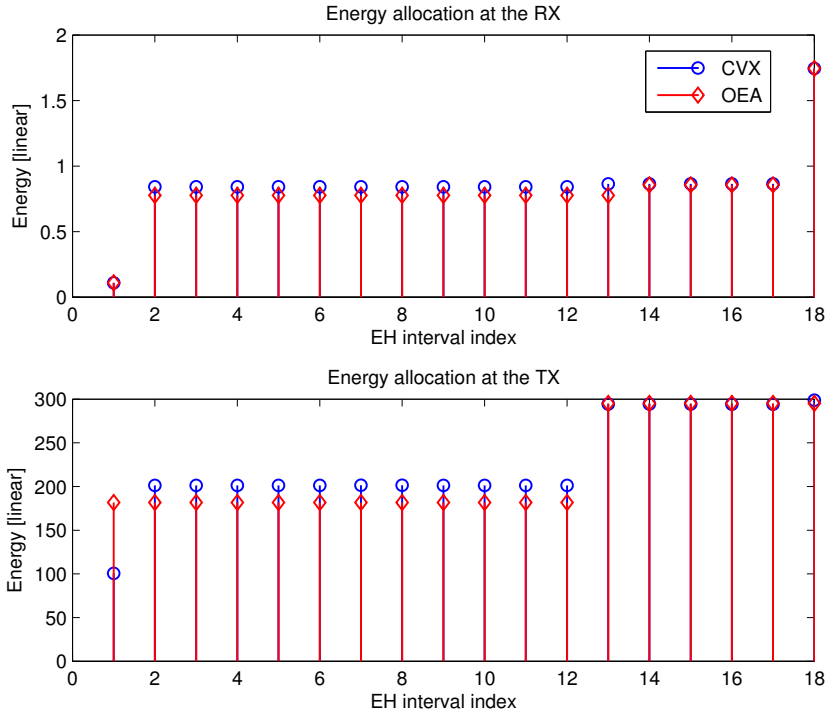


FIGURE 2.13 – Energy allocation at the TX and the RX, $M = 4$.

the general case in which both the TX and the RX harvest energy is analyzed. We have showed that, if EH profiles are similar, the optimization problem can be considerably simplified. We note the result obtained in Proposition 5 is general, and for example, can be used in a network setting in which a concave utility is to be maximized in the presence of EH nodes with similar harvesting profiles and having infinite size energy buffers. Numerical results show that the proposed policies not only outperform the greedy policies, but also achieve the performances which are quite close to the upper bound. We believe that our work sheds light on the design of feedback enabled multi-antenna systems when the nodes depend on EH devices for their energy.

## 2.8 Appendix

### 2.8.1 Proof of Lemma 1

Let $X_1 = [x_1 \ y_1 \ t_1]^{\mathrm{T}}, X_2 = [x_2 \ y_2 \ t_2]^{\mathrm{T}}$, we have

$$\begin{aligned} & h\left(\lambda X_1 + (1-\lambda) X_2\right) \\ & = \Theta g\left(\frac{\lambda y_1 + (1-\lambda) y_2}{\Theta}, \frac{f\left(\overline{x}, \overline{t}\right)}{\Theta}\right) \\ & \overset{(a)}{\geq} \Theta g\left(\frac{\lambda y_1 + (1-\lambda) y_2}{\Theta}, \frac{\lambda f_1 + (1-\lambda) f_2}{\Theta}\right) \\ & = \Theta g\left(\frac{\Theta_1 y_1}{\Theta \alpha_1} + \frac{\Theta_2 y_2}{\Theta \alpha_2}, \frac{\Theta_1 f_1}{\Theta \alpha_1} + \frac{\Theta_2 f_2}{\Theta \alpha_2}\right) \\ & \overset{(b)}{\geq} \Theta_1 g\left(\frac{y_1}{\alpha_1}, \frac{f_1}{\alpha_1}\right) + \Theta_2 g\left(\frac{y_2}{\alpha_2}, \frac{f_2}{\alpha_2}\right) \\ & = \lambda h\left(X_1\right) + (1-\lambda) h\left(X_2\right), \end{aligned} \tag{2.47}$$

where $\overline{x} \triangleq \lambda x_1 + (1-\lambda) x_2$, $\overline{t} \triangleq \lambda t_1 + (1-\lambda) t_2$, $f_1 \triangleq f\left(x_1, t_1\right)$, $f_2 \triangleq f\left(x_2, t_2\right)$, $\Theta_1 \triangleq \lambda\left(1 - \frac{t_1}{T}\right)$ and $\Theta_2 \triangleq (1-\lambda)\left(1 - \frac{t_2}{T}\right), \Theta = \Theta_1 + \Theta_2$, $\alpha_1 \triangleq \left(1 - \frac{t_1}{T}\right)$, $\alpha_2 \triangleq \left(1 - \frac{t_2}{T}\right)$. Here

(a) follows from the fact that $f\left(x, t\right)$ is concave, and $g\left(y, z\right)$ is monotonically increasing in each argument,

(b) follows from the fact that $\frac{\Theta_1}{\Theta} + \frac{\Theta_2}{\Theta} = 1$, and $g\left(y, z\right)$ is concave.

### 2.8.2 Proof of Proposition 1

Reproducing the ergodic rate bound in (2.13) with $p_k = P, \forall k$, we have

$$R^u\left(q_k, \tau_k\right) = t_k \log_2\left(1 + \frac{P f_k}{t_k}\right), \tag{2.48}$$

where $t_k \triangleq 1-\frac{\tau_k}{T}, f_k \triangleq (M-M-1(1+\frac{q_k}{\tau_k\sigma^2})^{\frac{-\tau_k}{M-1}})$. Since $b_k$ in (2.3) is concave in $q_k$ and $\tau_k$, it can be easily seen that $2^{-\frac{b_k}{M-1}} = \left(1+\frac{q_k}{\tau_k\sigma^2}\right)^{\frac{-\tau_k}{M-1}}$ is convex, and hence, $f_k$ is concave. Using Lemma 1 with $g(y,z) = \log_2(1+z)$ and $f_k$, we can see that $R_k^u$ is concave. Since the objective function in (2.20) is the summation of $R_k^u$'s, it is also concave.

### 2.8.3 Proof of Proposition 4

First, we show that $g(y,z) = \log_2(1+(1+y)z), (y,z) \in \mathbb{R}_+^2$ is concave for $y \geq 0, z \geq 1$. The Hessian of $g$ is given by

$$\mathbf{J} = \frac{1}{\beta}\begin{pmatrix} -z^2 & 1 \\ 1 & -(1+y)^2 \end{pmatrix}, \tag{2.49}$$

where $\beta = \log_e 2(1+(1+y)z)^2 > 0$. Consider $\boldsymbol{u}^{\mathrm{T}}\mathbf{J}\boldsymbol{u} = -\frac{1}{\beta}\left(a^2z^2 + b^2(1+y)^2 - 2ab\right)$, where $\boldsymbol{u} = [a\ b]^{\mathrm{T}} \in \mathbb{R}^2$. It can be easily seen that $\boldsymbol{u}^{\mathrm{T}}\mathbf{J}\boldsymbol{u} \leq 0$ for $ab \leq 0$. For $ab > 0$, since $z(1+y) \geq 1$, $\boldsymbol{u}^{\mathrm{T}}\mathbf{J}\boldsymbol{u} = -\frac{1}{\beta}\left[(az-b(1+y))^2 + 2ab(z(1+y)-1)\right] \leq 0$. As Hessian is negative semidefinite, $g(y,z)$ is concave. Reproducing the ergodic rate bound in (2.34), we have

$$R_k^{ub} = t_k \log_2\left(1+\left(1+\frac{p_k}{t_k}\right)\frac{f_k}{t_k}\right), \tag{2.50}$$

where $t_k$ and $f_k$ are as defined before.

By following the similar steps in Proposition 1, $f_k$ can be shown to be concave. Using Lemma 1 with $g(y,z)$ and $f_k$, we can see that $R_k^{ub}$ is concave. Since the objective function in (2.38) is the summation of $R_k^{ub}$'s, it is also concave.

### 2.8.4 Proof of Proposition 5

First, $(\boldsymbol{p}^*, \boldsymbol{q}^*)$ is shown to be the solution of (2.42) and then $\boldsymbol{\tau}^*$ is obtained by (2.43). Before solving (2.42), we prove that

$$\begin{aligned}(\boldsymbol{p}^*, \boldsymbol{q}^*) = &\arg\max_{g, p_k, q_k} \sum_{k=1}^{K} g(p_k, q_k) \\ &\text{s.t. } \forall k, (p_k, q_k) \in \tilde{\mathfrak{J}}, g \in \mathfrak{C},\end{aligned} \tag{2.51}$$

where $\mathfrak{C}$ is the set of all continuous concave functions. As (2.42) is a special case of (2.51), $(\boldsymbol{p}^*, \boldsymbol{q}^*)$ is also the solution of (2.42).

Before starting, we note that the notations and properties of the OEA algorithm discussed in Section A are used throughout the proof. By contradiction, let us assume that there exists a $[\hat{\boldsymbol{p}}^{\mathrm{T}}\ \hat{\boldsymbol{q}}^{\mathrm{T}}]^{\mathrm{T}} \neq [\boldsymbol{p}^{*\mathrm{T}}\ \boldsymbol{q}^{*\mathrm{T}}]^{\mathrm{T}}$ and $(\hat{\boldsymbol{p}}, \hat{\boldsymbol{q}})$

be the solution of (2.51). Then, by Theorem 3 we have,

$$\left[\hat{\boldsymbol{p}}^{\mathrm{T}}\ \hat{\boldsymbol{q}}^{\mathrm{T}}\right]^{\mathrm{T}} \preceq \left[\boldsymbol{p}^{\mathrm{T}}\ \boldsymbol{q}^{\mathrm{T}}\right]^{\mathrm{T}},\ \forall\,(\boldsymbol{p},\boldsymbol{q}) \in \tilde{\mathfrak{J}}. \tag{2.52}$$

Since $(\boldsymbol{p}^*, \boldsymbol{q}^*) \in \tilde{\mathfrak{J}}$, by (2.52) and Definition 3,

$$\left[\hat{\boldsymbol{p}}^{\mathrm{T}}\ \hat{\boldsymbol{q}}^{\mathrm{T}}\right]^{\mathrm{T}} = \left[\boldsymbol{p}^{*\mathrm{T}}\ \boldsymbol{q}^{*\mathrm{T}}\right]^{\mathrm{T}}\mathbf{D}. \tag{2.53}$$

By the feasibility constraint in (2.38b),

$$\sum_{j=B_{i-1}+1}^{B_i} \hat{q}_j \leq V_i = \sum_{j=B_{i-1}+1}^{B_i} e_j^r/L, \tag{2.54}$$

where $B_i$'s are the energy band indices as explained in Section A.

Applying (2.54) for $i = 1$, and remembering that $B_0 = 0$, we get

$$\sum_{j=1}^{B_1} \hat{q}_j = \sum_{j=1}^{B_1}\sum_{i=1}^{K} q_i^* d_{i,j} \leq V_1. \tag{2.55}$$

By (P1) and (P2) in Section A, $q_i^* = q_{(1)}^* + L_i$, where

$$\begin{aligned} L_i &= 0 \ \ \forall i \in [1 : B_1]\,, \\ L_i &> 0 \ \ \forall i \in [B_1 + 1 : K]\,. \end{aligned} \tag{2.56}$$

From (2.55) and (2.56)

$$\sum_{j=1}^{B_1}\sum_{i=1}^{K} q_{(1)}^* d_{i,j} + \sum_{j=1}^{B_1}\sum_{i=B_1+1}^{K} L_i d_{i,j} \leq V_1. \tag{2.57}$$

Using the fact that $\mathbf{D}$ is doubly stochastic and by (P1), $B_1 q_{(1)}^* = V_1$, and we have

$$\sum_{j=1}^{B_1}\sum_{i=B_1+1}^{K} L_i d_{i,j} \leq 0. \tag{2.58}$$

From (2.56) and (2.58), we get

$$d_{i,j} = 0, \ \ \forall i \in [B_1 + 1 : K]\,,\ \forall j \in [1 : B_1]\,. \tag{2.59}$$

As $\mathbf{D}$ is doubly stochastic, using (P1) and (2.59),

$$\hat{q}_j = \sum_{i=1}^{B_1} q_{(1)}^* \sum_{i=1}^{B_1} d_{i,j} = q_{(1)}^* = q_j^*, \forall j \in [1 : B_1]\,. \tag{2.60}$$

Since $\mathbf{D}$ is doubly stochastic, using (2.59), we get

$$\sum_{i=1}^{B_1}\sum_{j=1}^{K} d_{i,j} = B_1, \quad \sum_{i=1}^{B_1} d_{i,j} = 1, \ \forall j \in [1 : B_1]\,. \tag{2.61}$$

We can rewrite (2.61) as

$$\sum_{i=1}^{B_1}\sum_{j=1}^{K} d_{i,j} = \sum_{i=1}^{B_1}\sum_{j=1}^{B_1} d_{i,j} + \sum_{i=1}^{B_1}\sum_{j=B_1+1}^{K} d_{i,j}, \tag{2.62}$$

from which it follows that

$$\sum_{i=1}^{B_1}\sum_{j=B_1+1}^{K} d_{i,j} = 0, \tag{2.63}$$

and hence,

$$d_{i,j} = 0, \quad \forall i \in [1 : B_1]\,, \forall j \in [B_1 + 1 : K]\,. \tag{2.64}$$

Then applying (2.54) for $i = 2$,

$$\sum_{j=B_1+1}^{B_2} \hat{q}_j = \sum_{j=B_1+1}^{B_2}\sum_{i=1}^{K} q_i^* d_{i,j} \leq V_2. \tag{2.65}$$

By (P1) and (P2), we have $q_i^* = q_{(2)}^* + L_i$, where

$$\begin{aligned} L_i &< 0 \quad \forall i \in [1 : B_1]\,, \\ L_i &= 0 \quad \forall i \in [B_1 + 1 : B_2]\,, \\ L_i &> 0 \quad \forall i \in [B_2 + 1 : K]\,. \end{aligned} \tag{2.66}$$

From (2.65) and (2.66),

$$\sum_{j=B_1+1}^{B_2}\sum_{i=1}^{K} L_i d_{i,j} + \sum_{j=B_1+1}^{B_2}\sum_{i=1}^{K} q_{(2)}^* d_{i,j} \leq V_2. \tag{2.67}$$

Since $\mathbf{D}$ is doubly stochastic, by (P1), we obtain $(B_2 - B_1)\, q_{(2)}^* = V_2$, and using (2.64) and (2.66) in (2.67), we get

$$\sum_{j=B_1+1}^{B_2}\sum_{i=B_2+1}^{K} L_i d_{i,j} \leq 0, L_i > 0. \tag{2.68}$$

From (2.66) and (2.68) it can be concluded that

$$d_{i,j} = 0, \quad \forall i \in [B_2 + 1 : K]\,, \ \forall j \in [B_1 + 1 : B_2]\,. \tag{2.69}$$

As $\mathbf{D}$ is doubly stochastic, using (P1) together with (2.64) and (2.69), we have

$$\hat{q}_j = q^*_{(2)} \sum_{i=B_1+1}^{B_2} d_{i,j} = q^*_{(2)} = q^*_j, \forall j \in [B_1+1 : B_2]\,. \tag{2.70}$$

Again, since $\mathbf{D}$ is doubly stochastic, using (2.64) and (2.69),

$$\begin{aligned} &\sum_{i=B_1+1}^{B_2} \sum_{j=1}^{K} d_{i,j} = B_2 - B_1, \\ &\sum_{i=B_1+1}^{B_2} d_{i,j} = 1,\ \forall j \in [B_1+1 : B_2]\,. \end{aligned} \tag{2.71}$$

We can rewrite (2.71) as

$$\sum_{i=B_1+1}^{B_2} \sum_{j=1}^{K} d_{i,j} = \sum_{i=B_1+1}^{B_2} \sum_{j=B_1+1}^{B_2} d_{i,j} + \sum_{i=B_1+1}^{B_2} \sum_{j=B_2+1}^{K} d_{i,j}. \tag{2.72}$$

From (2.72) we can see that

$$\sum_{i=B_1+1}^{B_2} \sum_{j=B_2+1}^{K} d_{i,j} = 0, \tag{2.73}$$

and hence,

$$d_{i,j} = 0, \forall i \in [B_1+1 : B_2] \text{ and } \forall j \in [B_2+1 : K]\,. \tag{2.74}$$

Continuing this approach for $i = 3, ..., (|\mathcal{S}| - 1)$, we get $\hat{\boldsymbol{q}} = \boldsymbol{q}^*$. Since the EH profiles are similar, replacing $\hat{\boldsymbol{q}}$ by $\hat{\boldsymbol{p}}$ and $e^r_j$ by $e^t_j/T$ in the above proof, we reach the similar conclusion for $\hat{\boldsymbol{p}}$, i.e., $\hat{\boldsymbol{p}} = \boldsymbol{p}^*$. Therefore, $[\hat{\boldsymbol{p}}^{\mathrm{T}}\ \hat{\boldsymbol{q}}^{\mathrm{T}}]^{\mathrm{T}} = [\boldsymbol{p}^{*\mathrm{T}}\ \boldsymbol{q}^{*\mathrm{T}}]^{\mathrm{T}}$.

### 2.8.5 Proof of Lemma 4

Assume that at least one of the $p_k, q_k$ is not monotonically increasing in $k$. Without loss of generality (w.l.o.s) we consider the cases in which $p_k > p_{k+1}, q_k \geq q_{k+1}$ and $p_k < p_{k+1}, q_k > q_{k+1}$. In the case of $p_k > p_{k+1}, q_k \geq q_{k+1}$, we can construct a new feasible policy,

$$\begin{aligned} \tilde{p}_k = \tilde{p}_{k+1} &= \frac{p_k + p_{k+1}}{2}, \\ \tilde{q}_k = \tilde{q}_{k+1} &= \frac{q_k + q_{k+1}}{2}. \end{aligned} \tag{2.75}$$

Since the objective function is concave, by Jensen's inequality, the new policy strictly increases the objective. Finally considering the case where $p_k < p_{k+1}, q_k > q_{k+1}$, we can construct another feasible policy,

$$\begin{aligned} \tilde{p}_k = p_k,\ \tilde{p}_{k+1} = p_{k+1}, \\ \tilde{q}_k = q_{k+1},\ \tilde{q}_{k+1} = q_k. \end{aligned} \tag{2.76}$$

The function $R^{ub}$ with variables $p, q, \tau$ can be written as,

$$R^{ub}(p,q,\tau) = t\log_2\left(1+\left(\frac{1}{t}+\frac{p}{t^2}\right)f\right), \tag{2.77}$$

where $f \triangleq M-(M-1)\left(1+\frac{q}{\tau\sigma^2}\right)^{\frac{-\tau}{M-1}}$, $t \triangleq 1-\frac{\tau}{T}$ and $0 \le \tau < T$. The second order partial derivative of $R^{ub}(p,q,\tau)$ is given by,

$$\frac{\partial^2 R^{ub}}{\partial p \partial q} = \frac{\frac{\partial f}{\partial q}}{t\left(1+f/t+pf/t^2\right)^2}. \tag{2.78}$$

Since $f$ is monotonic in $q$, (2.78) is positive. As $\frac{\partial^2 R^{ub}}{\partial p \partial q} > 0$, by the definition of derivative,

$$\begin{aligned} R^{ub}(p,q,\tau) + R^{ub}(p+\delta, q+\alpha, \tau) > \\ R^{ub}(p+\delta,q,\tau) + R^{ub}(p,q+\alpha,\tau),\ \delta,\alpha>0. \end{aligned} \tag{2.79}$$

Since (2.79) holds for all $0 \le \tau < T$, we have

$$\begin{aligned} \tilde{R}^{ub}(p,q) + \tilde{R}^{ub}(q+\delta, q+\alpha) > \\ \tilde{R}^{ub}(p+\delta,q) + \tilde{R}^{ub}(p,q+\alpha), \end{aligned} \tag{2.80}$$

where $\tilde{R}^{ub}$ is obtained by,

$$\tilde{R}^{ub}(p,q) = \max_{\tau} R^{ub}(p,q,\tau). \tag{2.81}$$

Finally, using (2.76) and (2.80) we can see that the newly constructed policy strictly increases the objective.

### 2.8.6 Proof of Lemma 5

Let us assume that the transmission rates in the $k$-th and the $k+1$-th intervals are different, i.e., $\tilde{R}^{ub}(p_k,q_k) \neq \tilde{R}^{ub}(p_{k+1},q_{k+1})$. Before the $k+1$-th interval, the energy in the buffers of TX and the RX are $\Delta_r \triangleq \sum_{i=1}^{k} e_i^r - L\sum_{i=1}^{k} q_i$ and $\Delta_t \triangleq \sum_{i=1}^{k} e_i^t - LT\sum_{i=1}^{k} p_i$, respectively. W.l.o.s, we assume that $\Delta_r \le \Delta_t$. We can construct another feasible policy

$$\begin{aligned} \tilde{p}_k = p_k+\delta,\ \tilde{p}_{k+1} = p_{k+1}-\delta, \\ \tilde{q}_k = q_k+\delta,\ \tilde{q}_{k+1} = q_{k+1}-\delta, \end{aligned} \tag{2.82}$$

where $\delta$ is chosen such that $\delta < \Delta_r$ and $\tilde{q}_k < \tilde{q}_{k+1}$. Now, (2.82) can be written as

$$\begin{aligned} \tilde{p}_k &= \alpha p_k + (1-\alpha)\, p_{k+1},\ \tilde{p}_{k+1} = (1-\alpha)\, p_k + \alpha p_{k+1}, \\ \tilde{q}_k &= \alpha q_k + (1-\alpha)\, q_{k+1},\ \tilde{q}_{k+1} = (1-\alpha)\, q_k + \alpha q_{k+1}, \end{aligned} \tag{2.83}$$

where $\alpha = 1 - \delta/\left(q_{k+1} - q_k\right)$. Using Jensen's inequality

$$\sum_{j=k}^{k+1} \tilde{R}^{ub}\left(\tilde{p}_j, \tilde{q}_j\right) > \sum_{j=k}^{k+1} \tilde{R}^{ub}\left(p_j, q_j\right), \tag{2.84}$$

which concludes the proof.

### 2.8.7 Proof of Proposition 6

From the proof of Proposition 4, we know that $g\left(y,z\right) = \log_2\left(1 + \left(1+y\right)z\right), (y,z) \in \mathbb{R}_+^2$ is concave for $y \geq 0, z \geq 1$.

Reproducing the ergodic rate bound in (2.45), we have

$$R_k^{ub} = \log_2\left[1 + \left(1 + \frac{p_k}{\left(1 - \frac{1}{T}\right)}\right) f_k\right]. \tag{2.85}$$

where $f_k \triangleq \left(M - (M-1)\frac{1}{(1+q_k/\sigma^2)}\right)$.

The function $f_k$ can be easily shown to be concave. Using Lemma 1 with $g\left(y,z\right)$ and $f_k$, we can see that $R_k^{ub}$ is concave. Since the objective function in (2.45) is the summation of $R_k^{ub}$'s, it is also concave.

# Chapter 3

# Training Optimization in TDD MISO Broadcast Channels

## 3.1 Introduction

The downlink (DL) of a wireless communication system in which a multi-antenna transmitter (TX) communicating with multiple single antenna user terminals can be modeled as a MISO broadcast channel. Unlike the p2p MIMO communication channels, channel state information (CSI) at the TX in MISO broadcast channels is essential in achieving the large throughput gains as it allows the TX to serve multiple users in parallel [46], [53]. However, perfect CSI is an ideal assumption, and in practice this information must be acquired by the TX, which consumes resources of a communication system. In contrast to the p2p channels, studies in [46], [47] have shown that the quality of the CSI should be increased with the increase in transmission power to obtain the throughput gains.

In this chapter, we consider a MISO broadcast channel with EH user terminals. The work in [54] also considers a similar setting, but [54] uses a time division transmission strategy in which at each time based on the CSI obtained form the EH users, only the user with the largest channel gain is served. In this work we consider transmission schemes which use multi-antenna precoding techniques. Specifically, we consider a time-division-duplex (TDD) system where the DL channel can be estimated using the training sequences sent by the user terminals in the uplink (UL). Based on the obtained CSI, the TX designs a zero-forcing (ZF) precoding filter that reduces the inter-user interference. Training schemes that optimize the throughput are designed under the energy harvesting constraints at the user

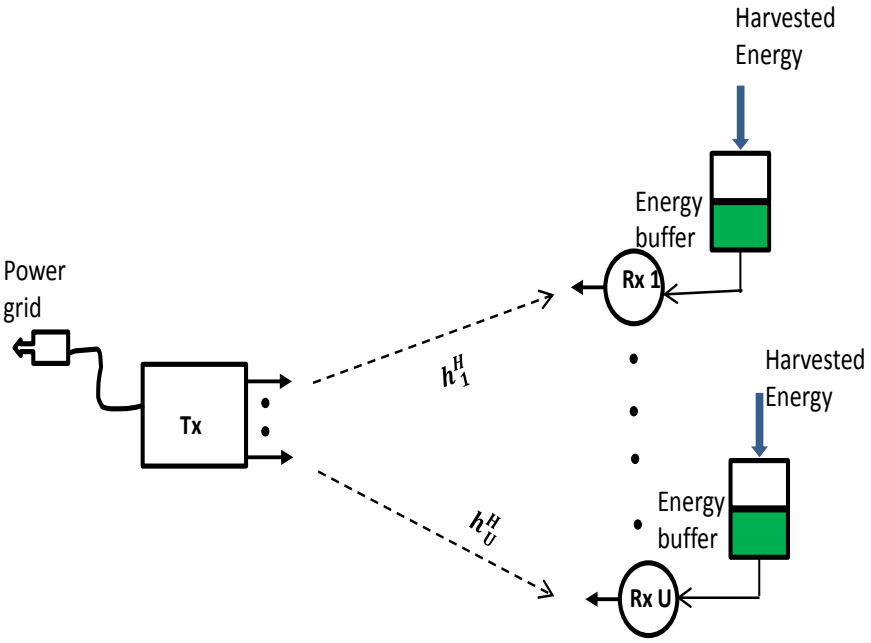


FIGURE 3.1 – MISO broadcast channel with EH user terminals.

terminals.

The main contributions of this chapter are the following :

- We derive an approximation of the ergodic sum rate and show that it is a concave function of the energy consumed in sending the pilot symbols.
- Using the offline optimization framework a lower bound on the throughput is obtained.
- A low complexity heuristic greedy algorithm is proposed whose performance is quite close to the optimal scheme.

## 3.2 System model

We consider a multiuser MISO system with one Base station (BS) equipped with $M$ antennas and $U \leq M$ single-antenna user terminals (UTs). Users harvest energy from the environment while the BS is connected to a fixed power supply as shown in the Fig. 3.1.

### 3.2.1 Energy Harvesting Model

The total observation time is divided into $K$ equal length EH intervals. At the beginning of the $k$-th EH interval, $k \in [1 : K]$, energy packet of size $e_{u,k}$ units arrives at the $u$-th UT. At each node, this energy is first stored in an infinite size energy buffer. We assume that all the harvested energy at

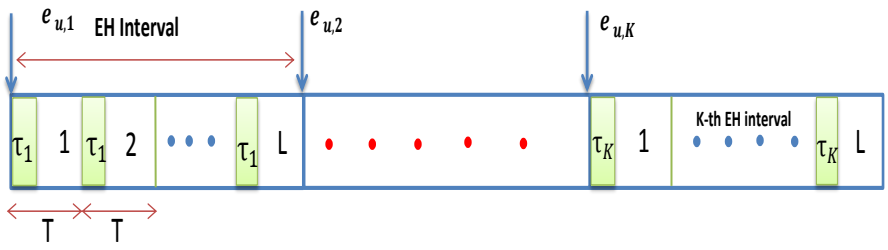


FIGURE 3.2 – Energy harvesting time frame structure of the $u$-th user.

the UTs is used for communication purposes, i.e., in providing channel state information to the BS.

### 3.2.2 Communication System Model

Each EH interval consists of $L$ data frames, each of length $T$ channel uses. We assume a block fading channel model. The channel between the BS and UTs is constant during $T$ channel uses of each frame, but changes in an independent and identically distributed (i.i.d.) fashion from one frame to another. The time frame structure is shown in Fig. 3.2.

The BS has $M > 1$ antennas, while all the UTs have a single antenna. The received signal by the $u$-th user on a given channel use in the $k$-th EH interval is given by

$$y_{u,k} = \boldsymbol{h}_{u,k}^{\mathrm{H}} \sum_{u=1}^{A_k} \boldsymbol{w}_{u,k} s_u + \eta_u, \tag{3.1}$$

where $A_k$ represents the number of active users in the $k$-th EH interval, $A_k = 1, 2, \ldots, U$, $\boldsymbol{h}_{u,k} \in \mathbb{C}^{M\times 1}$ represents the vector of channel coefficients from the BS to the $u$-th UT with i.i.d. $\mathcal{CN}(0,1)$ elements, $\boldsymbol{w}_{u,k} \in \mathbb{C}^{M\times 1}$ and $s_u \sim \mathcal{CN}(0, p_u)$ are the precoding vector and transmitted symbol of the $u$-th UT, and $\eta_u \sim \mathcal{CN}(0,1)$ represents the noise at the $u$-th UT. We assume equal power allocation among the active users, i.e., $\mathrm{E}|s_u|^2 = \frac{P}{A_k}$, where $P$ is the average transmission power constraint at the BS.

### 3.2.3 Channel Estimation and Transmission

We consider a TDD system in which the UL and DL use the same band in a time-sharing fashion. Therefore, BS can estimate the DL channel matrix from the known pilot symbols sent by the UTs in the UL. In each frame of the $k$-th EH interval, $\tau_k$ channel uses are dedicated for sending UL pilot symbols, and in the remaining $T - \tau_k$ channel uses, BS sends data to the UTs in DL exploiting the obtained CSI.

The imperfect CSI (of the $u$-th user) obtained by the BS on a given channel use in the EH interval $k$ is modeled as , [46]

$$\boldsymbol{h}_{u,k} = \sqrt{1 - \delta_{u,k}^2}\hat{\boldsymbol{h}}_{u,k} + \delta_{u,k}\boldsymbol{e}_{u,k}, \tag{3.2}$$

where the elements of $\hat{\boldsymbol{h}}_{u,k}$ and $\boldsymbol{e}_{u,k}$ are i.i.d. with $\mathcal{CN}(0,1)$, moreover the channel estimate $\hat{\boldsymbol{h}}_{u,k}$ and the estimation are $\boldsymbol{e}_{u,k}$ independent. Using the minimum mean square error (MMSE) estimation, the channel estimation error variance is given by [46]

$$\delta_{u,k}^2 = \frac{1}{1 + \tau_k p_{u,k}/\sigma^2}, \tag{3.3}$$

where $p_{u,k}$ is the power used in sending pilot symbols by the $u$-th user in each frame belonging to EH interval $k$ , and $\sigma^2$ is the UL Gaussian noise variance, which is assumed to be unity in the remainder of this chapter.

The whole multiuser channel matrix of the system is

$$\mathbf{H}_k = [\boldsymbol{h}_{1,k}, \boldsymbol{h}_{2,k}, \ldots, \boldsymbol{h}_{A_k,k}]^{\mathrm{H}}. \tag{3.4}$$

Similarly, the channel estimate matrix $\hat{\mathbf{H}}_k$ can be formed with the $u$-th row being $\sqrt{1 - \delta_{u,k}^2}\hat{\boldsymbol{h}}_{u,k}^{\mathrm{H}}$. Using the channel estimate $\hat{\mathbf{H}}_k$, the BS designs the ZF precoder

$$\mathbf{W}_k = \frac{\hat{\mathbf{H}}_k^{\mathrm{H}}\left(\hat{\mathbf{H}}_k\hat{\mathbf{H}}_k^{\mathrm{H}}\right)^{-1}}{\left\|\hat{\mathbf{H}}_k^{\mathrm{H}}\left(\hat{\mathbf{H}}_k\hat{\mathbf{H}}_k^{\mathrm{H}}\right)^{-1}\right\|} \tag{3.5}$$

With perfect CSI, ZF precoding results in complete removal of interference at the users. Although suboptimal at low signal-to-noise ratio (SNR), due to the analytical tractability, we focus on ZF precoder in this chapter. Note that ZF precoding is asymptotically optimal for large number of users [55], [56].

### 3.2.4 User Activity

As mentioned in the communication system model, in each EH interval $1 \leq A_k \leq U$ users are served by the BS. The user activity over the EH

intervals is modeled as a matrix $\mathcal{A}_{U\times K}$ with its elements $a_{u,k} \in \{0,1\}$ and has at least one non-zero element in each column. If UT $u$ is active and it is served by the BS in the $k$-th EH interval, then $a_{u,k} = 1$ and it will participate in sending pilot symbols in the UL. If $a_{u,k} = 0$ then the UT is not served by the BS and therefore $p_{u,k} = 0$ i.e., UT $u$ remains silent and will not send any pilot symbols in the $k$-th EH interval. The total number of active users in the $k$-th EH interval, $A_k = \sum_{u=1}^{U} a_{u,k}$.

### 3.2.5 Performance Metric

We assume that the length of the EH interval is very large compared to the channel coherence time (i.e., $L$ is very large). As a result, the achievable ergodic rate for the $u$-th user in the $k$-th EH interval is given by

$$R_{u,k} = \begin{cases} 0, \text{ if } a_{u,k} = 0 \\ t_k \, \mathrm{E}_{\boldsymbol{e}_{u,k},\hat{\boldsymbol{h}}_{u,k}} \log\left(1 + \frac{\frac{P}{t_k A_k} S_{u,k}}{1+\frac{P}{t_k A_k} I_{u,k}}\right), \text{ if } a_{u,k} = 1 \end{cases} \tag{3.6}$$

where the signal term $S_{u,k} = |\boldsymbol{h}_{u,k}^{\mathrm{H}} \boldsymbol{w}_{u,k}|^2$, the interference term $I_{u,k} = \sum_{j\neq u} |\boldsymbol{h}_{u,k}^{\mathrm{H}} \boldsymbol{w}_{j,k}|^2$, and $t_k \triangleq \left(1 - \frac{\tau_k}{T}\right)$. Note that since the BS is silent for the first $1 - t_k$ fraction of the total time $T$, by transmitting with power $\frac{P}{t_k}$ in the remaining fraction, the average transmission power is maintained at $P$.

## 3.3 Throughput maximization

The problem of maximizing the sum throughput of the users by the end of the $K$-th EH interval can be formulated as

$$\underset{p_{u,k},\tau_k,\mathcal{A}}{\text{maximize}} \quad \sum_{k=1}^{K}\sum_{u=1}^{U} R_{u,k} \tag{3.7a}$$

$$\text{s.t.} \quad L\sum_{j=1}^{l} \tau_j a_{u,j} p_{u,j} \leq \sum_{j=1}^{l} e_{u,j}, \ \forall u \in [1:U], \ \forall l \in [1:K] \tag{3.7b}$$

$$A_k \leq \tau_k < T, \ \tau_k \in \mathbb{N}, \ \forall k \in [1:K] \tag{3.7c}$$

$$p_{u,k} \geq 0, \ \forall k \in [1:K], \ \forall u \in [1:U] \tag{3.7d}$$

The constraints (3.7b) guarantee the *energy neutrality* of the system, i.e., at each node, energy consumed can not be more than the energy harvested till that time. Also, note that $A_k$ is the minimum number of training symbols required, due to the orthogonality of the pilot sequences [46].

The above problem is difficult to solve efficiently due to the following reasons. Since the optimization is over the set $\mathcal{A}$, which has binary variables $a_{u,k}$, it is a combinatorial optimization problem. Even if the user activity matrix is fixed, the optimization problem is not convex due to the constraints in

(3.7b), and also it is hard to get an insight on the convexity of the objective function which involves the joint expectation of several random variables. To overcome these difficulties, in the next section we formulate optimization problems using an approximation on the ergodic rate as the objective function. For a given user activity matrix $\mathcal{A}$, we show that these modified optimization problems are convex, then a greedy algorithm is proposed to reduce the complexity of optimization over $\mathcal{A}$.

### 3.3.1 Approximation

In this section, we use an approximation of the ergodic rate as the objective function for the throughput maximization problem. We first analyze the statistical properties of the signal and interference terms in the ergodic rate expression in (3.6) for the active user. Using the channel estimation model in (3.2), the signal term can be written as

$$\begin{aligned} S_{u,k} &= \frac{P}{t_k A_k} \left| \boldsymbol{h}_{u,k}^{\mathrm{H}} \boldsymbol{w}_{u,k} \right|^2 \\ &= \frac{P}{t_k A_k} \left| \sqrt{1-\delta_{u,k}^2}\, \hat{\boldsymbol{h}}_{u,k}^{\mathrm{H}} \boldsymbol{w}_{u,k} + \delta_{u,k} \boldsymbol{e}_{u,k}^{\mathrm{H}} \boldsymbol{w}_{u,k} \right|^2 \end{aligned} \tag{3.8}$$

Now the average of this signal term is given by

$$\begin{aligned} \mathrm{E}\left[S_{u,k}\right] &= \frac{P}{t_k A_k} \mathrm{E}_{\boldsymbol{e}_{u,k}, \hat{\boldsymbol{h}}_{u,k}} \left| \sqrt{1-\delta_{u,k}^2}\, \hat{\boldsymbol{h}}_{u,k}^{\mathrm{H}} \boldsymbol{w}_{u,k} + \delta_{u,k} \boldsymbol{e}_{u,k}^{\mathrm{H}} \boldsymbol{w}_{u,k} \right|^2 \\ &\overset{(a)}{=} \frac{P}{t_k A_k} \mathrm{E} \left( \left| \sqrt{1-\delta_{u,k}^2}\, \hat{\boldsymbol{h}}_{u,k}^{\mathrm{H}} \boldsymbol{w}_{u,k} \right|^2 + \left| \delta_{u,k} \boldsymbol{e}_{u,k}^{\mathrm{H}} \boldsymbol{w}_{u,k} \right|^2 \right) \\ &\overset{(b)}{=} \frac{P}{t_k A_k} \left[ (M - A_k + 1) \left(1-\delta_{u,k}^2\right) + \delta_{u,k}^2 \right] \end{aligned} \tag{3.9}$$

where

(a) follows from the facts that $\boldsymbol{e}_{u,k}$ and $\hat{\boldsymbol{h}}_{u,k}$ are independent with zero mean, and $\boldsymbol{e}_{u,k}$ and $\boldsymbol{w}_{u,k}$ are also independent,

(b) follows from the facts that the unit norm ZF precoding vector $\boldsymbol{w}_{u,k}$ is the projection of $\hat{\boldsymbol{h}}_{u,k}$ on the Null space of dimension $M - A_k + 1$ spanned by $\boldsymbol{h}_{u \neq j}, k = 1, \ldots, A_k$, therefore $|\hat{\boldsymbol{h}}_{u,k}^{\mathrm{H}} \boldsymbol{w}_{u,k}|^2$ is a chi-square random variable with $2(M - A_k + 1)$ degrees of freedom i.e., $|\hat{\boldsymbol{h}}_{u,k}^{\mathrm{H}} \boldsymbol{w}_{u,k}|^2 \sim \chi^2_{2(M-A_k+1)}$ [57], [58]. Since $\boldsymbol{w}_{u,k}$ is independent of $\boldsymbol{e}_{u,k}$, $|\boldsymbol{e}_{u,k}^{\mathrm{H}} \boldsymbol{w}_{u,k}|^2 \sim \chi^2_2$ [57], [58].

Similarly, using (3.2), the interference term can be written as

$$\begin{aligned} I_{u,k} &= \frac{P}{t_k A_k} \sum_{j \neq u} \left| \boldsymbol{h}_{u,k}^{\mathrm{H}} \boldsymbol{w}_{j,k} \right|^2 \\ &= \frac{P}{t_k A_k} \sum_{j \neq u} \left| \sqrt{1-\delta_{u,k}^2}\, \hat{\boldsymbol{h}}_{u,k}^{\mathrm{H}} \boldsymbol{w}_{j,k} + \delta_{u,k} \boldsymbol{e}_{u,k}^{\mathrm{H}} \boldsymbol{w}_{k,j} \right|^2 \\ &\overset{(a)}{=} \frac{P}{t_k A_k} \delta_{u,k}^2 \sum_{j \neq u} \left| \boldsymbol{e}_{u,k}^{\mathrm{H}} \boldsymbol{w}_{j,k} \right|^2 \\ &\overset{(b)}{=} \frac{P}{t_k A_k} \delta_{u,k}^2 \sum_{j \neq u} Y_j \end{aligned} \tag{3.10}$$

where $Y_j = \left| \boldsymbol{e}_{u,k}^{\mathrm{H}} \boldsymbol{w}_{j,k} \right|^2$ and $Y_j \sim \chi_2^2$. Here

(a) follows from the fact that ZF precoding vector $\boldsymbol{w}_{j,k}$ is orthogonal to $\hat{\boldsymbol{h}}_{u,k}$,

(b) follows from the fact that $\boldsymbol{w}_{j,k}$ is independent of $\boldsymbol{e}_{u,k}$, $|\boldsymbol{e}_{u,k}^{\mathrm{H}} \boldsymbol{w}_{j,k}|^2 \sim \chi_2^2$ [57], [58].

The average of this interference term is given by

$$\mathrm{E}\left[I_{u,k}\right] = \frac{P}{t_k A_k} \left(A_k - 1\right) \delta_{u,k}^2.$$

An approximation of the ergodic rate of active user in (3.6), $R_{u,k}^a \approx R_{u,k}$, is given by

$$\begin{aligned} R_{u,k}^a &\overset{(a)}{=} t_k \, \mathrm{E}_{\boldsymbol{e}_{u,k}, \hat{\boldsymbol{h}}_{u,k}} \log \left( 1 + \frac{\frac{P}{t_k A_k} (1-\delta_{u,k}^2) \left| \hat{\boldsymbol{h}}_{u,k}^{\mathrm{H}} \boldsymbol{w}_{u,k} \right|^2}{1 + \frac{P}{t_k A_k} \sum_{j \neq u} \left| \boldsymbol{h}_{u,k}^{\mathrm{H}} \boldsymbol{w}_{j,k} \right|^2} \right) \\ &\overset{(b)}{=} t_k \, \mathrm{E} \log \left( 1 + \frac{\frac{P}{t_k A_k} h\left(\tau_k, p_{u,k}\right) Y_u}{1 + \frac{P}{t_k A_k} g\left(\tau_k, p_{u,k}\right) \sum_{j \neq u} Y_j} \right), \end{aligned} \tag{3.11}$$

where $Y_u = |\hat{\boldsymbol{h}}_{u,k}^{\mathrm{H}} \boldsymbol{w}_{u,k}|^2$, $h\left(\tau_k, p_{u,k}\right) \triangleq \left(M - A_k + 1\right) \left(1 - \frac{1}{1+\tau_k p_{u,k}}\right)$ and $g\left(\tau_k, p_{u,k}\right) \triangleq \frac{1}{1+\tau_k p_{u,k}}$. Here

(a) follows from making the error $\boldsymbol{e}_{u,k} = 0$ in the signal term of $R_{u,k}$ in (3.6),

(b) follows from substituting (3.3) and (3.10).

Using (3.11) as the objective function, the modified optimization problem can be written as

$$\underset{p_{u,k},\tau_k,\mathcal{A}}{\text{maximize}} \quad \sum_{k=1}^{K}\sum_{u=1}^{U} R_{u,k}^{a} \tag{3.12a}$$

$$\text{s.t.} \quad L\sum_{j=1}^{l}\tau_j a_{u,j}p_{u,j} \leq \sum_{j=1}^{l} e_{u,j},\ \forall u \in [1:U],\ \forall l \in [1:K] \tag{3.12b}$$

$$A_k \leq \tau_k < T,\ \tau_k \in \mathbb{N},\ \forall k \in [1:K] \tag{3.12c}$$

$$p_{u,k} \geq 0,\ \forall k \in [1:K],\ \forall u \in [1:U] \tag{3.12d}$$

Note that is still hard to solve as it involves binary variables $a_{u,k}$'s and the constraints in (3.12b) and (3.12c) are not convex. However, we now show that (3.12) can be simplified. We start with the following lemma.

**Lemma 8.** *The function*

$$g\left(x\right) = x\log\left(1+\frac{a+b}{x}\right) - x\log\left(1+\frac{b}{x}\right),\ a \geq 0,\ b \geq 0 \tag{3.13}$$

*is monotonically increasing for* $x > 0$.

*Proof.* The derivative of $g$ is

$$g^{'}\left(x\right) = \log\left(1+\frac{a+b}{x}\right) - \frac{\frac{a+b}{x}}{1+\frac{a+b}{x}} - \left[\log\left(1+\frac{b}{x}\right) - \frac{b/x}{1+b/x}\right]. \tag{3.14}$$

Using the fact that $f\left(y\right) = \log\left(1+y\right) - \frac{y}{1+y}$ is a monotonically increasing function and $f\left(y\right) > 0, \forall y > 0$, we conclude that $g^{'}\left(x\right) > 0, x \neq 0$ and hence $g\left(x\right)$ is a monotonically increasing function. □

**Proposition 8.** *Let* $\tau_k^*$ *be the optimal solution of (3.12), then* $\tau_k^* = A_k$

*Proof.* For a fixed value of $q_{u,k} = \tau_k p_{u,k}$, if $R_{u,k}^{a}$ is monotonically decreasing function of $\tau_k$, then $\tau_k^* = A_k$. The approximation $R_{u,k}^{a}$ in terms of $q_{u,k} = \tau_k p_{u,k}$ can be written as

$$R_{u,k}^{a}\left(t_k\right) = t_k\log\left(1+\frac{a+b}{t_k}\right) - t_k\log\left(1+\frac{b}{t_k}\right), \tag{3.15}$$

where $a = \frac{P}{A_k}Y_u\left(1-\frac{1}{1+q_{u,k}}\right)$ and $b = \frac{P}{A_k}\frac{1}{1+q_{u,k}}\sum_{j\neq u}Y_j$. From Lemma 1 and (3.15), we conclude that $R_{u,k}^{a}$ is monotonically increasing function of $t_k$ for fixed $q_{u,k}$, and hence monotonically decreasing in $\tau_k$. □

Using the above result, (3.12) can be simplified to

$$\underset{q_{u,k},\mathcal{A}}{\text{maximize}} \quad \sum_{k=1}^{K}\sum_{u=1}^{U}\hat{R}^{a}_{u,k} \tag{3.16a}$$

$$\text{s.t.} \quad L\sum_{j=1}^{l}a_{u,j}q_{u,j} \leq \sum_{j=1}^{l}e_{u,j},\ \forall u \in [1:U],\ \forall l \in [1:K] \tag{3.16b}$$

$$q_{u,k} \geq 0,\ \forall k \in [1:K],\ \forall u \in [1:M] \tag{3.16c}$$

where, $\hat{R}^{a}_{u,k} = 0$ for $a_{u,k} = 0$ and for $a_{u,k} = 1$

$$\hat{R}^{a}_{u,k} = \hat{t}_k \,\mathrm{E}\log\left(1 + \frac{\frac{PY_k}{\hat{t}_k A_k}\left(1-\hat{g}\left(q_{u,k}\right)\right)}{1+\frac{P}{\hat{t}_k A_k}\hat{g}\left(q_{u,k}\right)\sum_{j\neq u}Y_j}\right), \tag{3.17}$$

$\hat{g}\left(q_{u,k}\right) \triangleq \frac{1}{1+q_{u,k}}$ and $\hat{t}_k \triangleq \left(1-\frac{A_k}{T}\right)$.

**Proposition 9.** *For a given user activity matrix $\mathcal{A}$, the objective function of the optimization problem (3.16) is concave.*

*Proof.* Rewriting (3.17) for the active user,

$$\hat{R}^{a}_{u,k} = \hat{t}_k \,\mathrm{E}\log\left(1 + a\left(1-\frac{b}{q_{u,k}+b}\right)\right), \tag{3.18}$$

where $a = \frac{PY_u}{\hat{t}_k A_k} \geq 0$ and $b = 1 + \frac{P\sum_{j\neq u}Y_j}{\hat{t}_k A_k} \geq 0$. Since expectation is a linear operation, and the distributions of $\sum_{j\neq u}Y_j$ and $Y_u$ are not functions of $q_{u,k}$, it can be easily seen that $\hat{R}^{a}_{u,k}$ is a concave function. Since the objective is summation of $\hat{R}^{a}_{u,k}$'s, it is also concave. □

Since the objective function is convex and the constraints in (3.16b) are linear for a given $\mathcal{A}$, it has a unique maximizer [48]. Also, note that for a given $\mathcal{A}$, the optimization problem (3.16) is separable in terms of the users as the rate of $k$-th user $\hat{R}^{a}_{u,k}$ depends only on $q_{u,k}$. Using the concavity of the objective function, we can show that for certain $\mathcal{A}$'s the optimal energy allocation can be obtained using a simple algorithm.

We start by introducing some notation. Let $\mathcal{D}_u$ be the set of EH interval indices where the $u$-th user is active, i,e., $\mathcal{D}_u = \{k : a_{u,k} = 1\}$. The number of elements in the set $\mathcal{D}_u$ is denoted by $|\mathcal{D}_u|$. The matrix $\mathbf{I}_K\left(\mathcal{D}_u\right)$ is obtained by keeping only the columns with indices in $\mathcal{D}_u$ from the $K \times K$ identity matrix $\mathbf{I}_K$. If $a_{u,k} = 0$, then there is no incentive for the $u$-th user to send pilot symbols in this interval, therefore, without loss of optimality we only consider optimal energy allocation schemes where $q^{*}_{u,k} = 0, \forall k \notin \mathcal{D}_u$.

Let $\tilde{\boldsymbol{q}}_u = [\tilde{q}_{u,1}, \ldots, \tilde{q}_{u,|\mathcal{D}_u|}]$ be the vector obtained by removing the elements $q_{u,k} = 0$ from $\boldsymbol{q}_u$. Mathematically,

$$\tilde{\boldsymbol{q}}_u = \boldsymbol{q}_u \mathbf{I}_K(\mathcal{D}_u), \tag{3.19}$$

where $\boldsymbol{q}_u = [q_{u,1}, q_{u,2}, \ldots, q_{u,K}]$. For example, if $K = 4$ and $\boldsymbol{a}_u = [1, 0, 1, 0]$, then $\tilde{\boldsymbol{q}}_u = [q_{u,1}, q_{u,3}]$. Since $q^*_{u,k} = 0, \forall k \notin \mathcal{D}_u$, we can rewrite the objective function in (3.17) for the $u$-th user as

$$\sum_{k=1}^{|\mathcal{D}_u|} \hat{R}^a(\tilde{q}_{u,k}). \tag{3.20}$$

Now we focus on the constraints in (3.17). These constraints can be modified into an equivalent form using the energy allocation $\tilde{\boldsymbol{q}}$ and an EH profile $\tilde{\boldsymbol{e}}_u$ as described below. Suppose there exists $j \in [1 : K]$ and $l \in [1 : j]$ such that $a_{u,j} = 1$ and $a_{u,j-l} = 0$, then $q^*_{u,m} = 0,\ j - l \leq m \leq j - 1$. Since the harvested energy can only be used in future time slots this is equivalent to a new EH profile where $e_{u,m} = 0, j - l \leq m \leq j - 1$ and $e_{u,j} = \sum_{m=j-l}^{j} e_{u,m}$. Therefore the new EH profile with $e_{u,k} = 0$ for $a_{u,k} = 0$, and the non-zero elements obtained by the above procedure is equivalent to the original EH profile. Let $\tilde{\boldsymbol{e}}_u$ denote the modified EH profile of the $u$-th user obtained by

$$\tilde{\boldsymbol{e}}_u = \boldsymbol{e}_u \mathbf{B}\mathbf{I}_K(\mathcal{D}_u), \tag{3.21}$$

where, the matrix

$$\mathbf{B}(l,k) = \begin{cases} 1, \forall l \in [k - j + 1 : k], \text{ if } a_{u,k} = 1,\ a_{u,k-j} = 1, \text{ and } a_{u,l} = 0 \\ 0, \text{otherwise.} \end{cases} \tag{3.22}$$

For example, consider a case where $K = 4$ and $\boldsymbol{e}_u = [e_{u,1}, e_{u,2}, e_{u,3}, e_{u,4}]$. If $\boldsymbol{a}_u = [1, 0, 1, 0]$, then the modified EH profile is $\tilde{\boldsymbol{e}}_u = [e_{u,1}, e_{u,2} + e_{u,3}]$.

Using the modified EH profile $\tilde{\boldsymbol{e}}_u$ and the energy allocation $\tilde{\boldsymbol{q}}_u$, for the $u$-th user, the optimization problem can be written as,

$$\underset{\tilde{q}_{u,k}}{\text{maximize}} \quad \sum_{i=1}^{|\mathcal{D}_u|} \hat{R}^a(\tilde{q}_{u,k}) \tag{3.23a}$$

$$\text{s.t.} \quad \sum_{j=1}^{l} \tilde{q}_{u,j} \leq \sum_{j=1}^{l} \frac{\tilde{e}_{u,j}}{L},\ \forall l \in [1 : |\mathcal{D}_u|] \tag{3.23b}$$

$$\tilde{q}_{u,k} \geq 0,\ \forall k \in [1 : |\mathcal{D}_u|] \tag{3.23c}$$

**Proposition 10.** *If the number of active users are equal in all the EH intervals where user k is active, i.e., $A_k = A, \forall k \in \mathcal{D}_u$ then the energy allocation $\tilde{\boldsymbol{q}}^*_u \preceq \tilde{\boldsymbol{q}}_u,\ \forall \tilde{\boldsymbol{q}}_u$ satisfying* (3.23*b*) *and* (3.23*c*) *is optimal.*

*Proof.* Since the objective function in (3.23) is symmetric and concave in $\tilde{q}_{u,k}$'s, by Theorem 2, $\tilde{\boldsymbol{q}}^*_u \preceq \tilde{\boldsymbol{q}}_u$. The energy vector $\tilde{\boldsymbol{q}}^*_u$ is obtained by using the OEA algorithm given Chapter 2 with the energy profile $\tilde{\boldsymbol{e}}_u$. □

## 3.4 Greedy user activation

The algorithm starts with the initial user activity matrix $\mathcal{A} = \mathbf{1}_{U\times K}$. For this given $\mathcal{A}$, the energy allocation is obtained by solving (3.12). Starting with the first EH interval, at each iteration, the algorithm removes the user $u$ with the smallest training energy $q_{u,1}$ and then solves (3.12) with this updated user activity matrix. If this results in an increase in the objective, the initial user activity matrix is updated. This process is continued until the objective is increased or there is only one active user left in the EH interval. Similar procedure is carried in the next EH interval. The steps are summarized in Algorithm 2 given below.

**Input** : EH intervals $K$ ; Harvested energy $\boldsymbol{e}_k$'s
**Output**: $\mathcal{A}$, $\boldsymbol{q}_k$'s, $\boldsymbol{\tau}$

`// initialization`
$\mathcal{A} := \mathbf{1}_{U\times K}$;
$\tilde{\mathcal{A}} = \mathcal{A}$, $\tau_k = \sum_{u=1}^{U} a_{u,k}, \forall k$.

**for** $k = 1 : K$ **do**
  **while** $\tau_k > 1$ **do**
    (i) Solve (3.12) with $\boldsymbol{e}_k$'s and $\mathcal{A}$
    (ii) $t = \underset{k,a_{u,k}>0}{\arg\min}\ q_{u,k}$
    (iii) Set $\tilde{\mathcal{A}}(t,k) = 0$
    (iv) Solve (3.12) with $\boldsymbol{e}_k$'s and $\tilde{\mathcal{A}}$
    **if** *(Objective is decreased from (i) to (iv))* **then**
      **break** ;
    **end**
    (v) Set $\mathcal{A} = \tilde{\mathcal{A}}$ ;
    (vi) $\tau_k = \sum_{u=1}^{U} a_{u,k}$
  **end**
**end**

**Algorithm 2:** Greedy user activation algorithm

## 3.5 Numerical Results

In this section, numerical simulations are used to illustrate the ergodic rate performance of the proposed training schemes. In Fig. 3.3, throughput of different schemes is shown for various DL SNRs. The number of EH intervals is assumed to be $K = 4$, number of BS antennas $M = 4$ and total number of users $U = 3$, therefore the number of active users in the $k$-th EH interval can be $A_k = \{1, 2, 3\}$. The length of each data frame is $T = 200$ ms. The EH profile is chosen as (normalized by the number of frames $L$ in each EH

interval)

$$\mathbf{E} = \begin{bmatrix} 3 & 15 & 1.5 & 3 \\ 1 & 0.6 & 2 & 6 \\ 20 & 0 & 0 & 0 \end{bmatrix}, \tag{3.24}$$

where each row represents the energy harvested by the user over time. The proposed scheme in Fig. 3.3 represents an achievable ergodic rate, and it is obtained by using the optimal training policy for (3.12). In the scheme where all users are active i.e., $\mathcal{A} = \mathbf{1}_{U\times K}$, the optimal training scheme is obtained by solving (3.12). In the naive scheme, $\mathcal{A} = \mathbf{1}_{U\times K}$, and at each user the energy spent in training is equal to the harvested energy of that user in each EH interval. The optimal energy allocated by the proposed scheme $\mathbf{Q}$ for the EH profile in (3.24) at DL SNR of 25 dB is shown below.

$$\mathbf{Q} = \begin{bmatrix} 3 & 15 & 0 & 0 \\ 0 & 0 & 3.6 & 6 \\ 0 & 20 & 0 & 0 \end{bmatrix}, \tag{3.25}$$

where each row represents the energy allocated for training by the user over time. We can see that the proposed scheme switch-off users with less energy (resulting in poor CSI) in some EH intervals. Also, note that the users with less harvested energy, for example user 2, accumulates the energy in the first few EH intervals by remaining silent, and uses this accumulated energy in the later intervals to provide accurate CSI. These effects are due to the fact that accurate CSI is needed at the BS for achieving higher throughput at high DL SNRs [47], [46].

In Fig. 3.4, we compare the ergodic rate of proposed scheme when all users have high harvested energy. The EH profile is chosen as (normalized by the number of frames $L$ in each EH interval)

$$\mathbf{E} = \begin{bmatrix} 22 & 15.4 & 13.2 & 22 \\ 10 & 6 & 20 & 4 \\ 30 & 15 & 4.5 & 10.5 \end{bmatrix}. \tag{3.26}$$

From Fig. 3.4, it can be seen that the performance of the scheme where all the users are active in all EH intervals is quite close to the one in which optimal user activation is performed. Since all the users have high harvested energy, BS can support more users (because of accurate CSI) for moderately high SNRs as opposed in the previous setting where some users are switched off due to their low harvested energy.

Finally, in Fig. 3.5 we compare the performance of the proposed scheme with the less complex greedy user activation algorithm proposed in Algorithm 2, for the harvested energy profile in (3.24). The greedy user activation outperforms the scheme where all the users are active in each EH interval.

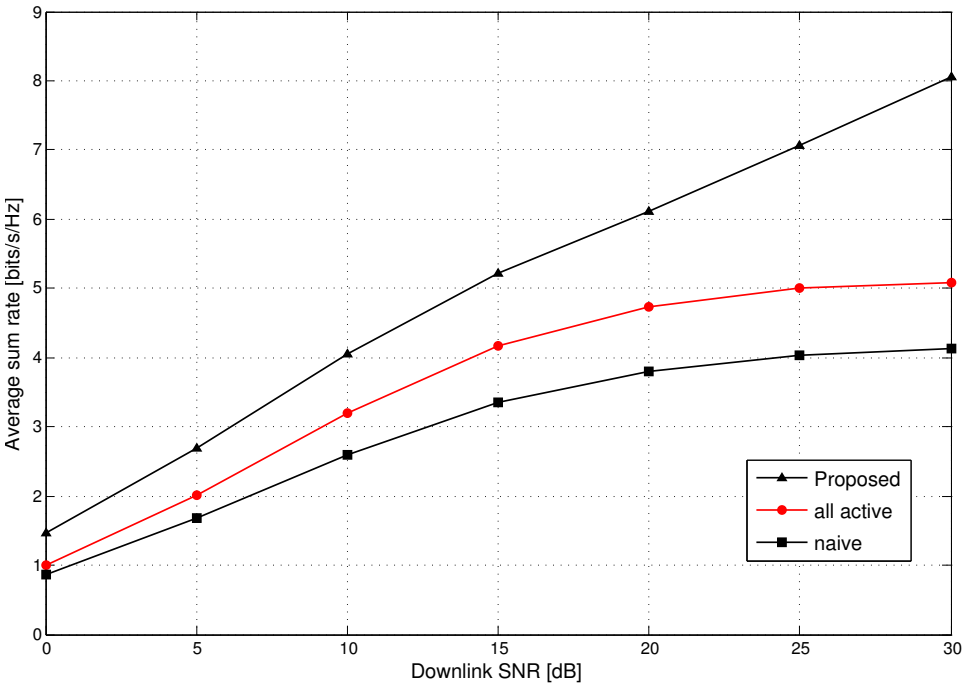


FIGURE 3.3 – Ergodic rate for different policies, $M = 4$, $U = 3$ and $K = 4$.

## 3.6 Conclusion

We have studied the problem of designing training schemes with EH constraints in a MISO broadcast channel when the user terminals harvest energy from the environment. Since the exact expression of the throughput is complicated, a concave approximation has been used as objective function in the formulated optimization problem. The energy allocation policy for sending pilot symbols turns out to be quite different from single user case. Completely turning-off users with less energy (resulting in poor CSI) is optimal in some cases.

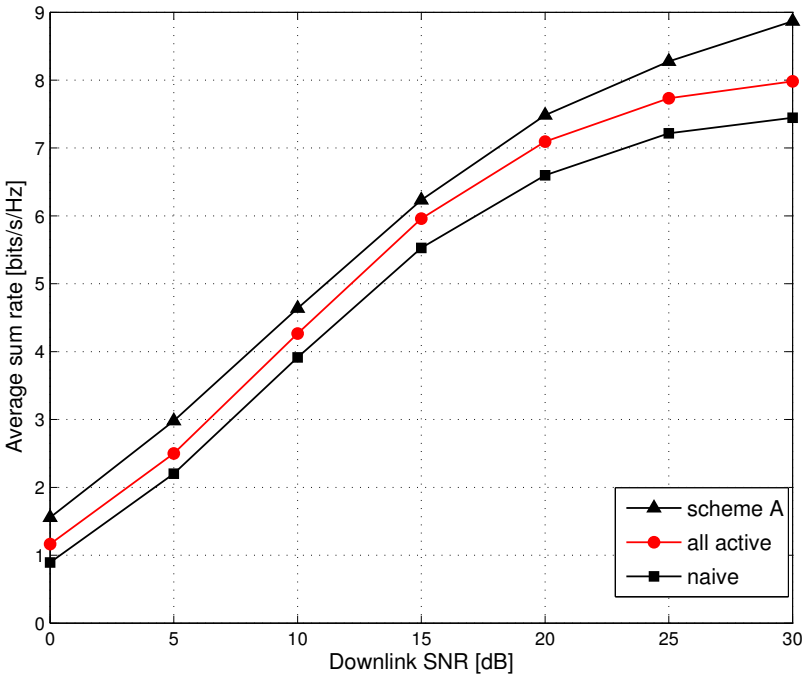


FIGURE 3.4 – Ergodic rate for different policies with high harvested energies, $M = 4$, $U = 3$ and $K = 4$.

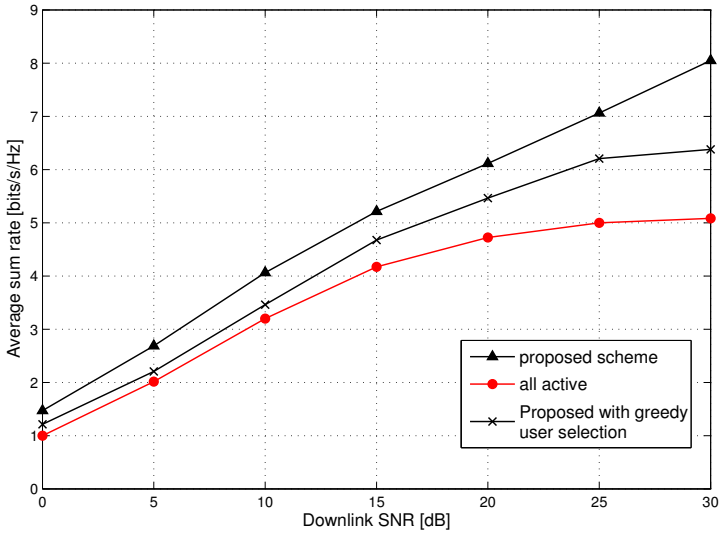


FIGURE 3.5 – Ergodic rate with greedy user activation, $M = 4$, $K = 3$ and $N = 4$.

# Chapter 4

# Distributed Compression and Transmission with Energy Harvesting Sensors

## 4.1 Introduction

A wireless sensor node collects samples from a source (typically a physical phenomenon in its surrounding environment), processes, and communicates these samples to a fusion center over a wireless radio channel. A network of such nodes can be used to gather information about a time varying process that is possibly correlated across space and time. In these settings, the aim is to design transmission and compression schemes which minimize the reconstruction distortion of the source at the fusion center.

Different from the works [18–22] where the focus is on designing transmission schemes that maximize the throughput under the energy harvesting (EH) constraints, the works in [59–61] consider the aspects of source sample acquisition, compression rate and transmission with EH constraints in a point-to-point setting. In [60], the problem of distortion minimization in a fading channel with an EH transmitter is considered. Taking into account the variation in energy arrivals, source variances and channel gains, the optimal compression and transmission rates are found using the offline optimization framework. A simple *directional 2D waterfilling* algorithm is proved to be optimal under a strict delay constraint. In [61], the distortion performance is studied using a stochastic EH model.

In this chapter, we extend the distortion minimization problem to a network setting. To the best of our knowledge, distributed source coding with

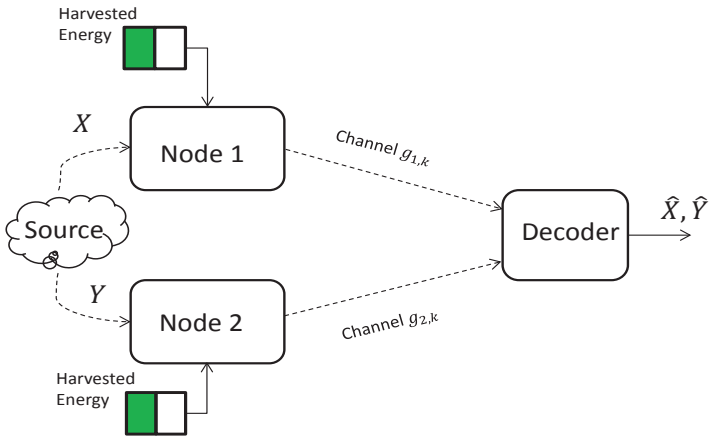


FIGURE 4.1 – Distributed sensing and transmission with EH nodes.

EH nodes from a rate-distortion perspective has not been studied before. Probably [62] is the closest work that considered distributed compressive sensing in an EH sensor network, however, it ignores transmission and coding aspects.

We consider a system of two sensor nodes which observe correlated source samples, and wish to communicate their samples to the destination over orthogonal fading channels with minimum average end-to-end distortion. The goal is to see how the correlation and the EH affect the coordination among the nodes in compression and transmission schemes. The main contribution of this chapter is to characterize the Pareto boundary of the distortion region of the quadratic Gaussian two-encoder source coding problem [63] under EH constraints. As we shall see, the resource allocation policy that optimizes the distortion outperforms the throughput optimization schemes which ignore the variation in source statistics.

## 4.2 System Model

We consider a system consisting of two sensor nodes where each node observes and samples a common physical phenomenon locally, and hence the samples are correlated. Then the nodes send their information to the destination over orthogonal wireless channels as shown in Fig. 4.1. Both nodes harvest energy from the environment, and are equipped with individual energy buffers for storage.

### 4.2.1 Energy Harvesting Model

A time slotted system with $K$ unit duration TSs is considered. At the beginning of the $k$-th TS, $k \in [1:K]$, new energy packets of sizes $e_{1,k}$ and $e_{2,k}$ units arrive at node 1 and 2, respectively. At each node the harvested energy is stored in an infinite size battery and it is used only for communication purposes, i.e., the energy consumed in sampling, compression, etc., is ignored here, and can be considered as an extension. Intially the battery doesnt have any stored energy.

### 4.2.2 Sensing and Communication Model

The observed physical phenomena at the two nodes are modeled as correlated Gaussian random processes. In the $k$-th TS, node 1 and node 2 collect samples $\boldsymbol{x}_k^n = [x_{1,k}, x_{2,k}, \ldots, x_{n,k}]$ and $\boldsymbol{y}_k^n = [y_{1,k}\, y_{2,k}, \ldots, y_{n,k}]$, respectively. The elements of $\boldsymbol{x}_k^n$, $\boldsymbol{y}_k^n$ are independent copies of the random variable $\{(X_k, Y_k)\}$, which is modeled as a bi-variate Gaussian random variable with the following probability density function (PDF) :

$$f_{X_k,Y_k}(x_k, y_k) = \frac{1}{2\pi|\Lambda_k|^{1/2}} \exp\left\{-\frac{1}{2}\boldsymbol{v}_k{}^T \Lambda_k{}^{-1} \boldsymbol{v}_k\right\},$$

where $\boldsymbol{v}_k = [x_k\ y_k]^{\mathrm{T}}$ and the covariance matrix $\Lambda_k$ is given by

$$\Lambda_k = \begin{pmatrix} \sigma_{X_k}^2 & \rho_k \sigma_{X_k}\sigma_{Y_k} \\ \rho_k \sigma_{X_k}\sigma_{Y_k} & \sigma_{Y_k}^2 \end{pmatrix},\ -1 < \rho_k < 1.$$

We assume that the duration of each TS is large enough (i.e., large $n$) to invoke the information theoretic arguments. We consider strict delay constraints, and assume that all samples collected in the beginning of the TS $k$ must be sent to the destination within the same TS.

The sensed data is sent to the destination over orthogonal channels. Each TS consists of $n$ channel uses. The channel between the $i$-th node ($i \in \{1, 2\}$) and the destination in the $k$-th TS is modeled as a memoryless additive white Gaussian noise (AWGN) channel with unit noise variance and a fixed channel gain $g_{i,k}$. Due to the large $n$ assumption, the maximum transmission rate of the $i$-th node in the $k$-th TS is given by $r_{i,k} \triangleq \frac{1}{2}\log_2(1 + g_{i,k}p_{i,k})$ bits/channel use, where $p_{i,k}$ is the average transmission power of node $i$ in $k$-th TS.

Some comments on the general characteristics of the optimal transmission strategies are in order. First, since the energy packets are available only at the beginning of a TS, and the channel gain remains constant throughout a TS, it is not hard to see that constant power transmission is optimal in each TS, while the transmission power may change from one TS to another. Additionally, since the channels are orthogonal, source-channel separation is optimal in this setting [64].

For a given power/rate allocation, the achievable distortion region in the $k$-th TS is given by [63]

$$\mathcal{D}_k = \mathcal{D}_{1,k} \cap \mathcal{D}_{2,k} \cap \mathcal{D}_{12,k}, \tag{4.1}$$

where the sets describing $\mathcal{D}_k$ are defined as :

$$\mathcal{D}_{1,k} = \left\{ (d_{1,k}, d_{2,k}) : d_{1,k} \geq \frac{\sigma_{X_k}^2}{2^{2r_{1,k}}} \left(1 - \rho_k^2 + \rho_k^2 2^{-2r_{2,k}}\right) \right\},$$

$$\mathcal{D}_{2,k} = \left\{ (d_{1,k}, d_{2,k}) : d_{2,k} \geq \frac{\sigma_{Y_k}^2}{2^{2r_{2,k}}} \left(1 - \rho_k^2 + \rho_k^2 2^{-2r_{1,k}}\right) \right\},$$

and finally,

$$\mathcal{D}_{12,k} = \left\{ (d_{1,k}, d_{2,k}) : d_{1,k} d_{2,k} \geq \sigma_{X_k}^2 \sigma_{Y_k}^2 \beta\left(r_{1,k}, r_{2,k}\right) \right\},$$

where

$$\beta\left(r_{1,k}, r_{2,k}\right) = \rho_k^2 2^{-4(r_{1,k}+r_{2,k})} + \frac{1-\rho_k^2}{2^{2(r_{1,k}+r_{2,k})}},$$

$d_{i,k}$ and $r_{i,k}$ are the achievable distortion and transmission/compression rate of node $i$ in TS $k$, respectively.

### 4.2.3 Problem Formulation

The average distortion achieved for the data transmitted by the $i$-th sensor node over $K$ TSs is denoted by $D_i = \frac{1}{K}\sum_{k=1}^{K} d_{i,k}$. We define the distortion region $\mathcal{D}^\star$ as

$$\mathcal{D}^\star = \left\{ (D_1, D_2) : (d_{1,k}, d_{2,k}) \in \mathcal{D}_k \ \forall k, (\boldsymbol{p}_1, \boldsymbol{p}_2) \in \mathfrak{F} \right\},$$

where $\boldsymbol{p}_i = [p_{i,1}, p_{i,2}, \ldots, p_{i,K}], i \in \{1,2\}$ and $\mathfrak{F}$ is given by

$$\mathfrak{F} = \left\{ (\boldsymbol{p}_1, \boldsymbol{p}_2) : \sum_{j=1}^{k} p_{i,j} \leq \sum_{j=1}^{k} e_{i,j},\ p_{i,j} \geq 0, \forall i, \forall k \right\}. \tag{4.2}$$

The above set represents the *energy neutrality* of the system, i.e., at each node, energy consumed cannot be more than the energy harvested till that time.

Our goal is to characterize the *Pareto boundary* of the region $\mathcal{D}^\star$. This boundary consists of operating points $(D_1, D_2)$ such that it is impossible to improve the distortion of one node, without simultaneously increasing the other node's distortion.

## 4.3 Characterizing the Pareto boundary of $\mathcal{D}^\star$

We start by investigating the convexity of $\mathcal{D}^\star$, which will be useful in the characterization of its Pareto boundary. The distortion region in the $k$-th TS in terms of the transmission powers $p_{i,k}$ can be written as

$$\mathcal{D}_k = \left\{ (d_{1,k}, d_{2,k}) : d_{1,k} \geq f_{1,k}, d_{2,k} \geq f_{2,k}, d_{2,k} \geq \frac{f_{12,k}}{d_{1,k}} \right\}, \tag{4.3}$$

where the functions $f_{1,k} \triangleq f_{1,k}(p_{1,k}, p_{2,k})$, $f_{2,k} \triangleq f_{2,k}(p_{1,k}, p_{2,k})$ and $f_{12,k} \triangleq f_{12,k}(p_{1,k}, p_{2,k})$ are obtained by substituting $r_{i,k} \triangleq \frac{1}{2}\log_2(1 + g_{i,k}p_{i,k})$ in the three sets describing $\mathcal{D}_k$ in (4.1).

**Proposition 11.** *The functions $f_{1,k}(p_{1,k}, p_{2,k})$, $f_{2,k}(p_{1,k}, p_{2,k})$ and $\frac{f_{12,k}(p_{1,k}, p_{2,k})}{d_{1,k}}$ are jointly convex in $p_{1,k}$, $p_{2,k}$ and $d_{1,k}$.*

*Proof.* See Appendix. □

**Proposition 12.** *$\mathcal{D}^\star$ is a convex region.*

*Proof.* Let two distinct distortion pairs achieved by the power allocation policies $(\boldsymbol{p}_1, \boldsymbol{p}_2)$ and $(\tilde{\boldsymbol{p}}_1, \tilde{\boldsymbol{p}}_2)$ belonging to the set $\mathfrak{F}$ be denoted by $(D_1, D_2)$ and $(\tilde{D}_1, \tilde{D}_2)$, respectively. Every point on the line segment joining the points $(D_1, D_2)$ and $(\tilde{D}_1, \tilde{D}_2)$ can be represented by $(\hat{D}_1, \hat{D}_2) = \alpha(D_1, D_2) + (1-\alpha)(\tilde{D}_1, \tilde{D}_2), 0 \leq \alpha \leq 1$. By finding a feasible power allocation policy that achieves the distortion pair $(\hat{D}_1, \hat{D}_2)$, we prove that $\mathcal{D}^\star$ is a convex set. We can write

$$(\hat{D}_1, \hat{D}_2) = \left( \frac{1}{K}\sum_{k=1}^{K} \hat{d}_{1,k}, \frac{1}{K}\sum_{k=1}^{K} \hat{d}_{2,k} \right), \tag{4.4}$$

where $\hat{d}_{i,k} \triangleq \alpha d_{i,k} + (1-\alpha)\tilde{d}_{i,k},\ i \in \{1,2\}$. Using the conditions in $\mathcal{D}_{1,k}$ we have

$$\begin{aligned} \hat{d}_{1,k} &\geq \alpha f_{1,k}(p_{1,k}, p_{2,k}) + (1-\alpha) f_{1,k}(\tilde{p}_{1,k}, \tilde{p}_{2,k}) \\ &\overset{(a)}{\geq} f_{1,k}(\hat{p}_{1,k}, \hat{p}_{2,k}), \end{aligned} \tag{4.5}$$

where $(a)$ follows from the convexity of $f_{1,k}$, and the definition $\hat{p}_{i,k} \triangleq \alpha p_{i,k} + (1-\alpha)\tilde{p}_{i,k}$. Similarly, we can show that

$$\hat{d}_{2,k} \geq f_{2,k}(\hat{p}_{1,k}, \hat{p}_{2,k}). \tag{4.6}$$

Finally, considering the constraint in $\mathcal{D}_{12,k}$,

$$\begin{aligned} \hat{d}_{2,k} &\geq \alpha \frac{f_{12,k}(p_{1,k}, p_{2,k})}{d_{1,k}} + (1-\alpha)\frac{f_{12,k}(\tilde{p}_{1,k}, \tilde{p}_{2,k})}{\tilde{d}_{1,k}} \\ &\overset{(b)}{\geq} \frac{f_{12,k}(\hat{p}_{1,k}, \hat{p}_{2,k})}{\hat{d}_{1,k}}, \end{aligned} \tag{4.7}$$

where $(b)$ follows from the convexity of $f_{12,k}/d_{1,k}$.

Since $(\boldsymbol{p}_1, \boldsymbol{p}_2) \in \mathfrak{F}$ and $(\tilde{\boldsymbol{p}}_1, \tilde{\boldsymbol{p}}_2) \in \mathfrak{F}$, it can be easily seen that $(\hat{\boldsymbol{p}}_1, \hat{\boldsymbol{p}}_2) \in \mathfrak{F}$. From (4.5), (4.6) and (4.7), we have $(\hat{d}_{1,k}, \hat{d}_{2,k}) \in \mathcal{D}_k$. Using (4.4) and the definition of $\mathcal{D}^\star$, we conclude that $(\hat{D}_1, \hat{D}_2) \in \mathcal{D}^\star$, and hence the proof. $\square$

Since $\mathcal{D}^\star$ is a convex region, the Pareto boundary is the closure of all the points $(\mathrm{D}_1^\star, \mathrm{D}_2^\star)$, where $(\mathrm{D}_1^\star, \mathrm{D}_2^\star)$ is the solution to the following optimization problem

$$\min_{(D_1, D_2)} \ \mu_1 D_1 + \mu_2 D_2 \ \ \text{s.t} \ (D_1, D_2) \in \mathcal{D}^\star \tag{4.8}$$

for some $\boldsymbol{\mu} = [\mu_1 \ \mu_2]^{\mathrm{T}} \in \mathbb{R}_+^2$. We examine two different cases of (4.8) depending on the choice of $\boldsymbol{\mu}$.

### 4.3.1 Source coding with a helper node ($\mu_1 = 0$ or $\mu_2 = 0$)

In this subsection, we focus on the scenario in which the decoder is interested in minimizing the distortion of one of the source component, and treats the other component information as side information. Without loss of generality, we consider minimizing the distortion $D_1$. Since the decoder is only interested in decoding $X_k$, the distortion incurred in decoding $Y_k$, $d_{2,k}$, is ignored. Thus, in this case the distortion region is given by [65]

$$\mathcal{D}_k = \Big\{ (d_{1,k}, d_{2,k}) : d_{1,k} \geq f_{1,k}(p_{1,k}, p_{2,k}) \Big\}. \tag{4.9}$$

The power allocation policy that minimizes $D_1$ is obtained by solving the following optimization problem

$$\min_{p_{i,k}, d_{1,k}} \quad \sum_{k=1}^{K} d_{1,k} \tag{4.10a}$$

$$f_{1,k}(p_{1,k}, p_{2,k}) - d_{1,k} \leq 0, \quad k \in [1:K] \tag{4.10b}$$

$$\sum_{j=1}^{l} p_{i,j} \leq \sum_{j=1}^{l} e_{i,j}, \ i \in \{1,2\}, \ l \in [1:K], \tag{4.10c}$$

$$p_{i,k} \geq 0 \quad i \in \{1,2\}, \ k \in [1:K]. \tag{4.10d}$$

Since the distortion is minimized, the constraint (4.10b) is satisfied with equality for the optimal solution. Using Proposition 11, we can see that (4.10) is a convex optimization problem, and the Karush-Kuhn-Tucker (KKT) conditions provide the necessary and sufficient conditions for optimality [48].

The Lagrangian of (4.10) can be defined as

$$\begin{aligned}\mathcal{L} \triangleq &\sum_{k=1}^{K} f_{1,k}(p_{1,k}, p_{2,k}) + \sum_{j=1}^{K} \lambda_j \left( \sum_{k=1}^{j} p_{1,k} - \sum_{k=1}^{j} e_{1,k} \right) \\ &+ \sum_{j=1}^{K} \psi_j \left( \sum_{k=1}^{j} p_{2,k} - \sum_{k=1}^{j} e_{2,k} \right) + \sum_{k=1}^{K} \eta_k p_{1,k} + \sum_{k=1}^{K} \phi_k p_{2,k},\end{aligned} \tag{4.11}$$

where $\lambda_j \geq 0, \psi_j \geq 0, \eta_k \geq 0$ and $\phi_k \geq 0$ are the Lagrange multipliers corresponding to (4.10c) and (4.10d). Taking the derivative of (4.11) with respect to $p_{1,k}$, and using the complimentary slackness conditions, we obtain

$$p_{1,k} = W_k \left[\vartheta_k - H_k\right]^+, \tag{4.12}$$

where $W_k \triangleq \sqrt{\frac{\sigma_{X_k}^2}{g_{1,k}} \left(1 - \rho_k^2 + \frac{\rho_k^2}{\left(1+p_{2,k}g_{2,k}\right)}\right)}$, $H_k \triangleq \frac{1}{W_k g_{1,k}}$ and the water level $\vartheta_k \triangleq \frac{1}{\left(\sqrt{\sum_{j=k}^{K} \lambda_j}\right)}$. Similarly,

$$p_{2,k} = B_k \left[\gamma_k - L_k\right]^+, \tag{4.13}$$

where $B_k \triangleq \frac{\sigma_{Y_k}\rho_k}{\sqrt{g_{2,k}(1+p_{1,k}g_{1,k})}}$, $L_k \triangleq \frac{1}{B_k g_{2,k}}$ and the water level $\gamma_k \triangleq \frac{1}{\sqrt{\sum_{j=k}^{K} \psi_j}}$, From (4.12) and (4.13) we can see that optimal $p_{i,k}$'s are dependent, and it is difficult to obtain a closed form expression, however, an iterative directional 2D waterfilling algorithm to obtain the optimal policy is provided.

Given the optimal power allocation of the second node, denoted as $\boldsymbol{p}_2^*$, the optimal $\boldsymbol{p}_1^*$ is obtained by solving

$$\min_{p_{1,k}} \sum_{k=1}^{K} f_{1,k}(p_{1,k}, p_{2,k}^*) \text{ s.t } (\boldsymbol{p}_1, \boldsymbol{p}_2^*) \in \mathfrak{F}. \tag{4.14}$$

By using KKT conditions, it can be easily seen that $p_{1,k}^*$ is obtained by plugging $p_{2,k}^*$ into the expression in (4.12). This solution can be interpreted as directional 2D water-filling [60]. A graphical illustration of the solution for $p_{1,k}^*$ is given in Fig. 4.2, for $K = 3$ TSs. Precisely, in the $k$-th TS we have rectangles of width $W_k$ and height $H_k$. The harvested energy is poured over the level $H_k$ up to the water level $\vartheta_k$. The shaded area below the water level $\vartheta_k$ and above $H_k$ represents the power allocated in TS $k$. The directional taps in Fig. 4.2 represent the fact that energy can be flow only in forward direction. We refer the reader to [60] for the details of the algorithm.

Since (4.10) is a convex optimization problem, and the constraint set can be written as the Cartesian product of two sets, it can be shown that an alternating minimization algorithm, alternating between vectors $\boldsymbol{p}_1$ and $\boldsymbol{p}_2$, converges to the global optimum [66]. Therefore, we use directional 2D

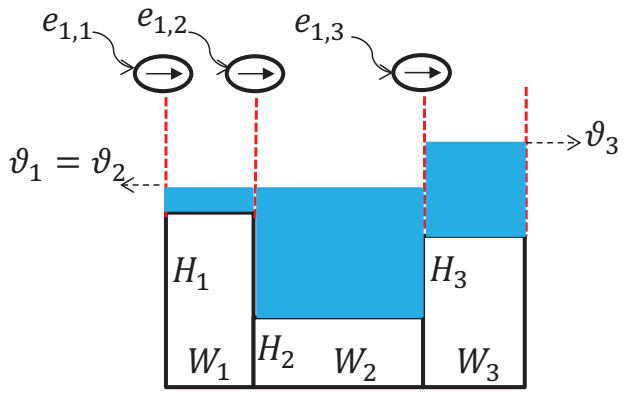


FIGURE 4.2 – 2D waterfilling interpretation.

water-filling in an alternating fashion until the solution converges. We denote $(\mathrm{D}_{1,m}, \mathrm{D}_{2,h})$ as the optimal distortion tuple obtained when $\mu_2 = 0$. Similarly, we obtain $(\mathrm{D}_{1,h}, \mathrm{D}_{2,m})$ when $\mu_1 = 0$.

### 4.3.2 Weighted sum distortion ($\mu_1 > 0, \mu_2 > 0$)

The points in between $(\mathrm{D}_{1,m}, \mathrm{D}_{2,h})$ and $(\mathrm{D}_{1,h}, \mathrm{D}_{2,m})$ that lie on the Pareto boundary are obtained by solving (4.8) for $\boldsymbol{\mu} > 0$. The optimization problem is given by

$$\min_{p_{i,k}, d_{i,k}} \quad D_s = \mu_1 \sum_{k=1}^{K} d_{1,k} + \mu_2 \sum_{k=1}^{K} d_{2,k} \tag{4.15a}$$

$$(d_{1,k}, d_{2,k}) \in \mathcal{D}_k, \ \ k \in [1:K] \tag{4.15b}$$

$$(\boldsymbol{p}_1, \boldsymbol{p}_2) \in \mathfrak{F}. \tag{4.15c}$$

Since $\mathcal{D}_k$ is a convex set (by Proposition 12), and the other constraints are linear, (4.15) is a convex optimization problem. To further understand the structure of the optimal solution, the optimization is performed in two steps. First, consider

$$\tilde{D}_s(\boldsymbol{p}_1, \boldsymbol{p}_2) = \min_{d_{i,k}} D_s \text{ s.t } (d_{1,k}, d_{2,k}) \in \mathcal{D}_k \ \forall k. \tag{4.16}$$

We now illustrate the solution of (4.16) graphically in Fig. 4.3. Since there is no dependency among the distortion sets $\mathcal{D}_i, \mathcal{D}_j, i \neq j$, the optimization can be performed separately for each TS. In the $k$-th TS, depending on the slope

of the line $\mu_1 d_{1,k} + \mu_2 d_{2,k}$, it is not hard to see that the optimal solution must occur at one of the following three points :

$$\left(d_{1,k}^*, d_{2,k}^*\right) = \begin{cases} \mathrm{A} \triangleq \left(f_{1,k}, \frac{f_{12,k}}{f_{1,k}}\right), \\ \mathrm{B} \triangleq \left(\frac{f_{12,k}}{f_{2,k}}, f_{2,k}\right), \text{ or} \\ \mathrm{C} \triangleq \left(\sqrt{\frac{\mu_2}{\mu_1} f_{12,k}}, \sqrt{\frac{\mu_1}{\mu_2} f_{12,k}}\right), \end{cases} \tag{4.17}$$

as shown in Fig. 4.3. Since (4.15) is a convex optimization problem, the function $\tilde{D}_s$ is convex with domain $\{(\boldsymbol{p}_1, \boldsymbol{p}_2) : (\boldsymbol{p}_1, \boldsymbol{p}_2) \in \mathfrak{F}, (d_{1,k}, d_{2,k}) \in \mathcal{D}_k \forall k\}$ [48, 3.2.5].

Using (4.16) and (4.17), the second step of the optimization is given by

$$\min_{p_{i,k}} \qquad \tilde{D}_s\left(\boldsymbol{p}_1, \boldsymbol{p}_2\right) = \mu_1 \sum_{k=1}^{K} d_{1,k}^* + \mu_2 \sum_{k=1}^{K} d_{2,k}^* \tag{4.18a}$$

$$(\boldsymbol{p}_1, \boldsymbol{p}_2) \in \mathfrak{F}. \tag{4.18b}$$

Using the above analysis, we now provide a simplified way of obtaining the Pareto optimal points of $\mathcal{D}^*$ in a static setting.

### A Static setting

In the static setting, the source statistics and the channel gains do not vary with time, i.e., $\sigma_{X_k}^2 = \sigma_X^2, \sigma_{Y_k}^2 = \sigma_Y^2, \rho_k = \rho, g_{i,k} = g_i, \forall i, k$, and the EH profiles are *similar*. The EH profiles are similar in the sense that the most majorized feasible vectors obtained from the EH profiles of the two nodes, have the same structure. For better presentation, we restate the definition of similar EH profiles, which is already provided in Chapter 2.

**Definition 5.** *The EH profiles are said to be similar if the most majorized feasible vectors $(\boldsymbol{p}_1^*, \boldsymbol{p}_2^*)$, where $\boldsymbol{p}_1^* \preceq \boldsymbol{p}_1, \boldsymbol{p}_2^* \preceq \boldsymbol{p}_2, \forall (\boldsymbol{p}_1, \boldsymbol{p}_2) \in \mathfrak{F}$, have the same structure i.e., $\forall k$, $p_{1,k}^* = p_{1,k+1}^*$ iff $p_{2,k}^* = p_{2,k+1}^*$, and $p_{1,k}^* \neq p_{1,k+1}^*$ iff $p_{2,k}^* \neq p_{2,k+1}^*$.*

**Proposition 13.** *In the static setting, all points on the Pareto boundary of $\mathcal{D}^*$ are obtained by the power allocation $(\boldsymbol{p}_1^*, \boldsymbol{p}_2^*)$, where $\boldsymbol{p}_1^* \preceq \boldsymbol{p}_1, \boldsymbol{p}_2^* \preceq \boldsymbol{p}_2 \ \forall \left(\boldsymbol{p}_1, \boldsymbol{p}_2\right) \in \mathfrak{F}$.*

*Proof.* Since $\sigma_{X_k}^2 = \sigma_X^2, \sigma_{Y_k}^2 = \sigma_Y^2, \rho_k = \rho, g_{i,k} = g_i, \forall i, k$, we have $f_{i,k}(p_{1,k}, p_{2,k}) = f_i(p_{1,k}, p_{2,k}),\ \forall i, k$ and $f_{12,k}(p_{1,k}, p_{2,k}) = f_{12}(p_{1,k}, p_{2,k}),\ \forall k$. Therefore, using (4.17) in the static setting, we can write $d_{i,k}^*(p_{1,k}, p_{2,k}) = d_i^*(p_{1,k}, p_{2,k}) \forall i, k$. Since $d_{i,k}^* = d_i^*,\ \forall k$, we can see that the function $\tilde{D}_s\left(\boldsymbol{p}_1, \boldsymbol{p}_2\right)$ is symmetric. Using the convexity and symmetry of $\tilde{D}_s$, and by using the proof similar to the one of Proposition 5 in Chapter 2, we can prove that the power allocation vectors $\boldsymbol{p}_1^*$ and $\boldsymbol{p}_2^*$ are optimal. Once $(\boldsymbol{p}_1^*, \boldsymbol{p}_2^*)$ is obtained, the optimal distortion region $\mathcal{D}_k^*$ for TS $k$ is given by (4.1). Depending on $\boldsymbol{\mu}$, using $\mathcal{D}_k^*$ and (4.17), we obtain $(d_{1,k}^*, d_{2,k}^*)$ and then $(\mathrm{D}_1^\star, \mathrm{D}_2^\star)$. □

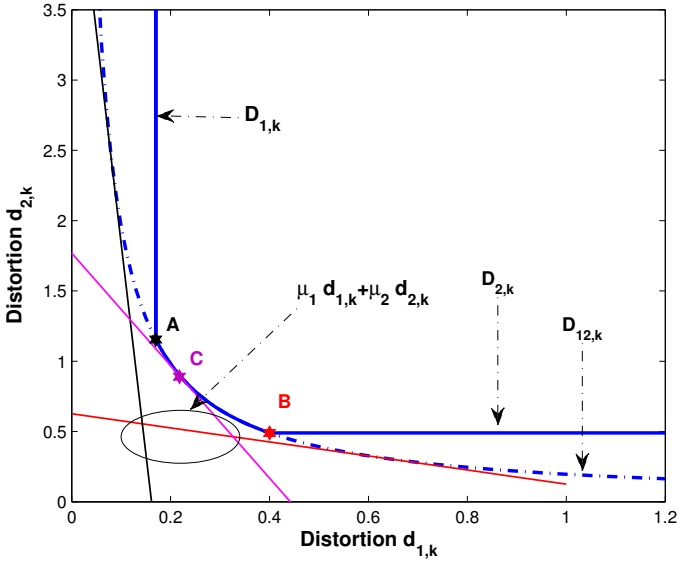


FIGURE 4.3 – Distortion region $\mathcal{D}_k$, lines $\mu_1 d_{1,k} + \mu_2 d_{2,k}$ for different $\boldsymbol{\mu}$.

We could not find a simple algorithm to solve (4.15) in a non-static setting, therefore we resort to numerical methods.

## 4.4 Numerical Results

In this section, numerical simulations are used to illustrate the Pareto boundary of the distortion region. We consider $K = 6$ TSs. The harvested energy vectors are chosen as $\boldsymbol{e}_1 = [4, 2, 5, 4, 3, 10]$ and $\boldsymbol{e}_2 = [4, 0.5, 3.5, 2.5, 3, 4]$. The variance of the sources are given by $\boldsymbol{\sigma}_X^2 = [3, 0.2, 2, 0.4, 1.4, 0.3]$ and $\boldsymbol{\sigma}_Y^2 = [0.8, 2, 3.6, 4.8, 1.2, 2.3]$. The correlation coefficient among the observed source samples is $\boldsymbol{\rho} = [0.95, 0.4, 0.5, 0.3, 0.8, 0.1]$. Fig. 4.3 shows the Pareto boundary of $\mathcal{D}^\star$ when the channel gains are chosen as $\boldsymbol{g}_1 = [0, 0.9, 0.2, 0, 0.8, 0.3]$ and $\boldsymbol{g}_2 = [0.5, 0, 0.8, 0.9, 0.1, 0.9]$. The points $(\mathrm{D}_{1,m}, \mathrm{D}_{2,h})$ and $(\mathrm{D}_{1,h}, \mathrm{D}_{2,m})$ correspond to the distortion pairs when node 2 or node 1 acts as the helper node, respectively. The remaining boundary, shown in green in Fig. 4.4, is obtained by numerically solving (4.15) for different $\boldsymbol{\mu} \in \mathbb{R}_+^2$ pairs. The points $\mathrm{B}_1$ and $\mathrm{B}_2$ are obtained when each node greedily maximizes the total number of bits transmitted till the end of $K$-th TS irrespective of the source statistics. In each TS, at each node, the compression rate is equal to the transmission rate. The power allocation at $i$-th node is obtained by using directional waterfilling with $\boldsymbol{e}_i$ and $\boldsymbol{g}_i$ [18], [20].

For the static scenario, same energy harvesting profiles are used with $\sigma_X^2 = 2, \sigma_Y^2 = 1, \rho_k = 0.6\ \forall k$, and all channel gains are assumed to be

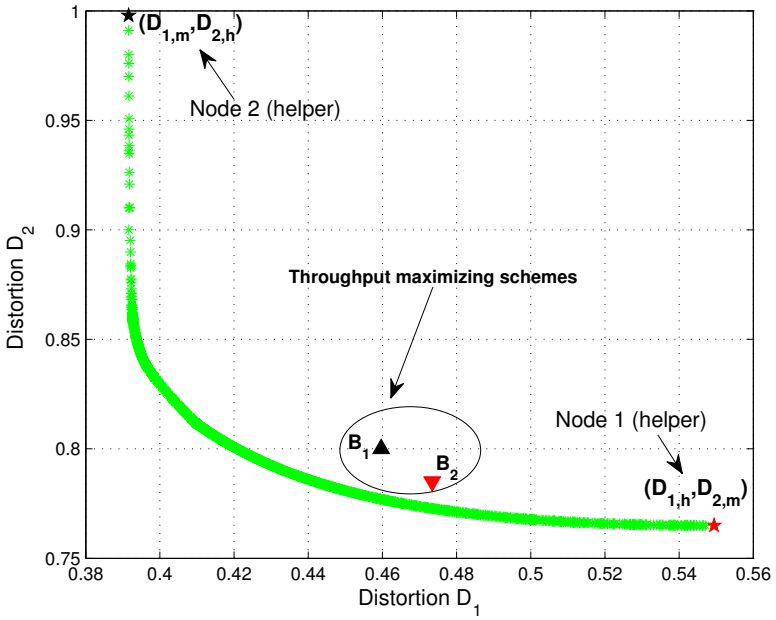


FIGURE 4.4 – Pareto boundary of $\mathcal{D}^*$.

unity. The most majorized feasible vectors for the given harvesting profiles are given by $\boldsymbol{p}_1^* = [3, 3, 4, 4, 4, 10]$ and $\boldsymbol{p}_2^* = [2.5, 2.5, 3, 3, 3, 4]$, and hence the harvesting profiles are similar. Note that, since the source statistics are not varying in time, power allocation polices $\boldsymbol{p}_1^*$ and $\boldsymbol{p}_2^*$ are also throughput optimal. The Pareto boundary of the distortion region for the static scenario is shown Fig. 4.5.

## 4.5 Conclusion

We have determined the Pareto boundary of the the distortion region of the quadratic Gaussian two-encoder source coding problem with EH nodes. Specific points on this boundary are obtained by using an iterative directional 2D waterfilling algorithm. In the static case, we have shown that all points on the Pareto boundary are obtained by the most majorized feasible power allocation policies.

## 4.6 Appendix

### 4.6.1 Proof of Proposition 11

Since $r_{i,k}$ is concave in $p_{i,k}$, it can be easily seen that $2^{-r_{1,k}}$ and $2^{-(r_{1,k}+r_{2,k})}$ are convex. Since the summation of convex functions is convex, $f_1\left(p_{1,k}, p_{2,k}\right)$

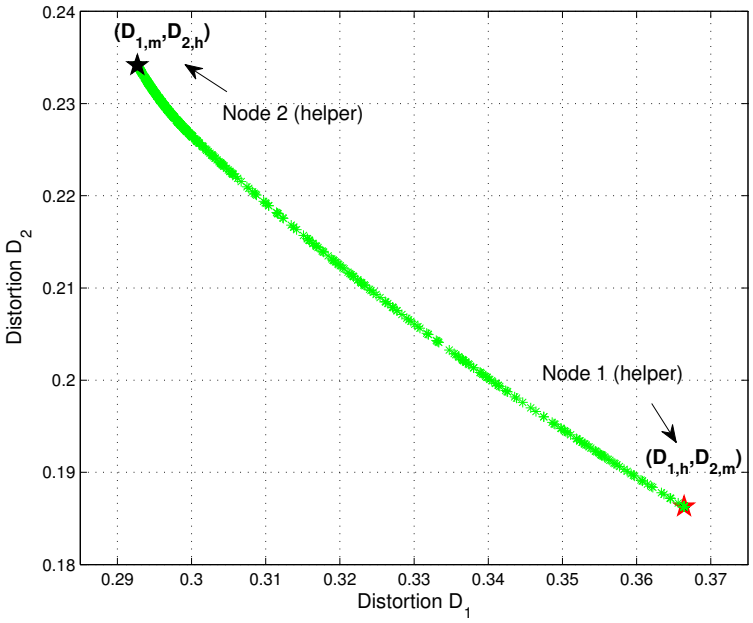


FIGURE 4.5 – Pareto boundary of $\mathcal{D}^*$ for the static scenario.

is convex. Similarly, we can show that $f_2\left(p_{1,k}, p_{2,k}\right)$ is also convex. To show that the final function is convex as well, consider the following functions :

$$h\left(x\right) = \sqrt{\rho_k^2 2^{-4x} + (1-\rho_k^2)2^{-2x}},$$

and the quadratic-over-linear function [48]

$$g(x, d_{1,k}) = \frac{x^2}{d_{1,k}},\ d_{1,k} > 0.$$

The derivative of $h$ is given by

$$h^{'}\left(x\right) = -\log_e 2 \left[ h\left(x\right) + \frac{\rho_k^2}{\sqrt{\rho_k^2 16^x + (1-\rho_k^2)64^x}} \right].$$

It can be seen that $h^{'}(x)$ is monotonically increasing, and therefore $h(x)$ is convex. The function $g(x, d_{1,k})$ is convex for $d_{1,k} > 0$ [48]. Using the above defined functions we can write

$$\frac{f_{12}(p_{1,k}, p_{2,k})}{d_{1,k}} = g\left(h\left(p_{1,k}, p_{2,k}\right), d_{1,k}\right), \tag{4.19}$$

where $h\left(p_{1,k}, p_{2,k}\right) = h\left(r_{1,k} + r_{2,k}\right)$.

The function $h\left(p_{1,k}, p_{2,k}\right)$ is convex since $h(x)$ is convex and non-increasing, and $r_{i,k}$ is concave. Using the fact that $h\left(p_{1,k}, p_{2,k}\right)$ and $g(x, d_{1,k})$ are convex, and monotonicity of $g$ in the first argument, we can easily prove that $\frac{f_{12}(p_{1,k}, p_{2,k})}{d_{1,k}}$ is convex.

# Chapter 5

# Harvesting and Compression of Information from an Ambient Energy Source

## 5.1 Introduction

A wireless sensor node collects samples of a physical phenomenon in its surrounding environment, processes and sends them to a destination. The block diagram of a typical sensor node powered by an ambient energy source is shown in Fig. 5.1. In Fig. 5.1, there are two transducers, one converts the ambient energy into an electrical signal, and the other transducer (or sensing unit) converts the physical phenomenon of interest into an electrical signal. The output of the first transducer (energy harvester) is given to an energy buffer such as super capacitor or rechargeable battery. This harvested energy can be later used to power different components of the sensor. The output signal of the second transducer is fed to a sampling circuit which converts the continuous analog signal into discrete time samples. These samples are then given to a communication subsystem where they are processed by the encoder and then transmitted by the radio unit.

In some scenarios, the ambient energy source from which the sensor harvests energy and the information source from which the sensor collects samples might be the same. For example, a sensor node wishes to send information about the intensity of the solar irradiation in its surroundings, and at the same time depends on the energy harvested from it. In this case also we can follow similar architecture as in Fig. 5.1, with two transducers one for harvesting one for sensing. However, provision of two traducers with the

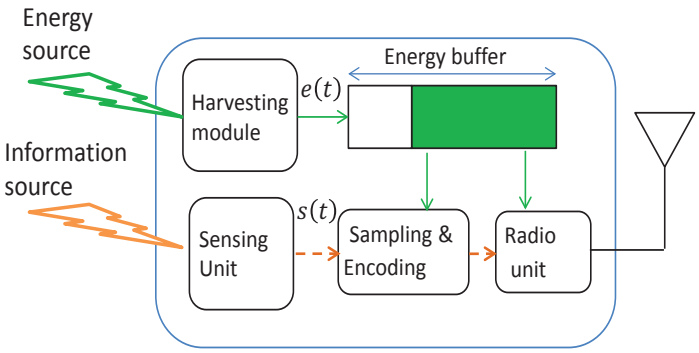


FIGURE 5.1 – An EH sensor node with different energy and information sources.

same functionality may not be allowable as they occupy more chip-area. So, if there is only one transducer in the system, the output electrical signal now contains both the energy to be harvested and the information about source samples to be transmitted.

Such architectures are desirable in some applications and are of practical interest [67–69]. Interestingly, the work in [67] considered our envisaged system model. In [67], there is a single piezoelectric (PZT) transducer which produces an electrical signal from the vibrations. The sensor node is interested in some measurements from this vibration and also at the same time harvest energy produced from it. A time division modeled is used, where for some portion of time the electrical signal is fed to the harvester (charging a capacitor in their model), and in the reaming time measurements are performed using the output electrical signal from the transducer. However, the work considers on powering the whole sensor node and focuses on the practical implementation aspects.

In this chapter, we use a rather abstract model where the encoder has to send the information about the signal obtained from the transducer to a destination and at the same time relies on the harvesting energy from it. The model is shown in Fig. 5.2. We propose some practical schemes that efficiently utilizes the electrical signal generated from the ambient energy and information source for both communication and harvesting purposes. The aim is to send the source samples to the destination with minimum average end-to-end distortion while using the harvested energy from the same source.

Finally, we investigate a scenario where the sensor has two energy sup-

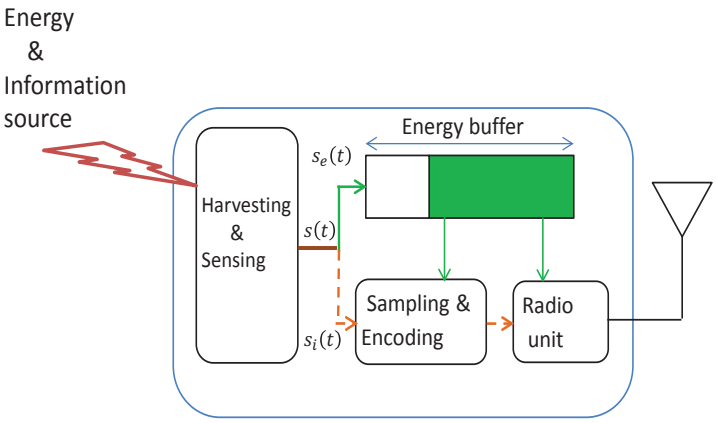


FIGURE 5.2 – An EH sensor node with the same energy and information source.

plies, one from the traditional limited energy in the battery, and the other form the harvest energy from the source itself. In this scenario, we design schemes that intelligently use both the traditional limited energy and the energy harvested from the source, so as to satisfy some QoS constraints on the average distortion while minimizing the usage of traditional limited energy.

## 5.2 System model

The output electrical waveform of the transducer in the time interval $[0, T]$ is denoted by $s(t), t \in [0, T]$. We model $s(t)$ as an ergodic and stationary Gaussian random process with zero mean and variance $\sigma_s^2$. The zero mean assumption is due to the fact that the DC part in the electri signal doesn't carry any information and can be harvested entirely, an hence, no tradeoff to look into. We also assume $s(t)$ to be a band limited signal i.e., there are no frequencies higher than $B$ hertz in $s(t)$. By using Nyquist sampling theorem, perfect reconstruction of $s(t)$ is possible from the discrete samples taken $T_s = 1/2B$ seconds apart. Given the sampling period $T_s$, the interval $[0, T]$ corresponds to $n = T/T_s$ samples. For convenience we assume $n = T$ (i.e., $T_s = 1$).

Whether laws of physics allows us to harvest all the energy from the signal $s(t)$ without any loss of information in it, and then later use it for sampling and encoding purposes (or vice versa), is not clear to us. In this work, ignoring

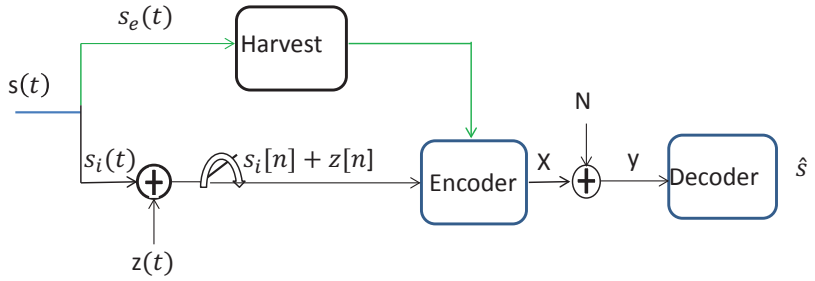


FIGURE 5.3 – An abstract model for division of the source signal.

this subtle issue, we deal with current practical circuit limitations where this is not possible. Along the lines of works in [70], [71] where the focus was on decoding information and harvesting energy from the same radio signal, we use practical designs where the signal $s\,(t)$ is split into two separate streams $s_e\,(t)$ and $s_i\,(t)$, such that sum of the energies in the both streams is equal to the energy in the signal $s\,(t)$. The signal $s_e\,(t)$ is given to the harvesting system and the signal $s_i\,(t)$ is given to the sampling system and later to the encoder. An abstract model of the considered system is shown in Fig. 5.3.

The sampling process is noisy and the received samples at the encoder are given by

$$\tilde{\boldsymbol{s}}^n = \boldsymbol{s}_i^n + \boldsymbol{z}^n \tag{5.1}$$

where $\boldsymbol{s}_i^n = [s_{i1}, s_{i2}, \ldots, s_{in}]$, $\boldsymbol{z}^n = [z_1, z_2, \ldots, z_n]$ and $\tilde{\boldsymbol{s}}^n = [\tilde{s}_1, \tilde{s}_2, \ldots, \tilde{s}_n]$. The noise samples are assumed to be i.i.d Gaussian with zero mean and variance $\sigma_z^2$, and they are independent of the source signal. The samples $\tilde{\boldsymbol{s}}^n$ are then given to the encoder which maps them into the channel input $\boldsymbol{x}^n = [x_1, x_2, \ldots, x_n]$. The encoded samples are then transmitted over a memoryless AWGN channel with zero mean and noise variance $\sigma_n^2$. We assume that the duration of time interval $T$ is large enough (i.e., large $n$) to invoke the information theoretic arguments.

We now state some well known definitions and results from the rate-distortion theory that are used in this chapter.

**Definition 6.** *[72] The rate-distortion function of the source $S$ with reconstruction distortion $D$ is defined as*

$$R(D) = \min_{p_{\hat{S}|S}: Ed(S,\hat{S}) \leq D} I(S;\hat{S}),$$

*where $p_{\hat{S}|S}$ is the conditional PDF of the reconstructed source $\hat{S}$ for a given input $S$, $Ed(S,\hat{S})$ is the distortion measure and $I(S;\hat{S})$ denotes the mutual information between $S$ and $\hat{S}$.*

**Definition 7.** *[72] The capacity of the channel $p_{Y/X}$ with average transmission power constraint $P$ is defined as*

$$C(P) = \max_{p_X : E[X^2] \leq P} I(X;Y),$$

*where $p_{Y|X}$ is the conditional PDF of the output of the channel $Y$ for the input symbol $X$, $p_X$ is the PDF of the input $X$ and $I(X;Y)$ denotes the mutual information between $X$ and $Y$.*

**Theorem 4.** *[72] Any communication system for a discrete-time memoryless source with $k$ samples, transmitted over $n$ channel uses of a discrete-time memoryless channel with $k \to \infty, n \to \infty$ such that $k/n = \kappa$, satisfies*

$$\kappa R(D) \leq C(P), \tag{5.2}$$

*where $D$ is the distortion incurred and $C(P)$ is the capacity of the channel with the power constraint $P$.*

**Theorem 5.** *[73], [74] The distortion-rate function of a remote memory less Gaussian source of zero mean and variance $\sigma_s^2$ observed with additive independent memory less Gaussian noise of zero mean and variance $\sigma_z^2$ is*

$$D_{remote}(R) = \frac{\sigma_s^2 \sigma_z^2}{\sigma_s^2 + \sigma_z^2} + \frac{\sigma_s^4}{\sigma_s^2 + \sigma_z^2} 2^{-2R}. \tag{5.3}$$

We now propose some practical schemes for the model shown in Fig. 5.3.

## 5.3 Practical Architectures

In this section we propose three architectures based on the energy conservation principle i.e, the sum of energies given to the sampling and the encoder system is equal to the energy in the output signal of the transducer.

### 5.3.1 Energy splitting

In this scheme, the source signal $s(t)$ is divided into two signals $s_e(t)$ and $s_i(t)$ with $s_e(t) = \sqrt{1-\alpha}s(t)$ given to the harvester and $s_i(t) = \sqrt{\alpha}s(t)$ to the sampling system. The splitting parameter $0 \leq \alpha \leq 1$ ensures the energy conservation is obeyed. We assume that the harvested energy from $s_e(t)$ is used to transmit the encoded source samples over $n$ channel uses, hence, the average transmission power using energy splitting approach is given by

$$P_e = \lim_{T \to \infty} \frac{1}{T} \int_{t=0}^{T} \left| \sqrt{1-\alpha} s(t) \right|^2 dt. \tag{5.4}$$

Since the random process $s(t)$ is ergodic, (5.4) can be written as

$$P_e = (1-\alpha)\sigma_s^2. \tag{5.5}$$

Using the equality in (5.2) with $k = n$, the average power $P_e$, and the rate-distortion of the Gaussian remote source (5.3), we obtain

$$\mathrm{E}\left|\sqrt{\alpha}s - \hat{s}\right|^2 = \frac{\alpha\sigma_s^2\sigma_z^2}{\alpha\sigma_s^2+\sigma_z^2} + \frac{\alpha^2\sigma_s^4}{\alpha\sigma_s^2+\sigma_z^2}\frac{1}{(1+\frac{P_e}{\sigma_n^2})}. \tag{5.6}$$

Using (5.5) and (5.6), the reconstruction distortion

$$D_e \triangleq \mathrm{E}\left|s - \frac{\hat{s}}{\sqrt{\alpha}}\right|^2 = \frac{\sigma_s^2\sigma_z^2}{\alpha\sigma_s^2+\sigma_z^2} + \frac{\alpha\sigma_s^4}{\alpha\sigma_s^2+\sigma_z^2}\frac{\sigma_n^2}{(\sigma_n^2+(1-\alpha)\sigma_s^2)}. \tag{5.7}$$

The optimal splitting parameter $\alpha^*, \alpha^* \in [0,1]$ that minimizes $D_e$ is given by

$$\alpha^* = \begin{cases} 0.5, & \text{if } \sigma_z^2 = \sigma_n^2 \\ \frac{1+\frac{\sigma_n^2}{\sigma_s^2}}{1-\frac{\sigma_n^2}{\sigma_z^2}}\left(1-\sqrt{1-\frac{1-\frac{\sigma_n^2}{\sigma_z^2}}{1+\frac{\sigma_n^2}{\sigma_s^2}}}\right), & \text{otherwise.} \end{cases} \tag{5.8}$$

### 5.3.2 Time splitting

In this scheme, the source signal $s(t)$ is divided into two signals $s_e(t)$ and $s_i(t)$ with $s_e(t) = s(t), t \in [0,(1-\beta)T]$ given to the harvester and $s_i(t) = s(t), t \in ((1-\beta)T, T]$ to the sampling system. Hence, we have $\beta n$ source samples. The splitting parameter $0 \leq \beta \leq 1$ ensures the energy conservation is obeyed. Since we assume that the collected source samples are transmitted in $n$ channel uses, the average transmission power with time splitting approach is given by

$$P_t = \lim_{T\to\infty}\frac{1}{T}\int_{t=0}^{(1-\beta)T} |s(t)|^2\, dt. \tag{5.9}$$

Since the random process $s(t)$ is ergodic,

$$P_t = (1-\beta)\sigma_s^2. \tag{5.10}$$

Since $\beta n$ source samples are to be transmitted over $n$ channel uses, using the equality in (5.2) with $\kappa = \beta$, (5.3), and (5.10) we have

$$D_t \triangleq \mathrm{E}\,|s-\hat{s}|^2 = (1-\beta)\sigma_s^2 + \beta\left[\frac{\sigma_s^2\sigma_z^2}{\sigma_s^2+\sigma_z^2} + \frac{\sigma_s^4}{\sigma_s^2+\sigma_z^2}\frac{1}{(1+\frac{P_t}{\sigma_n^2})^{1/\beta}}\right] \tag{5.11}$$

The optimal splitting parameter is obtained by solving

$$\frac{\partial D_t}{\partial \beta}|_\beta = 0,\ 0 \leq \beta \leq 1. \tag{5.12}$$

There is no closed form expression for the optimal $\beta^*$, however it can be obtained by using a simple one dimensional search in the interval $[0, 1]$.

### 5.3.3 Time and energy splitting

In this case we combine both the above mentioned strategies. The source signal $s\,(t)$ is divided into two signals $s_e\,(t)$ and $s_i\,(t)$ with

$$s_e\,(t) = \begin{cases} s(t), \text{ for } \ t \in [0, (1-\beta)T] \\ \sqrt{1-\alpha}s(t), \text{ for } \ t \in ((1-\beta)T, T] \end{cases} \tag{5.13}$$

given to the harvester and $s_i\,(t) = \sqrt{\alpha}s(t), t \in ((1-\beta)T, T]$ to the sampling system. Hence, we have $\beta n$ source samples. Since we assume that the collected source samples are transmitted in $n$ channel uses, the average harvested power is given by

$$P_h = \lim_{T\to\infty} \frac{1}{T} \int_{t=0}^{(1-\beta)T} |s(t)|^2\, dt + \lim_{T\to\infty} \frac{1}{T} \int_{t=(1-\beta)T}^{T} \left|\sqrt{1-\alpha}s(t)\right|^2 dt. \tag{5.14}$$

Since $s\,(t)$ is stationary and ergodic,

$$P_h = (1-\beta)\sigma_s^2 + \beta(1-\alpha)\sigma_s^2. \tag{5.15}$$

Since $\beta n$ source samples are to be transmitted in $n$ channel uses, using the equality in (5.2) with $\kappa = \beta$, (5.3), and (5.15) we have

$$\mathrm{E}\left|s - \frac{\hat{s}}{\sqrt{\alpha}}\right|^2 = (1-\beta)\sigma_s^2 + \beta\left[\frac{\sigma_s^2\sigma_z^2}{\alpha\sigma_s^2+\sigma_z^2} + \frac{\alpha\sigma_s^4}{\alpha\sigma_s^2+\sigma_z^2}\frac{1}{(1+\frac{P_h}{\sigma_n^2})^{1/\beta}}\right] \tag{5.16}$$

Note that there is no closed form expression for the optimal $\alpha^*$ and $\beta^*$ that minimizes (5.16), therefore we revert to numerical methods.

## 5.4 Performance comparison

The signal to noise ratio at the encoder (SNRE) is defined as

$$SNR = 10\log_{10}\left(\frac{\sigma_s^2}{\sigma_z^2}\right).$$

In Fig. 5.4 the distortion performance of the proposed architectures are compared for different sampling noise variances while varying the signal power

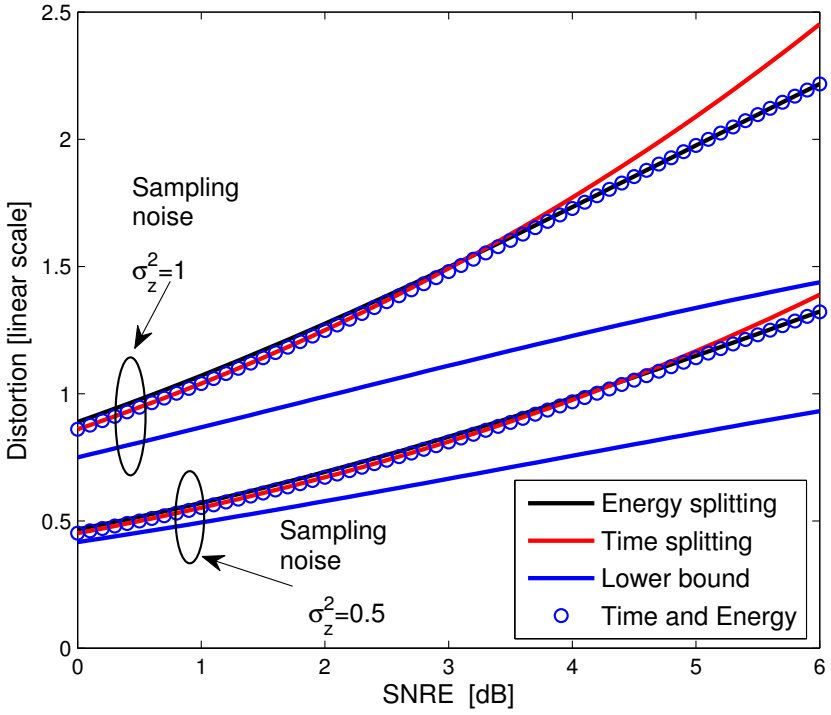


FIGURE 5.4 – Distortion for different sampling noise.

$\sigma_s^2$, thus varying the SNRE. The channel noise variance is assumed to be $\sigma_n^2 = 1$. The lower bound is obtained under the assumption that the encoder can measure and at the same time harvest all the energy from the source signal. As expected the scheme where both time and energy splitting parameters are optimized outperforms the other schemes. However, note that energy division approach performs quite well at all SNREs. As we can see the distortion performance differs for different sampling noise variance even though the SNRE is same.

In Fig. 5.5, we compare the distortion for the proposed schemes for high SNRE. The sampling and channel noise variances are assumed to be $\sigma_z^2 = 1$ and $\sigma_n^2 = 1$, respectively. For high SNRE, energy splitting scheme achieves the distortion quite close to the lower bound and there seems to be a constant gap in the distortion performance.

## 5.5 QoS with conventional power supply

From the results and analysis from the previous sections, we can see that energy splitting is a simple scheme where the optimal splitting parameter

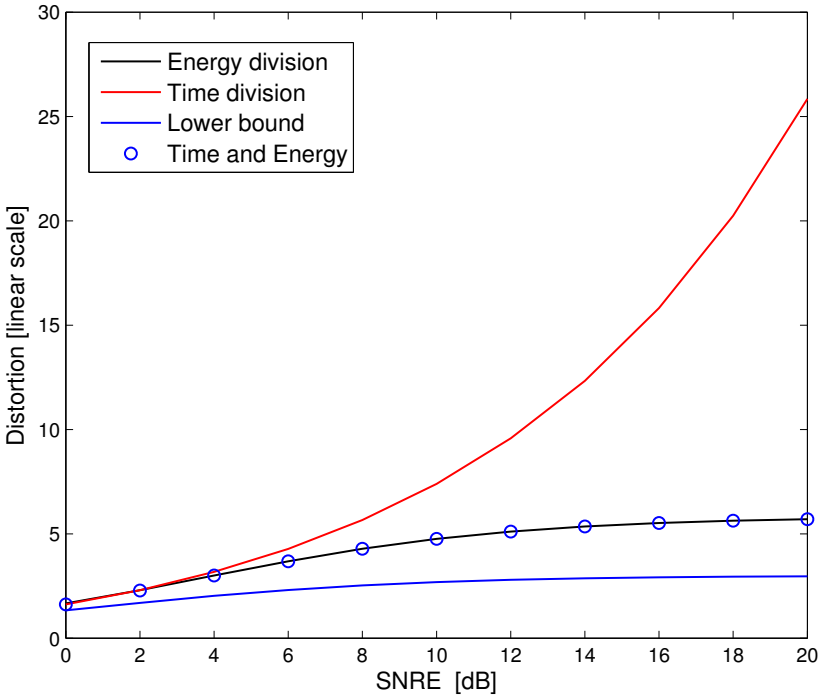


FIGURE 5.5 – Distortion performance of the proposed schemes.

can be expressed in closed form, and it performs very well at all SNREs. In this section, we apply the proposed energy splitting architecture to a scenario where the sensor node can harvest energy from the source signal, and also has conventional power supply. The aim is to satisfy some QoS constraints on the distortion with the minimal possible usage of conventional power supply.

### 5.5.1 System model

We consider a time slotted system with $N$ time slots (TSs), each of duration $T$. In the $i$-th TS, $i \in [1:N]$, output electrical waveform of the transducer is modeled as an ergodic and stationary Gaussian random process with zero mean and variance $\sigma_{s_i}^2$. The remaining sampling an communication model is assumed to be same in each TS, as described in Section 5.2. We use an energy splitting model with splitting parameter $\alpha_i$ in the $i$-th TS. The harvested energy is stored in an infinite size battery and it is used only for communication purposes. In each TS, the sensor draws power $p_i$ units from the conventional power supply and $h_i T$ units of energy from the harvested energy. Using (5.3), the achievable distortion in the $i$-th TS is given by

$$D_i = \frac{\sigma_{s_i}^2 \sigma_z^2}{\alpha_i \sigma_{s_i}^2 + \sigma_z^2} + \frac{\alpha \sigma_{s_i}^4}{\alpha \sigma_{s_i}^2 + \sigma_z^2} \frac{\sigma_n^2}{(\sigma_n^2 + h_i + p_i)}. \tag{5.17}$$

By using both the harvested and conventional power supplies, the sensor node has to make sure that the QoS constraint $D_i \leq Q_i$ is satisfied in each TS. Since the traditional power supply is costly and non-renewable, we wish to minimize its usage while satisfying the QoS constraints. The problem of minimizing of traditional power consumption with QoS constraints can be formulated as

$$\min_{b_i, h_i, \alpha_i} \quad \sum_{i=1}^{N} b_i \tag{5.18a}$$

$$\text{s.t.} \quad D\left(\sigma_{s_j}^2, b_i, h_i, \alpha_i\right) \leq Q_i, \ \forall i \in [1:N] \tag{5.18b}$$

$$\sum_{j=1}^{l} h_j \leq \sum_{j=1}^{l} (1-\alpha_i)\sigma_{s_j}^2, \ \forall l \in [1:N] \tag{5.18c}$$

$$0 \leq \alpha_i \leq 1, \ b_i \geq 0 \ \text{ and } h_i \geq 0, \ \forall i \in [1:N] \tag{5.18d}$$

Using (5.17), we can rewrite the QoS constraint in (5.18b) as

$$b_i \geq f_i \triangleq \frac{\sigma_n^2 \sigma_{s_i}^4 \alpha_i}{(Q_i - \sigma_{s_i}^2)(\alpha_i \sigma_{s_i}^2 + \sigma_z^2)} - h_i - \sigma_n^2 \tag{5.19}$$

Now using (5.19) and the constraint $b_i \geq 0$ the optimization can be simplified to

$$\min_{h_i,\alpha_i} \quad \sum_{i=1}^{N} \max\left(0, f_i\right) \tag{5.20a}$$

$$\text{s.t.} \quad \sum_{j=1}^{l} h_j \leq \sum_{j=1}^{l} (1-\alpha_i)\sigma_{s_j}^2, \ \forall l \in [1:N] \tag{5.20b}$$

$$0 \leq \alpha_i \leq 1, \ h_i \geq 0, \ \forall i \in [1:N] \tag{5.20c}$$

**Remark 4.** *The optimization problem in (5.18) may not have a feasible solution. This is due to the fact that the first term in the summation in (5.17) is independent of the power used for transmission, hence, even if $p_i = \infty$, the distortion cannot be made arbitrarily small.*

**Remark 5.** *We only consider cases where the QoS metric of average distortion in the i-th TS follows $Q_i < \sigma_{s_i}^2$. If it is not the case, the solution is trivial as there is no need for transmission as the intended distortion is equal to the source variance in that TS.*

Based on the above remarks, if the given QoS constraints are feasible, then by considering cases where $Q_i < \sigma_{s_i}^2$, we can see that the function $f_i$ is jointly convex in $\alpha_i$ and $h_i$. Since $f_i$ is convex, the function $\max(0, f_i)$ is also convex, and hence the objective function in (5.20). Since the objective function in (5.20) is concave and the constraints are linear, it has a global minimizer [48]. We use efficient numerical methods (CVX) to solve the optimization problem.

### 5.5.2 Numerical Results

We consider $K = 6$ TSs. The variance of the source over TSs is given by $\boldsymbol{\sigma_s^2} = [10, 1, 5, 2.5, 10, 0.5]$. The sampling and channel noise variances are assumed to be $\sigma_z^2 = 0.01$ and $\sigma_n^2 = 1$, respectively. In Fig. 5.6 we compare the power drawn from the conventional power supply source with and without the energy splitting module in the sensor node for various QoS requirements. The QoS requirement is specified by the signal to distortion ratio

$$Q_d = 10 \log_{10} \left( \frac{\sigma_{s_i}^2}{D_i} \right).$$

By choosing a proper value for $D_i$, we make the QoS requirement same in all the TSs. From Fig. 5.6, we can see that harvesting energy from the source results in significant reduction in conventional power utilization.

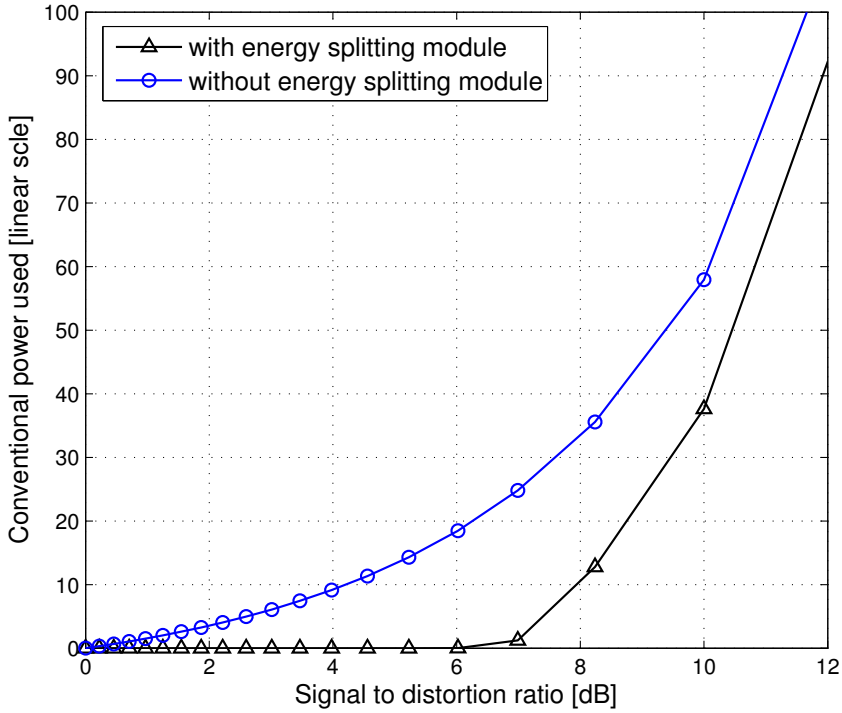


FIGURE 5.6 – Non-renewable power consumption for various QoS constraints.

## 5.6 Conclusion

We have proposed three practical architectures that utilize the electrical signal generated from the energy/information source, and compared their performance in terms of average distortion. Owing to its analytical tractability and good distortion performance, we used energy division model in an application where we have shown that significant reduction in the consumption of non-renewable energy can be attained by harvesting energy from the energy/information source, when the data sent by the sensor node has to satisfy some QoS requirements on the distortion.

# Chapter 6

# Conclusion

The focus of this thesis has been on the design of transmission and feedback strategies taking into account the time varying nature of energy supplies at the communication nodes. A summary the contributions are given below.

- In Chapter 2, we have focused on the design of transmission and feedback policies that maximizes the throughput in a p2p MISO channel with EH nodes. Since the exact expressions of throughput are complicated, concave upper bounds have been used as the objective functions in the formulated optimization problems. By exploiting the convexity and symmetry properties of the formulated optimization problems, and using tools from majorization theory, we have devised simple algorithms to obtain the optimal energy management policies at the TX and the RX. Numerical results show that the optimal policies obtained for these modified problems outperform the naive scheme in which no intelligent management of energy is performed.
- In Chapter 3, we have considered a TDD MISO broadcast channel where the downlink channel is estimated from the pilot symbols sent by the user terminals. Training schemes that optimize the throughput are designed under the energy harvesting constraints at the user terminals. The optimal training scheme turns out to be quite different from the single user scenario considered in the previous chapter. Completely turning-off users with less harvested energy (resulting in poor CSI) is optimal in some cases.
- In Chapter 4, we have determined the achievable distortion region when the correlated source samples are transmitted by two energy harvesting sensor nodes to the destination over orthogonal fading channels. Assuming non-causal knowledge of these time varying source

statistics, energy arrivals and the channel gains, i.e., under the offline optimization framework, we have obtained the optimal transmission and coding schemes that achieve the points on the Pareto boundary of the total distortion region. An iterative directional 2D waterfilling algorithm is proposed to obtain two specific points on this boundary.

- In Chapter 5, we have considered a scenario where both the information and the energy source for an EH node are the same. We proposed and compared some practical schemes that use the electrical signal generated by the source to reduce the distortion in the transmitted data. We have also shown that when the sensor node can harvest energy form the source signal and use it in conjunction with the conventional power supply to satisfy QoS (distortion) constraints on the transmitted data, significant reduction in the usage of non-renewable energy can be achieved.

A brief summary of the future research directions are described below.

- In Chapter 2, we assumed that the energy consumed at the RX is only due to the CSI exchange process. However, if we consider a bi-direction communication where the RX also has data to transmit, how the harvested energy should be divided in transmission and feedback schemes ? The problem can be formulated as a weighted sum throughput of uplink and downlink rates subjected to the energy harvesting constraints at the TX and the RX. Also, one can consider a finite battery and also relax the assumption of the perfect feedback channel without any errors.
- In Chapter 3, we considered a TDD system and further work is needed to compare with other feedback models such as a FDD system. Although, ZF precoding is optimal at high SNRs, for low SNRs better rate is obtained by using other precoding techniques such as MMSE precoding. Although, might be challenging, it would interesting to see whether the feedback policies change with the choice of such precoding schemes. Recently it has been shown that delayed CSI can also bring significant benefits in the performance of a MISO broadcast channel [75]. Since an EH user terminal can delay its CSI feedback until it has sufficient energy, an interesting problem arises : given an EH profile, when and with what quality the user should feedback the CSI ?
- In Chapter 4, we have assumed that the energy consumed in only transmission of the source samples. However, sensing and processing of the source samples also incurs some energy consumption. In [76] it is shown that, when sampling costs are taken into account, in some cases, it is optimal to not sample some fraction of the total samples. One can model the sampling costs along the lines of [76], and to see how they affect the coordination among the sensor nodes in the considered system model.

- The idea of harvesting and sending information about the same source is quite new and there are plenty of possible extensions. In Chapter 5, we have assumed that the source is memoryless. However, if the samples are correlated, intuitively we can harvest more energy as loss of information in a sample due to the harvesting can be partially obtained from another correlated sample. Another interesting scenario is when multiple nodes observe a correlated source similar to the model considered in Chapter 4, and coordinate their actions in harvesting and transmission schemes.

# Chapter 7

# Résumé

## 7.1 Résumé [Français]

Au cours de la dernière décennie, nous avons observé à une croissance rapide du nombre de appareils de communication, et cette tendance devrait se poursuivre tant que les technologies essentielles telles que des objets connectes façonnent l'avenir de technologies d'information et de communication. Cette croissance a entraîné une augmentation considérable de la demande d'énergie, donc l'empreinte carbone de l'écosystème des ICT ne peut plus être ignoré.

De plus, dans les systèmes de communication traditionnelle alimentés par batterie, où le infrastructure énergétique n'est pas disponible après le déploiement, énergie limitée dans la batterie devient le goulot d'étranglement car elle détermine le lifetime de réseau.

Alimenter appareil de communication avec des sources d'énergie ambiante, grâce à technologie de récupération l'énergie, non seulement réduit l'empreinte carbone du secteur de ICT mais aussi augmente l'autonomie des réseaux de communication que dépend de la batterie. Un appareil de récupération d'énergie peut piéger l'énergie de l'entourant environnement (sources typiques sont l'énergie solaire, le vent, les vibrations, thermique, etc.). Cependant, variabilité dans temps de l'énergie ambiant modifie la conception de stratégies de communication tres différente de la systèmes traditionnelle.

En dehors de la récupération d'énergie, un débit plus élevé peut être obtenu dans un system sans fil en concevant des systèmes de transmission basé sur des informations de canal de propagation. Comme les techniques d'adaptation de canal exigent d'avoir une certaine connaissance de l'état du canal sans fil envoyé au émetteur, l'augmentation du débit vient a un coût de

l'estimation de l'information de canal qui consomment des ressources dans un système de communication, particulièrement, l'energie. En outre, lorsque l'objectif dans un système de communication est à envoyer des informations sur la source à une destination avec au minimum distortion erreur, des stratégies de transmission et de compression a être conçu sur la base à la fois sur la variable temps des conditions de canal et la statistiques de la source.

Cette thèse porte sur la conception de stratégies de transmission prenant en compte le coût de l'obtention des informations d'état de canal (CSI) à l'émetteur, et les statistiques de sources variables dans le temps lorsque la communication dispositifs reposent sur l'énergie récoltée (donc variant dans le temps) des fournitures. Plus précisément, dans le chapitre 2, nous considérons un multiple-input single output (MISO) système de communication de sortie dans lequel l'émetteur et le récepteur ont des capacités de récupération d'énergie. Le récepteur est intéressé par l'envoi de la CSI à l'émetteur pour aider à améliorer la debit. Par la modélisation de l'énergie consommée dans l'obtention de la CSI, nous visons à maximiser la débit, sous réserve des contraintes de récupération d'énergie à l'émetteur et le récepteur.

Dans le prolongement du scénario de MISO p2p, au chapitre 3, un canal MISO broadcast où un émetteur multi-antenne sert de multiples terminaux utilisateurs de récolte d'énergie est étudié. L'émetteur obtient la CSI en estimant le canal à partir de symboles pilotes envoyés par les terminaux utilisateurs. Les symboles pilotes qui optimisent le débit sont obtenus sous des contraintes de récupération d'énergie dans les terminaux d'utilisateurs.

Ensuite, au chapitre 4, on considère un système constitué de deux noeuds de capteur où chaque noeud observe et échantillons d'un phénomène physique commun localement, donc les échantillons sont corrélés. Ensuite, les nIJuds envoient leurs informations à la destination sur des canaux sansfil orthogonales. Dans ce scénario, on détermine la zone de distorsion possible pour les données transmises par les deux noeuds de capteur.

Enfin, on considère un système de communication où l'objectif est d'envoyer des informations sur la source d'énergie elle-même à une destination (mesure noeud) avec une moyenne de minimiser l'erreur quadratique distorsion. Plus précisément, le capteur mesures et envoie des informations sur le signal de la source tandis que dans le même temps repose sur l'énergie récupére de lui. Dans ce scénario, nous proposer des régimes qui utilise efficacement le signal électrique généré à partir de la source d'énergie ambiante pour minimiser moyenne distorsion.

## Chapitre 2 - Optimisation de p2p EH MISO systèmes de communication

Pour le meilleur de nos connaissances, un aspect commun de la plupart des travaux antérieurs traitant des problèmes d'allocation des ressources dans

les réseaux de communication EH est que le transmetteur (TX) est fourni avec des informations d'état de canal parfaite (CSI). La connaissance de CSI au TX est bénéfique dans la conception des techniques d'adaptation de canal optimales et les filtres TX dans les systèmes multi-antennes.

Toutefois, en pratique, le TX obtient cette information soit par de feedback où le récepteur (RX) envoie des bits quantifié de CSI ou en estimant le canal à partir de symboles pilotes envoyés par la RX. Des études récentes ont démontré que, bien que feedback améliore la performance du système, les ressources de feedback (puissance et de bande passante) sont limitées, et doit être dépensé à bon escient [41]. En conséquence, une question importante se pose : Comment les contraintes EH affecter la conception de réseaux sans fil avec feedback ?

Dans ce chapitre, l'optimisation d'une canal MISO EH avec feedback, où le feedback est utilisé pour améliorer le débit est étudié. En utilisant différents modèles de feedback, problèmes d'optimisation de débit sont formulés sous les contraintes EH au TX et RX. Nous essayons de répondre aux questions suivantes : Dans le cas de EH, l'énergie disponible pour le RX varie dans le temps. Devrait le RX envoyer feedback de sorte que même qualité de CSI est maintenue à la TX en tout temps ? Si oui, peut la qualité de CSI être améliorée en utilisant plus de bande passante lorsque l'énergie récoltée est faible au RX ?

Les principales contributions de ce chapitre sont les suivantes :

- Présentation pour la première fois les contraintes de récolte de l'énergie dans un canal à évanouissement MISO avec feedback.
- En utilisation de « offline optimisation », bornes limites supérieures inférieures sur le debit ergodique sous le EH contraintes sont obtenus.
- Outils de la théorie de Majoration sont utilisés pour dériver des algorithmes simples pour résoudre les problèmes d'optimisation formulés.

Le travail dans ce chapitre a été publié dans :

- *Rajeev Gangula, David Gesbert, Deniz Gunduz "Optimizing feedback in energy harvesting MISO communication channels", in proc. of IEEE Global Conference on Signal and Information Processing, December 3-5, 2013, Austin, TX, USA.*
- *Rajeev Gangula, David Gesbert, Deniz Gunduz "Optimization of energy harvesting MISO communication system with feedback", IEEE Journal on Selected Areas in Communications, vol.33, no.3, pp.396-406, March 2015.*

Le modèle d'un système de p2p MISO est montre dans Fig. 7.1, où à la fois le TX et le RX récupére de l'énergie de l'environnement. Chaque noeud est équipé d'un tampon particulier de l'énergie, soit une batterie rechargeable,

qui peut stocker l'énergie récupérée au niveau local.

Dans ce chapitre, nous utilisons EH model montre dans Fig. 7.2, pour évalue la performance des algorithmes proposés avec les algorithmes naïfs où aucune optimisation se fait sur l'utilisation de l'énergie récoltée.

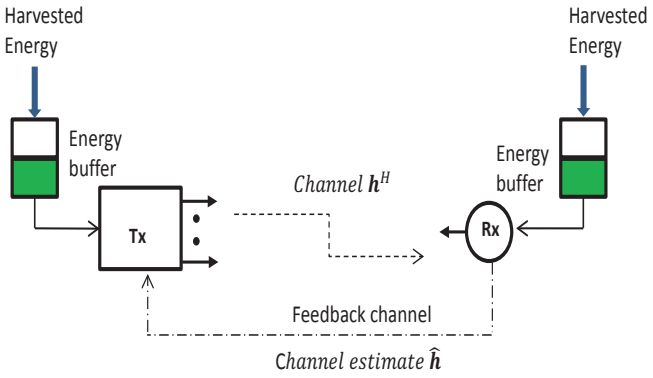


FIGURE 7.1 – Canal MISO avec TX et RX de la récupération d'énergie.

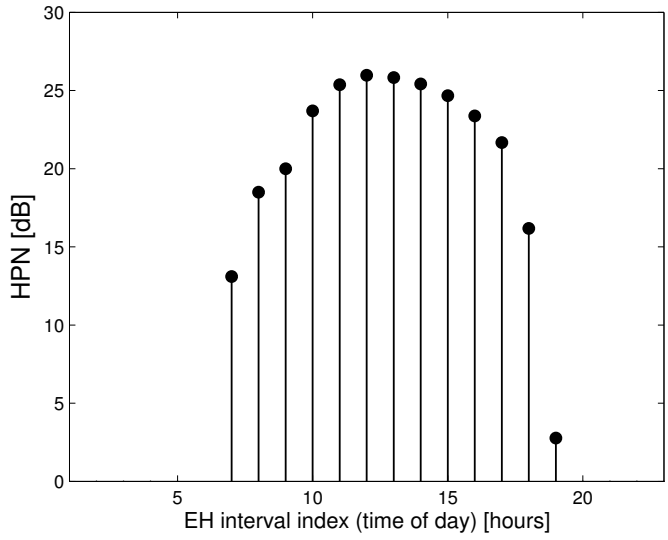


FIGURE 7.2 – Modèle pour un profil de l'énergie solaire a récupéree.

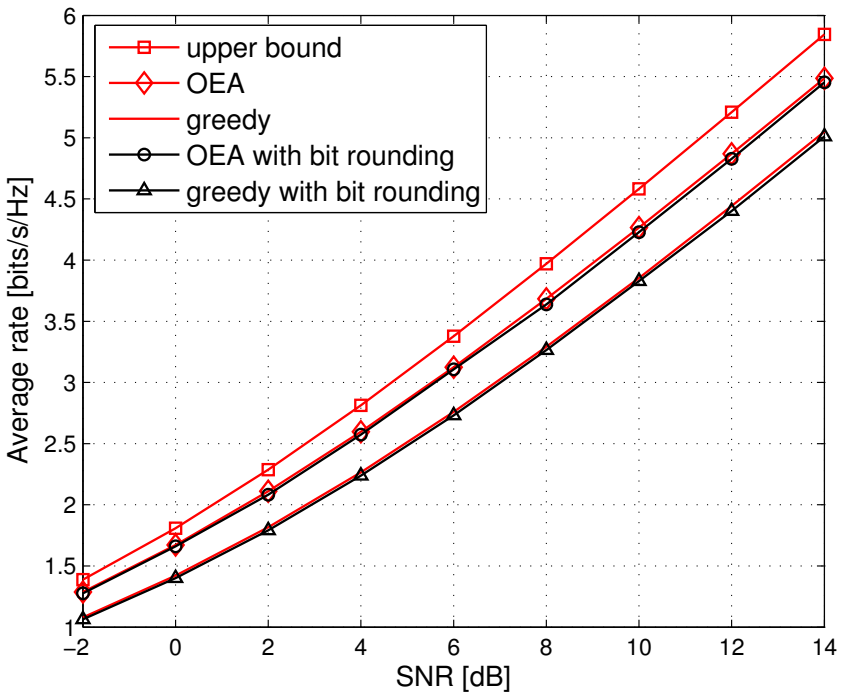


FIGURE 7.3 – Débit ergodique pour le scénario de canal non réciproque avec seulement un EH RX, et M = 4.

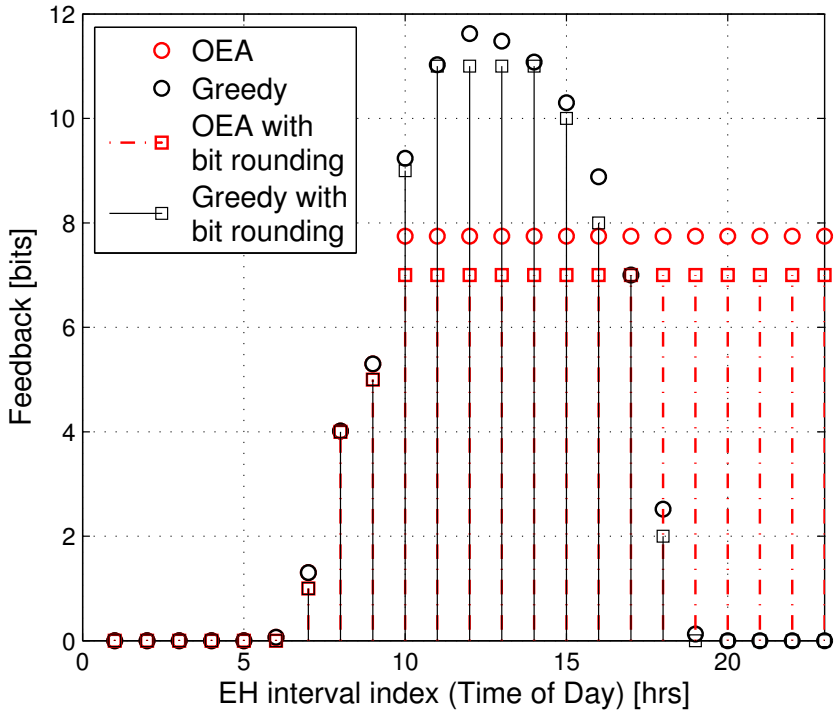


FIGURE 7.4 – Feedback à SNR de 10 dB, $M = 4$.

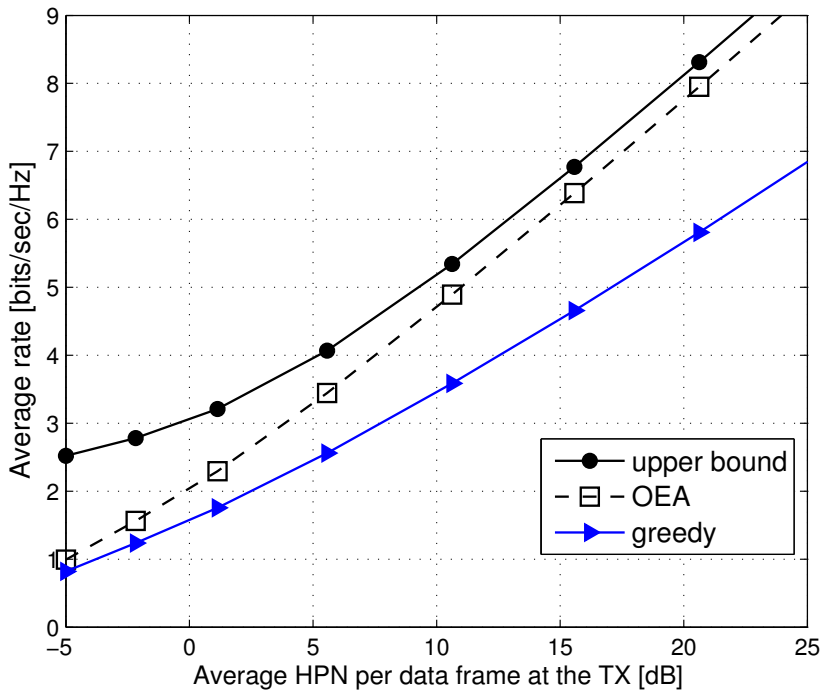


FIGURE 7.5 – Débit ergodique pour les profils EH similaires dans le scénario de canal non réciproque, $M = 4$.

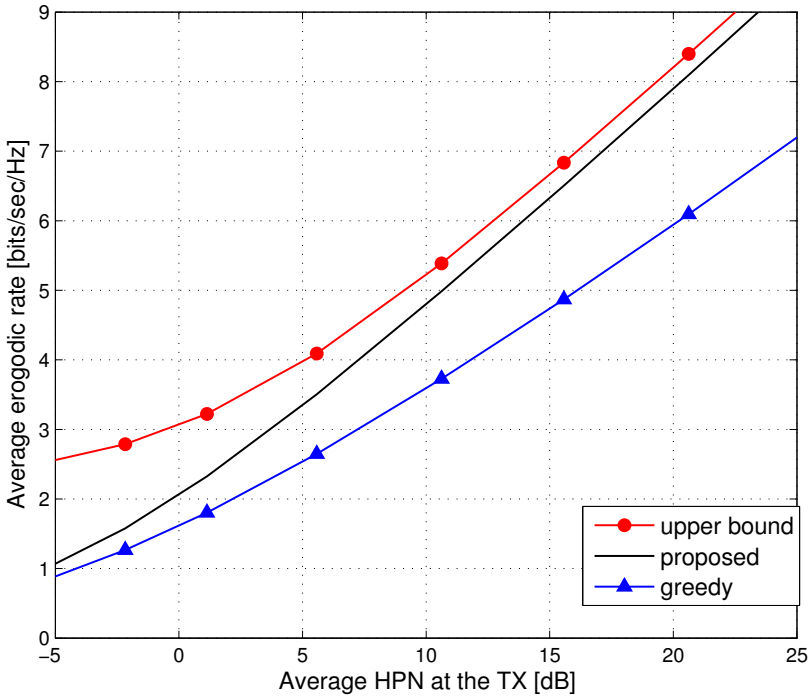


FIGURE 7.6 – Débit ergodique pour les profils EH similaires dans le scénario de canal réciproque, $M = 4$.

## Chapitre 3 - Optimisation de broadcast EH MISO systèmes de communication

Dans ce chapitre, nous considérons les transmissions d'un TX multi-antenne à plusieurs RXs avec seule antenne, qui modèle les transmissions à plusieurs utilisateurs en une seule cellule. Cette systeme est bien connu sous le nom de canal de MISO broadcast [46], [53].

Contrairement aux canaux de communication p2p MIMO, des informations d'état de canal (CSI) au TX dans canal MISO broadcast est essentielle à la réalisation des grands gains de débit car elle permet le TX à servir plusieurs utilisateurs en parallèle [46], [53]. Cependant, parfait CSI est une hypothèse idéale, et dans la pratique de cette l'information doit être acquise par le TX, qui consomme des ressources d'un système de communication. Contrairement aux canaux de p2p, des études dans [46], [47] ont montré que la qualité de la CSI doit être augmentée avec l'augmentation de la puissance de transmission pour obtenir des gains de débit.

Dans ce chapitre, nous considérons canal de MISO broadcast où les RXs récupérer l'énergie de l'environnement et le TX a une alimentation fixe. Le CSI au TX est obtenue par estimation du canal à partir de symboles pilotes envoyés par les terminaux utilisateurs (RXs). Plus précisément, nous considérons un système time-division-duplex (TDD) où le canal de down-link (DL) peut être estimé en utilisant les symboles pilotes émises par les terminaux d'utilisateurs dans up-link (UL). Sur la base de la CSI obtenu, le TX effectue le Zero-Forcing (ZF) précodage pour réduit l'inter-utilisateur interférences. Les symboles pilotes qui optimisent le débit sont déterminés sous la contraintes de récupération d'énergie aux terminaux.

Les principales contributions de ce chapitre sont les suivantes :

- Nous obtenons une approximation du débit de somme ergodique et montrons qu'il est une fonction concave de l'énergie consommée en envoyant les symboles pilotes.
- En utilisation de « offline optimisation », une borne inférieure sur le débit est obtenue.
- Un faible complexité heuristique algorithme glouton est proposé dont le rendement est assez proche au régime optimal.

Les contributions de ce chapitre seront bientôt soumis pour publication :

- *Rajeev Gangula, David Gesbert, Deniz Gunduz "Training optimization for Multiuser MISO Downlink with Energy Harvesting users" To be submitted.*

Le modèle d'un système de MISO broadcast où les RXs récupérer l'énergie de l'environnement et le TX a une alimentation fixe est montre dans Fig. 7.7.

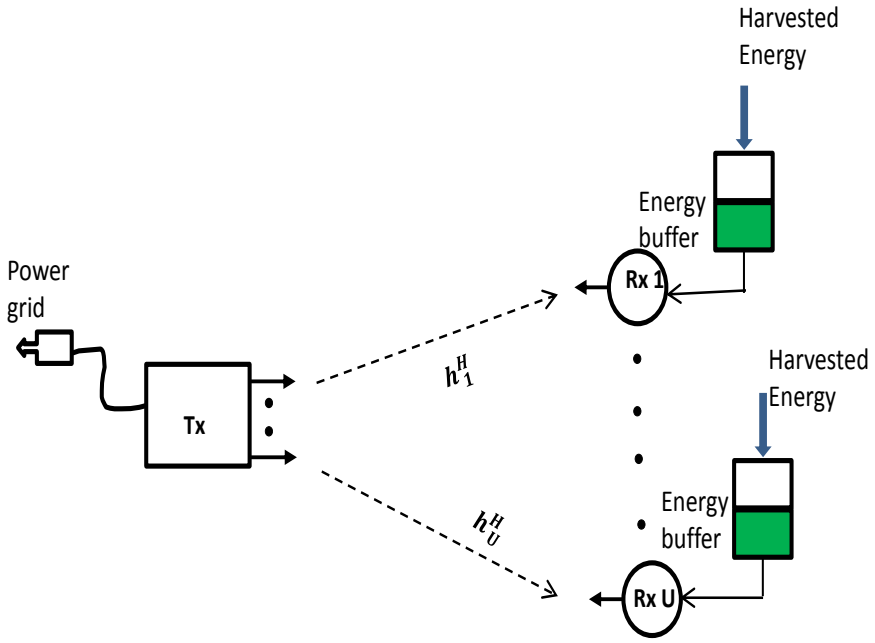


FIGURE 7.7 – Canal MISO broadcast avec EH noudes.

Dans le Fig. 7.8, nous utilisons EH model montre dans (7.1), pour évalue la performance des algorithmes proposés avec les algorithmes naïfs où aucune optimisation se fait sur l'utilisation de l'énergie récoltée et nombre de terminaux d'utilisateur. Le nombre d'intervalles EH est supposé être $K = 4$, nombre d'antennes de BS M $= 4$ et nombre total d'utilisateurs $U = 3$. Le modèle de EH est donné par

$$\mathbf{E} = \begin{bmatrix} 3 & 15 & 1.5 & 3 \\ 1 & 0.6 & 2 & 6 \\ 20 & 0 & 0 & 0 \end{bmatrix}, \tag{7.1}$$

où chaque rangée représente l'énergie récuperée par l'utilisateur au fil du temps. De même, dans le Fig. 7.9, nous utilisons EH model montre dans (7.2), pour évalue la performance des algorithmes proposés avec les algorithmes naïfs où aucune optimisation se fait sur l'utilisation de l'énergie récoltée et nombre de terminaux d'utilisateur. Le nombre d'intervalles EH est supposé être $K = 4$, nombre d'antennes de BS $M = 4$ et nombre total d'utilisateurs $U = 3$. Le modèle de EH est donné par

$$\mathbf{E} = \begin{bmatrix} 22 & 15.4 & 13.2 & 22 \\ 10 & 6 & 20 & 4 \\ 30 & 15 & 4.5 & 10.5 \end{bmatrix}. \tag{7.2}$$

Enfin, dans Fig. 7.10, nous comparons la performance du système proposé avec le moins complexe greddy user activation algorithme. Le greedy

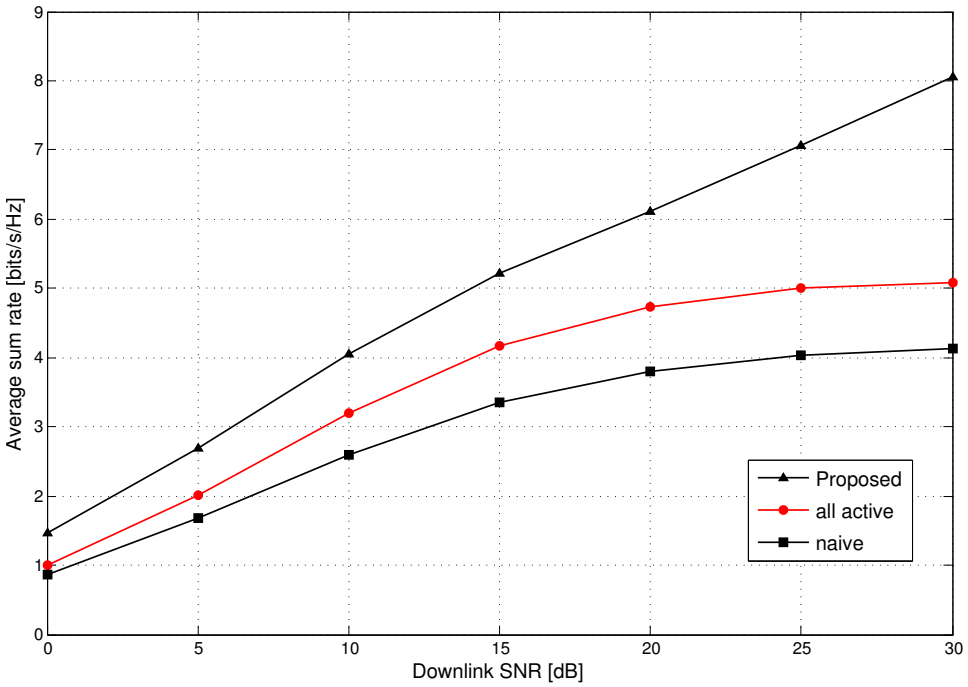


FIGURE 7.8 – Débit ergodique pour , $M = 4$, $U = 3$ and $K = 4$.

algorithme surpasse le système où tous les utilisateurs sont actifs dans chaque intervalle EH.

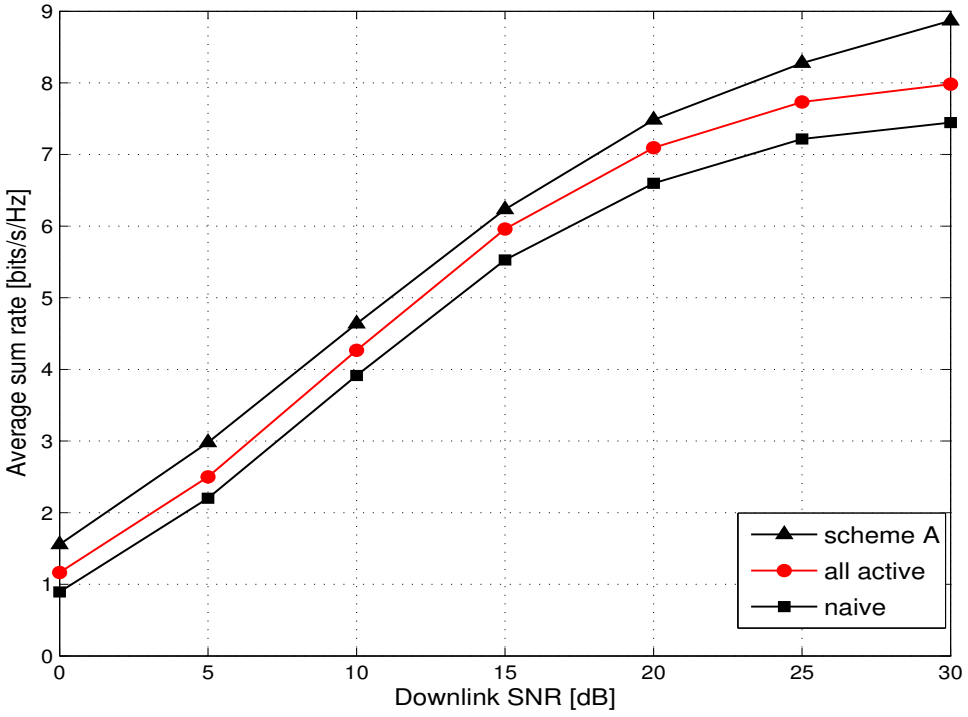


FIGURE 7.9 – Débit ergodique, $M = 4$, $U = 3$ and $K = 4$.

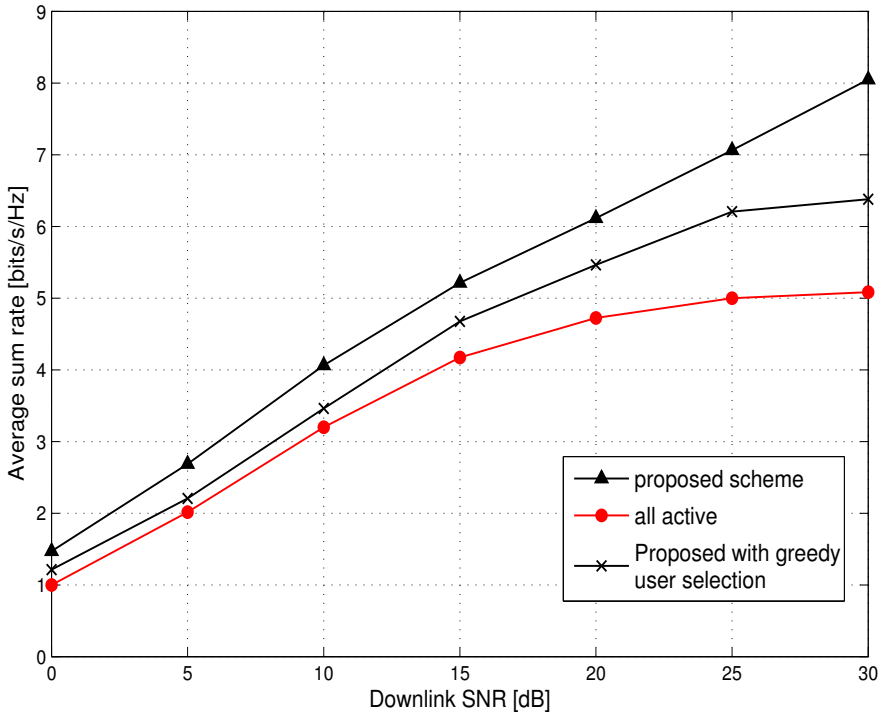


FIGURE 7.10 – Débit ergodique avec greedy algoritme, $M = 4$, $U = 3$ and $K = 4$.

## Chapitre 4 - Compression et de transmission Distribué avec des Capteurs à récupération de l'énergie

Un noeud de capteur sans fil recueille des échantillons d'une source (typiquement un physique phénomène dans son environnement), et communique ces échantillons à la destination sur un canal radio sans fil. Un réseau de ces noeuds peut être utilisé pour recueillir des informations sur un processus variant dans le temps qui est peut-être corrélée à travers l'espace et le temps. Dans ce scénario, le objectif est de concevoir des systèmes de transmission et de compression qui minimisent la reconstruction de distorsion de la source à la destination.

Dans [60], le problème de minimisation de la distorsion dans un canal sans fil avec un émetteur EH et un seul récepteur est considéré. Tenant compte de la variation de l'énergie récupère, variance statistique de la source et gains de canal, de débits optimaux des compression et de transmission sont trouvés en utilisant « offline optimisation » un simple algorithme « directional 2D waterfilling algorithm » est avérée optimal avec une contrainte de retard strictes. Dans [61], la performance de distorsion est étudiée en utilisant un modèle stochastique de EH.

Dans ce chapitre, nous étendons le problème de minimisation de la distorsion à un scénario de réseau. Pour le meilleur de nos connaissances, de codage source distribué avec des noeuds EH du point de vue de la théorie de distorsion-débit n'a pas été étudié avant. On considère un système constitué de deux noeuds de capteur où chaque noeud observe et échantillons d'un phénomène physique commun localement, donc les échantillons sont corrélés. Ensuite, les noeuds envoient leurs informations à la destination sur des canaux sans-fil orthogonales. Dans ce scénario, on détermine la zone de distorsion possible pour les données transmises par les deux noeuds de capteur. Le travail dans ce chapitre a été publié dans :

- *Rajeev Gangula, Deniz Gunduz, David Gesbert "Distributed compression and transmission with energy harvesting sensors", in Proc. of IEEE ISIT, Hong Kong, 2015.*

Les points $(\mathrm{D}_{1,m}, \mathrm{D}_{2,h})$ and $(\mathrm{D}_{1,h}, \mathrm{D}_{2,m})$ correspondant aux paires de distorsion lorsque respectivement le noeud 2 ou 1 agit comme le noeud d'aide. La limite reste, montré en vert dans la Fig. 7.12, représente les autres paires de distorsion de Pareto optimale. Les points $\mathrm{B}_1$ et $\mathrm{B}_2$ sont obtenus lorsque chaque noeud maximise goulûment le nombre total de bits transmis, quelles que soient les statistiques de source. Dans chaque fois, à chaque noeud, le débit de compression est égale à la débit de transmission.

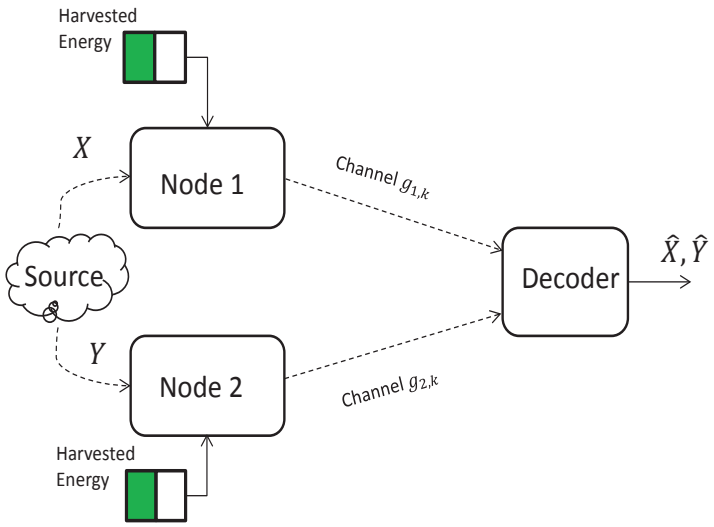


FIGURE 7.11 – Détection et la transmission distribuée avec des capteurs à récupération de l'énergie.

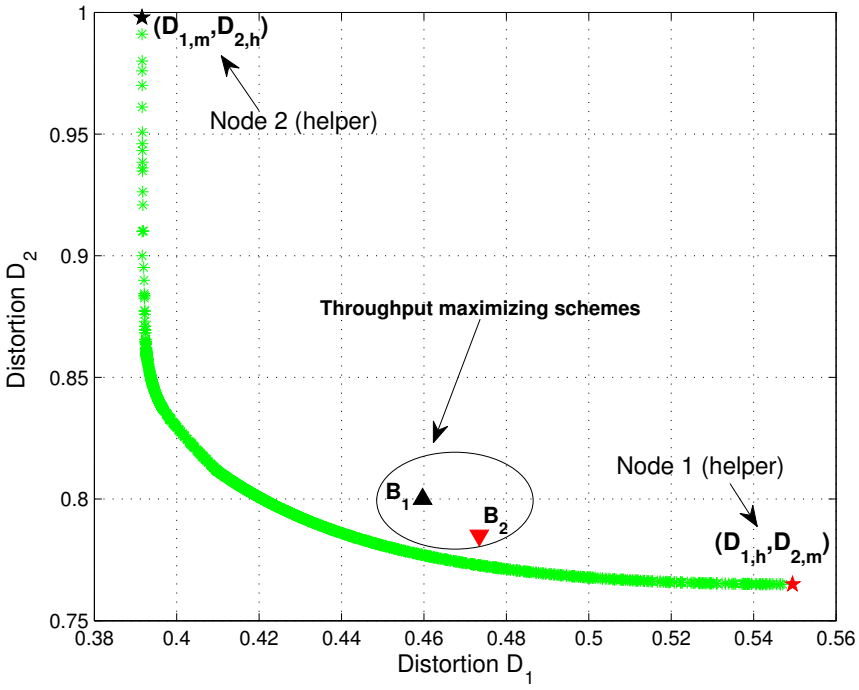


FIGURE 7.12 – Pareto frontier de $\mathcal{D}^*$.

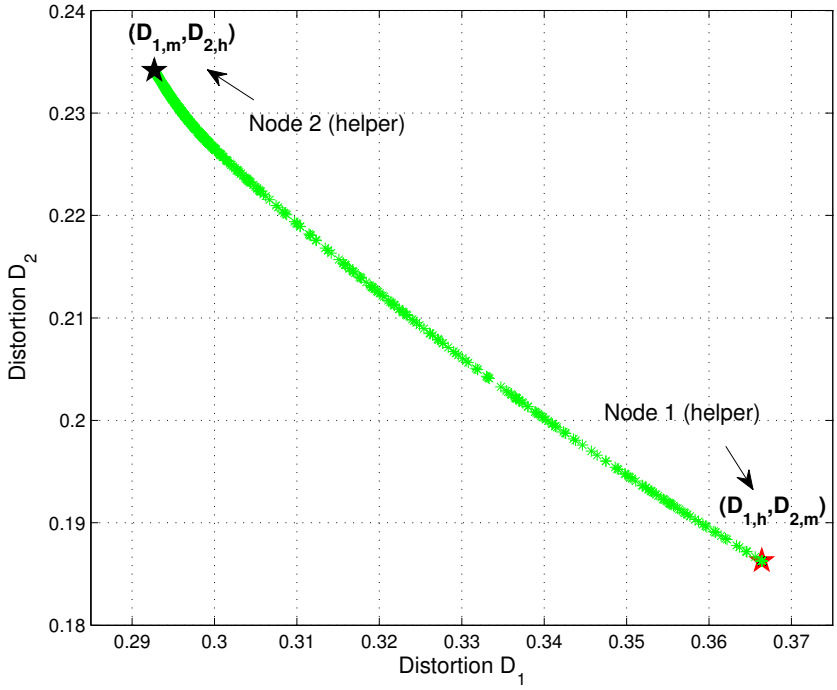


FIGURE 7.13 – Pareto frontier de $\mathcal{D}^*$ dans la scenario static.

## Chapitre 5 -La récupération et la compression de l'information à partir d'une source d'énergie ambiante

Le schéma synoptique d'un noeud de capteur typique alimenté par une source d'énergie ambiant est représenté sur la Fig. 7.14. Sur la Fig. 7.14, il y a deux transducteurs, une convertit l'énergie ambiante en un signal électrique, et l'autre transducteur (ou unité de détection) convertit le phénomène physique d'intérêt dans un signal électrique. La sortie du premier transducteur (collecteur d'énergie) est donnée à un réserve d'énergie tels que supercondensateur ou une batterie rechargeable. Cette énergie récupérée peut être utilisé ultérieurement pour alimenter les différents composants du capteur. Le signal de sortie du second transducteur est envoyé à un circuit d'échantillonnage qui convertit le signal analogique en échantillons de temps discrètes. Ces échantillons sont ensuite donnés à un sous-système de communication où ils sont traité par le codeur et ensuite transmis par la radio.

Dans certains cas, la source d'énergie ambiante à partir de laquelle le capteur récupère l'énergie, et la source d'informations à partir de laquelle le capteur recueille des échantillons peut être la même. Par exemple, un noeud de capteur souhaite envoyer des informations sur l'intensité de l'énergie solaire irradiation dans son environnement, et en même temps dépend de l'énergie récupérée de source solaire. Dans ce cas aussi, nous pouvons suivre l'architecture similaire à celle de la Fig. 7.14, avec deux transducteurs un pour la récupération et un pour la détection. Toutefois, la fourniture de deux détracteurs avec la même fonctionnalité peut ne pas être autorisée car ils occupent plus surface de puce. Donc, si il n'y a qu'un transducteur dans le système, le signal électrique de sortie maintenant contient à la fois l'énergie à récupérer et les informations sur les échantillons de source à transmettre.

Ces architectures sont souhaitables dans certaines applications et sont d'un intérêt pratique [67–69]. Fait intéressant, le travail [67] considéré notre envisagée modèle de système. Dans [67], il y a un seul piézo-électrique (PZT) transducteur qui produit un signal électrique à partir des vibrations. Le noeud de capteur est intéressé par quelques mesures de cette vibration et en même temps il récupère l'énergie de vibration. Une répartition dans le temps le modèle est utilisé, où, pour une certaine partie de temps du signal électrique est envoyé à la system de récupération (chargement d'un condensateur dans leur modèle), et les temps restantes des mesures sont effectuées en utilisant le signal électrique de sortie du transducteur. Cependant, le travail considère la mise sous tension du noeud de capteur ensemble et met l'accent sur la aspects pratiques de mise en oeuvre.

Dans ce chapitre, nous utilisons un modèle plutôt abstraite où le codeur doit envoyer les informations sur le signal issu du transducteur à une destination et en même temps appuie sur la récupération d'énergie à partir de cela. Le modèle est représenté sur la Fig. 7.15. Nous proposons des modèles pra-

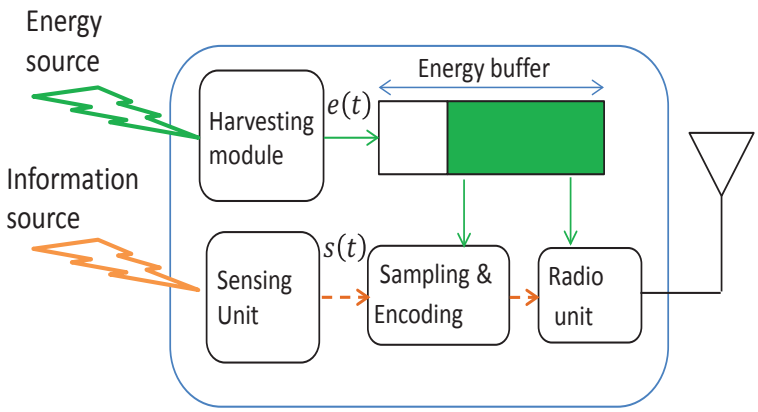


FIGURE 7.14 – Un noeud de capteur EH avec des sources d'énergie et d'information différents.

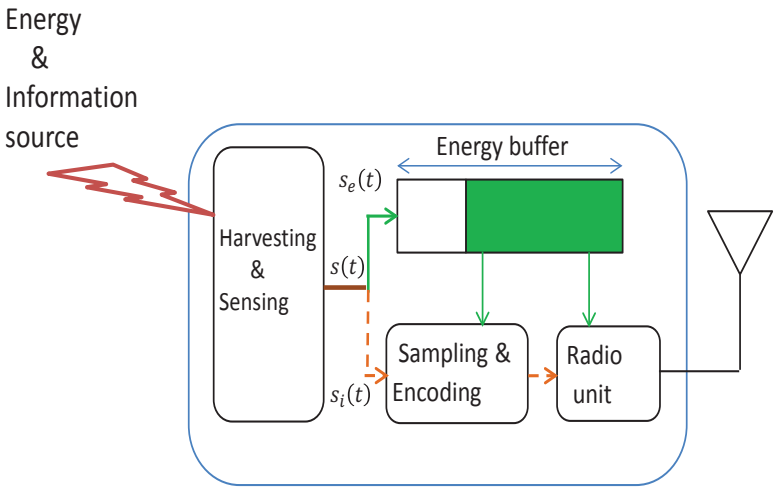


FIGURE 7.15 – Noeud de capteur EH avec la même source d'énergie et d'information.

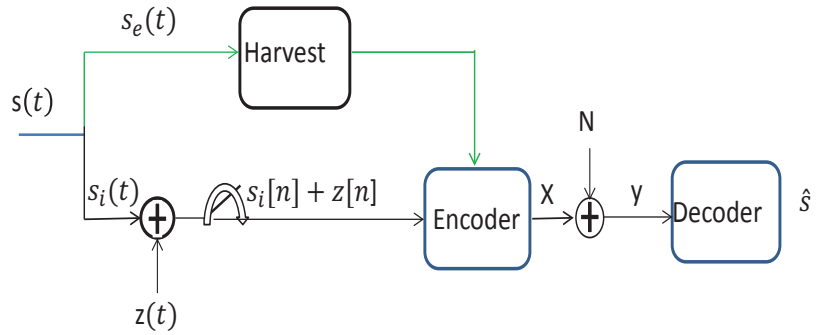


FIGURE 7.16 – Un modèle théorique pour la division du signal source.

tiques qui utilise efficacement le signal électrique généré à partir de l'énergie ambiante et source d'information pour la communication et à des fins de récolte. La objectif est d'envoyer les échantillons de source à la destination avec moyenne minimum distorsion tout en utilisant l'énergie récupérée à partir de la même source.

L'onde électrique de sortie du transducteur dans l'intervalle de temps $[0, T]$ est est désigné par $s(t), t \in [0, T]$. $s(t)$ est modélisée comme un processus aléatoire gaussienne ergodique et stationnaire avec moyenne nulle et de variance $\sigma_s^2$. Nous supposons $s(t)$ être une bande limitée de signal donc, il n'y a pas des fréquences supérieures à $B$ hertz dans $s(t)$. En utilisant le théorème d'échantillonnage de Nyquist, la reconstruction parfaite de $s(t)$ est possible à partir des échantillons discrètes prises $T_s = 1/2B$ secondes d'intervalle. Compte tenu de la période d'échantillonnage $T_s$, l'intervalle $[0, T]$ correspond à des échantillons $n = T/T_s$. Pour plus de commodité, nous supposons $n = T$ (à savoir, $T_s = 1$).

Nous utilisons des conceptions pratiques où le signal $s(t)$ est divisé en deux courants distincts $s_e(t)$ et $s_i(t)$, que la somme des énergies dans les courants des deux est égale à l'énergie dans le signal $s(t)$. Le signal $s_e(t)$ est utilisé pour récupération de l'énergie et le signal $s_i(t)$ est donné au système d'échantillonnage et par la suite à l'encodeur. Un modèle théorique du système considéré est représenté sur la Fig. 7.16.

## Architectures proposées

Dans cette section, nous proposons trois architectures basées sur le principe de conservation de l'énergie.

### Fractionnement de l'energie

Dans ce schéma, le signal source $s(t)$ est divisée en deux signals $s_e(t)$ et $s_i(t)$. $s_e(t)$ utilisé pour récupération de l'énergie, et $s_i(t)$ pour le système d'échantillonnage. Les paramètre de séparation $0 \leq \alpha \leq 1$ assure la conservation de l'énergie est obéi.

### Fractionnement dans le temps

Dans ce schéma, le signal source $s(t)$ est divisée en deux signals $s_e(t)$ et $s_i(t)$, ou $s_e(t) = s(t), t \in [0, (1-\beta)T]$ est utilisé pour récupération de l'énergie, et $s_i(t) = s(t), t \in ((1-\beta)T, T]$ est donné au système d'échantillonnage et par la suite à l'encodeur. Les paramètre de séparation $0 \leq \beta \leq 1$ assure la conservation de l'énergie est obéi.

### Fractionnement dans le temps et l'energie

Dans ce cas, nous combinons les deux les stratégies mentionnées ci-dessus. Le signal de source $s(t)$ est divisé en deux signaux $s_e(t)$ et $s_i(t)$ avec

$$s_e(t) = \begin{cases} s(t), \text{ for } t \in [0, (1-\beta)T] \\ \sqrt{1-\alpha}s(t), \text{ for } t \in ((1-\beta)T, T] \end{cases} \tag{7.3}$$

utilisé pour récupération de l'énergie, et $s_i(t) = \sqrt{\alpha}s(t), t \in ((1-\beta)T, T]$ est donné au système d'échantillonnage et par la suite à l'encodeur.

## Comparaison des performances

Le rapport signal sur bruit au niveau du codeur (SNRE) est définie comme

$$SNR = 10\log_{10}\left(\frac{\sigma_s^2}{\sigma_z^2}\right).$$

Dans la Fig. 7.17 distorsion des architectures proposées sont comparés pour différents écarts de bruit d'échantillonnage tout en faisant varier la puissance du signal $\sigma_s^2$, ainsi varier la SNRE. La variance du bruit de canal est supposé être $\sigma_n^2 = 1$. La borne inférieure est obtenue sous l'hypothèse que le codeur peut mesurer et en même temps il peut récolte de toute l'énergie du signal source. Comme prévu, le régime où les deux paramètres de temps et de fractionnement de l'énergie sont optimisées surpasse les autres régimes. Toutefois, notez que l'approche de la division de l'énergie effectue très bien

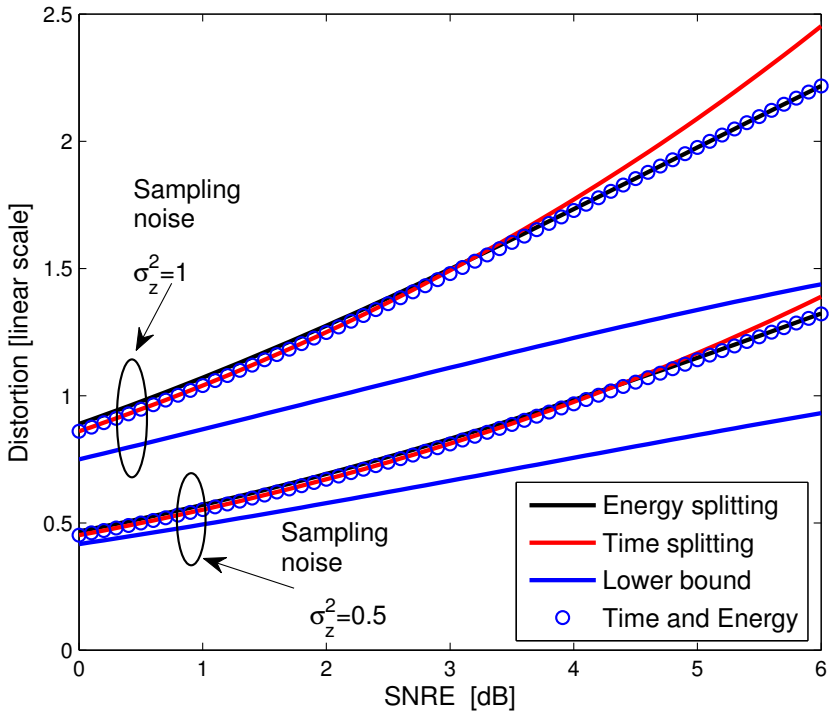


FIGURE 7.17 – Distorsion pour le bruit d'échantillonnage différents.

à tous les SNRE's. Comme nous pouvons voir la performance de distorsion diffère pour différents variance des bruits d'échantillonnage, même si le SNRE est la même.

Dans la Fig. 7.18, on compare la distorsion des architectures proposés-pour haute SNRE. Les écarts de bruit d'échantillonnage et le canal sont supposés être $\sigma_z^2 = 1$ and $\sigma_n^2 = 1$, respectivement. Pour la haute SNRE, architecture de fractionnement de l'énergie atteint la distorsion assez proche de la limite inférieure et il semble y avoir un écart constant dans l'exécution de la distorsion.

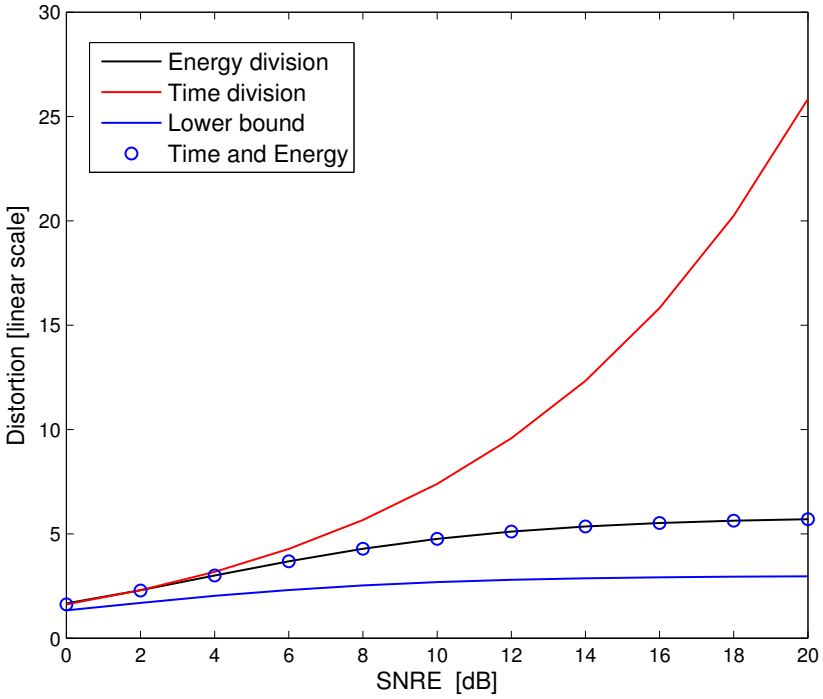


FIGURE 7.18 – Distorsion des architectures proposés.

# Bibliography


[1] S. Cui, A. Goldsmith, and A. Bahai, "Energy-efficiency of mimo and cooperative mimo techniques in sensor networks," *IEEE JSAC*, vol. 22, no. 6, pp. 1089–1098, Aug 2004.

[2] C. Isheden and G. Fettweis, "Energy-efficient multi-carrier link adaptation with sum rate-dependent circuit power," in *Proc. IEEE Glob. Telecom. Conf. (Globecom)*, Dec 2010, pp. 1–6.

[3] D. Feng, C. Jiang, G. Lim, J. Cimini, L.J., G. Feng, and G. Li, "A survey of energy-efficient wireless communications," *IEEE Communications Surveys Tutorials*, vol. 15, no. 1, pp. 167–178, First 2013.

[4] A. Bianzino, C. Chaudet, D. Rossi, and J. Rougier, "A survey of green networking research," *IEEE Communications Surveys Tutorials*, vol. 14, no. 1, pp. 3–20, First 2012.

[5] J. Baliga, R. Ayre, K. Hinton, and R. Tucker, "Green cloud computing : Balancing energy in processing, storage, and transport," *Proceedings of the IEEE*, vol. 99, no. 1, pp. 149–167, Jan 2011.

[6] A. Kansal, J. Hsu, S. Zahedi, and M. B. Srivastava, "Power management in energy harvesting sensor networks," *ACM Trans. Embed. Comput. Syst.*, vol. 6, no. 4, Sep. 2007.

[7] S. Sudevalayam and P. Kulkarni, "Energy harvesting sensor nodes : survey and implications," *IEEE Communications Surveys Tutorials*, vol. 13, no. 3, pp. 443–461, 2011.

[8] M. Krämer and A. Geraldy, "Energy measurements for Micaz node," *University of Kaiserslautern, Kaiserslautern, Germany, Technical Report KrGe06*, 2006.

[9] W. Du, F. Mieyeville, and D. Navarro, "Modeling energy consumption of wireless sensor networks by system C," in *Proc. International Conference on Systems and Networks Communications (ICSNC)*, Aug 2010, pp. 94–98.

[10] S. Baghaee, S. Chamanian, H. Ulusan, O. Zorlu, E. Uysal-Biyikoglu, and H. Kulah, "Demonstration of energy-neutral operation on a WSN testbed using vibration energy harvesting," in *Proc. European Wireless*, May 2014, pp. 1–6.

[11] R. Rajesh, V. Sharma, and P. Viswanath, "Information capacity of energy harvesting sensor nodes," in *ISIT*, 2011, pp. 2363–2367.

[12] O. Ozel and S. Ulukus, "Achieving AWGN capacity under stochastic energy harvesting," *IEEE Transactions on Information Theory*, vol. 58, no. 10, pp. 6471–6483, 2012.

[13] ——, "AWGN channel under time-varying amplitude constraints with causal information at the transmitter," in *Proc. Asilomar Conf. on Sign., Syst. and Computers*, Nov 2011, pp. 373–377.

[14] P. K. Deekshith, V. Sharma, and R. Rajesh, "AWGN Channel Capacity of Energy Harvesting Transmitters with a Finite Energy Buffer," *ArXiv e-prints*, Jul. 2013.

[15] Y. Dong and A. Ozgur, "Approximate capacity of energy harvesting communication with finite battery," in *ISIT*, June 2014, pp. 801–805.

[16] V. Jog and V. Anantharam, "An energy harvesting awgn channel with a finite battery," in *ISIT*, June 2014, pp. 806–810.

[17] R. A. Raghuvir, D. Rajan, and M. D. Srinath, "Capacity of the multiple access channel in energy harvesting wireless networks," in *Proc. Wireless Communications and Networking Conference (WCNC)*, 2012, pp. 898–902.

[18] O. Ozel, K. Tutuncuoglu, J. Yang, S. Ulukus, and A. Yener, "Transmission with energy harvesting nodes in fading wireless channels : optimal policies," *IEEE JSAC*, vol. 29, no. 8, pp. 1732–1743, 2011.

[19] J. Yang and S. Ulukus, "Optimal packet scheduling in an energy harvesting communication system," *IEEE Transactions on Communications*, vol. 60, no. 1, pp. 220–230, January 2012.

[20] C. K. Ho and R. Zhang, "Optimal energy allocation for wireless communications with energy harvesting constraints," *IEEE Transactions on Signal Processing*, vol. 60, no. 9, pp. 4808–4818, Sept. 2012.

[21] M. Antepli, E. Uysal-Biyikoglu, and H. Erkal, "Optimal packet scheduling on an energy harvesting broadcast link," *IEEE JSAC*, vol. 29, no. 8, pp. 1721–1731, 2011.

[22] J. Yang, O. Ozel, and S. Ulukus, "Broadcasting with an energy harvesting rechargeable transmitter," *IEEE Transactions on Wireless Communications*, vol. 11, no. 2, pp. 571–583, 2012.

[23] B. Devillers and D. Gunduz, "A general framework for the optimization of energy harvesting communication systems with battery imperfections," *Journal of Comm. and Nets*, vol. 14, no. 2, pp. 130–139, 2012.

[24] D. Gunduz and B. Devillers, "Two-hop communication with energy harvesting," in *CAMSAP*, 2011.

[25] O. Orhan and E. Erkip, "Optimal transmission policies for energy harvesting two-hop networks," in *CISS*, 2012.

[26] M. Gregori and M. Payaro, "Throughput maximization for a wireless energy harvesting node considering the circuitry power consumption," in *IEEE VTC Fall*, Sept. 2012.

[27] O. Orhan, D. Gunduz, and E. Erkip, "Optimal packet scheduling for an energy harvesting transmitter with processing cost," in *IEEE ICC*, June. 2013, pp. 3110–3114.

[28] D. Gunduz, K. Stamatiou, N. Michelusi, and M. Zorzi, "Designing intelligent energy harvesting communication systems," to appear in *IEEE Communications Magazine*, 2013.

[29] Q. Bai, A. Mezghani, and J. A. Nossek, "Throughput maximization for energy harvesting receivers," in *Smart Antennas (WSA), 2013 17th International ITG Workshop on*, March 2013.

[30] K. Tutuncuoglu and A. Yener, "Communicating with energy harvesting transmitters and receivers," in *ITA*, 2012.

[31] V. Sharma, U. Mukherji, V. Joseph, and S. Gupta, "Optimal energy management policies for energy harvesting sensor nodes," *IEEE Transactions on Wireless Communications*, vol. 9, no. 4, pp. 1326–1336, Apr 2010.

[32] N. Michelusi, K. Stamatiou, and M. Zorzi, "On optimal transmission policies for energy harvesting devices," in *Information Theory and Applications Workshop*, Feb 2012, pp. 249–254.

[33] M. Kashef and A. Ephremides, "Optimal scheduling for energy harvesting sources on time varying wireless channels," in *Proc. of Allerton Conf. on Comm. Control and Comp*, Sept 2011, pp. 712–718.

[34] B. Bacinoglu and E. Uysal-Biyikoglu, "Finite horizon online lazy scheduling with energy harvesting transmitters over fading channels," in *Proc. ISIT*, June 2014, pp. 1176–1180.

[35] L. Huang and M. J. Neely, "Utility optimal scheduling in energy-harvesting networks," *IEEE/ACM Trans. Netw.*, vol. 21, no. 4, pp. 1117–1130, Aug. 2013.

[36] P. Blasco, D. Gunduz, and M. Dohler, "A learning theoretic approach to energy harvesting communication system optimization," *IEEE Transactions on Wireless Communications*, vol. 12, no. 4, pp. 1872–1882, April 2013.

[37] D. Tse and P. Viswanath, *Fundamentals of wireless communication*. Cambridge university press, 2005.

[38] W. Santipach and M. Honig, "Optimization of training and feedback for beamforming over a MIMO channel," in *Proc. WCNC*, Mar 2007, pp. 1139–1143.

[39] ——, "Optimization of training and feedback overhead for beamforming over block fading channels," *IEEE Trans on Information Theory,*, vol. 56, no. 12, pp. 6103–6115, Dec. 2010.

[40] M. Kobayashi, N. Jindal, and G. Caire, "Training and feedback optimization for multiuser MIMO downlink," *IEEE Transactions on Communications*, vol. 59, no. 8, pp. 2228–2240, 2011.

[41] D. Love, R. Heath, V. K. N. Lau, D. Gesbert, B. Rao, and M. Andrews, "An overview of limited feedback in wireless communication systems," *IEEE JSAC*, vol. 26, no. 8, pp. 1341–1365, 2008.

[42] H. Edmundson, *Bounds on the Expectation of a Convex Function of a Random Variable.* RAND Corporation, 1957.

[43] A. W. Marshall, I. Olkin, and B. C. Arnold, *Inequalities : Theory of majorization and its applications.* Springer, 2010.

[44] C. K. Au-Yeung and D. Love, "On the performance of random vector quantization limited feedback beamforming in a MISO system," *IEEE Transactions on Wireless Commm*, vol. 6, no. 2, pp. 458–462, 2007.

[45] T. Yoo and A. Goldsmith, "Capacity and power allocation for fading MIMO channels with channel estimation error," *IEEE Transactions on Information Theory*, vol. 52, no. 5, pp. 2203–2214, May 2006.

[46] G. Caire, N. Jindal, M. Kobayashi, and N. Ravindran, "Multiuser MIMO achievable rates with downlink training and channel state feedback," *IEEE Transactions on Information Theory*, vol. 56, no. 6, pp. 2845–2866, Jun 2010.

[47] N. Jindal, "MIMO broadcast channels with finite-rate feedback," *IEEE Trans on Inf. Theory*, vol. 52, no. 11, pp. 5045–5060, 2006.

[48] S. Boyd and L. Vandenberghe, *Convex optimization.* New York, NY, USA : Cambridge University Press, 2004.

[49] B. Prabhakar, E. Uysal Biyikoglu, and A. El Gamal, "Energy-efficient transmission over a wireless link via lazy packet scheduling," in *IEEE INFOCOM*, vol. 1, 2001, pp. 386–394 vol.1.

[50] M. Zafer and E. Modiano, "A calculus approach to minimum energy transmission policies with QoS guarantees," in *INFOCOM*, 2005.

[51] S. Reddy and C. Murthy, "Dual-stage power management algorithms for energy harvesting sensors," *IEEE Trans on Wireless Comm*, vol. 11, no. 4, pp. 1434–1445, 2012.

[52] "Solar Resource and Meteorological Assessment Project (SOLRMAP)," `http://www.nrel.gov/midc/lmu/`.

[53] D. Gesbert, M. Kountouris, R. Heath, C.-B. Chae, and T. Salzer, "Shifting the mimo paradigm," *IEEE Signal Processing Magazine*, vol. 24, no. 5, pp. 36–46, Sep 2007.

[54] M. Shakiba-Herfeh and E. Uysal-Biyikoglu, "Optimization of feedback in a MISO downlink with energy harvesting users," in *Proc. IEEE EW*, May 2014.

[55] C. Swannack, E. Uysal-Biyikoglu, and G. Wornell, "Low complexity multiuser scheduling for maximizing throughput in the mimo broadcast channel," in *Allerton Conference on Communications, Control, and Computing, Monticello, IL, USA*, 2004.

[56] T. Yoo and A. Goldsmith, "On the optimality of multiantenna broadcast scheduling using zero-forcing beamforming," *IEEE JSAC*, vol. 24, no. 3, pp. 528–541, Mar 2006.

[57] N. Jindal, J. Andrews, and S. Weber, "Multi-antenna communication in ad hoc networks : Achieving MIMO gains with SIMO transmission," *IEEE Transactions on Communications*, vol. 59, no. 2, pp. 529–540, Feb 2011.

[58] J. Zhang, M. Kountouris, J. Andrews, and R. Heath, "Multi-mode transmission for the MIMO broadcast channel with imperfect channel state information," *IEEE Transactions on Communications*, vol. 59, no. 3, pp. 803–814, March 2011.

[59] P. Castiglione, O. Simeone, E. Erkip, and T. Zemen, "Energy management policies for energy-neutral source-channel coding," *IEEE Trans on Communications*, vol. 60, no. 9, pp. 2668–2678, Sep. 2012.

[60] O. Orhan, D. Gunduz, and E. Erkip, "Source-channel coding under energy, delay and buffer constraints," *IEEE Transactions on Wireless Communications*, vol. PP, no. 99, pp. 1–1, 2015.

[61] M. Motlagh, M. Khuzani, and P. Mitran, "On lossy source-channel transmission in energy harvesting communication systems," in *IEEE ISIT*, June 2014.

[62] W. Chen, Y. Andreopoulos, I. Wassell, and M. Rodrigues, "Towards energy neutrality in energy harvesting wireless sensor networks : A case for distributed compressive sensing ?" in *IEEE GLOBECOM*, Dec 2013.

[63] A. Wagner, S. Tavildar, and P. Viswanath, "Rate region of the quadratic Gaussian two-encoder source-coding problem," *IEEE Transactions on Information Theory*, vol. 54, no. 5, pp. 1938–1961, May. 2008.

[64] J.-J. Xiao and Z.-Q. Luo, "Multiterminal source-channel communication over an orthogonal Multiple-access channel," *IEEE Transactions on Information Theory*, vol. 53, no. 9, pp. 3255–3264, Sep. 2007.

[65] Y. Oohama, "Gaussian multiterminal source coding," *IEEE Trans on Info Theory*, vol. 43, no. 6, pp. 1912–1923, Nov. 1997.

[66] D. Bertsekas, *Nonlinear programming.* Athena Scientific, 1999.

[67] P. Miribel-Catala, J. Colomer-Fararons, J. Lafuente Brinquis, and J. Lopez-Sanchez, "Self-powered adaptive circuit sampling for a piezoelectric harvester," in *Proc. Design of Circuits and Integrated Circuits (DCIS)*, Nov 2014, pp. 1–6.

[68] M. Bafleur and J.-M. Dilhac, "Towards energy autonomy of wireless sensors in aeronautics applications : SMARTER collaborative project," in *Proc. IEEE International Conference on Green Computing and Communications and IEEE Internet of Things and IEEE Cyber, Physical and Social Computing*, Aug 2013.

[69] "SMARTER Project," `http://www.chistera.eu/projects/smarter`.

[70] R. Zhang and C. K. Ho, "MIMO broadcasting for simultaneous wireless information and power transfer," *IEEE Transactions on Wireless Communications*, vol. 12, no. 5, pp. 1989–2001, May 2013.

[71] L. Liu, R. Zhang, and K.-C. Chua, "Wireless information and power transfer : A dynamic power splitting approach," *IEEE Transactions on Communications*, vol. 61, no. 9, pp. 3990–4001, September 2013.

[72] T. M. Cover and J. A. Thomas, "Elements of information theory," 2012.

[73] R. Dobrushin and B. Tsybakov, "Information transmission with additional noise," *IRE Transactions on Information Theory*, vol. 8, no. 5, pp. 293–304, September 1962.

[74] J. Wolf and J. Ziv, "Transmission of noisy information to a noisy receiver with minimum distortion," *IEEE Transactions on Information Theory*, vol. 16, no. 4, pp. 406–411, Jul 1970.

[75] M. Maddah-Ali and D. Tse, "Completely stale transmitter channel state information is still very useful," *IEEE Transactions on Information Theory*, vol. 58, no. 7, pp. 4418–4431, July 2012.

[76] X. Liu, O. Simeone, and E. Erkip, "Energy-efficient sensing and communication of parallel gaussian sources," *IEEE Transactions on Communications*, vol. 60, no. 12, pp. 3826–3835, December 2012.